NON-LINEAR FINITE ELEMENT METHOD SIMULATION AND MODELING OF THE COLD AND HOT ROLLING PROCESSES

By

Alejandro Rivera Muñiz

Thesis submitted to the Faculty of the
Virginia Polytechnic Institute and State University
in partial fulfillment of the requirements for the degree of

Master of Science
in
Mechanical Engineering

Dr. Robert L. West – Committee Chair
Dr. John J. Lesko - Committee Member
Dr. Robert H. Sturges - Committee Member

January 8th, 2007
Blacksburg, Virginia

Keywords: Hot Rolling, Cold Rolling, Coupled Thermal-Mechanical, Non-Linear Finite Element Method, Plasticity, Rigid-Viscoplastic, Elastic-Plastic

© Alejandro Rivera, 2007

NON-LINEAR FINITE ELEMENT METHOD SIMULATION AND MODELING OF THE COLD AND HOT ROLLING PROCESSES

Alejandro Rivera

Abstract

A nonlinear finite element model of the hot and cold rolling processes has been developed for flat rolling stock with rectangular cross section. This model can be used to analyze the flat rolling of cold and hot steel rectangular strips under a series of different parameters, providing the rolling designer with a tool that he can use to understand the behavior of the steel as it flows through the different passes.

The models developed, take into account all of the non-linearities present in the rolling problem: material, geometric, boundary, and heat transfer. A coupled thermal-mechanical analysis approach is used to account for the coupling between the mechanical and thermal phenomena resulting from the pressure-dependent thermal contact resistance between the steel slab and the steel rolls.

The model predicts the equivalent stress, equivalent plastic strain, maximum strain rate, equivalent total strain, slab temperature increase, increase in roll temperature, strip length increase, slab thickness % reduction (draft), and strip's velocity increase, for both the cold and hot rolling processes. The FE model results are an improvement over the results obtained through the classical theory of rolling. The model also demonstrates the role that contact, plastic heat generation and friction generated heat plays in the rolling process.

The analysis performed shows that the steel in cold rolling can be accurately modeled using the elastic-plastic (solid Prandtl-Reuss) formulation, with a von Mises yield surface, the Praguer kinematic hardening rule, and the Ramberg-Osgood hardening material model. The FE models also demonstrate that the steel in hot rolling can be modeled using the rigid-viscoplastic (flow Levy-Mises) formulation, with a von Mises yield surface, and Shida's material model for high temperature steel where the flow stress is a function of the strain, strain rate, and the temperature.

Other important contributions of this work are the demonstration that in cold rolling, plane sections do not remain plane as the classic theory of rolling assumes. As a consequence, the actual displacements, velocity, and stress distributions in the workpiece are compared to and shown to be an improvement over the distributions derived from the classical theory. Finally, the stress distribution in the rolls during the cold rolling process is found, and shown to be analogous to the stress distribution of the Hertz contact problem.

Keywords: Hot Rolling, Cold Rolling, Coupled Thermal-Mechanical, Non-Linear Finite Element Method, Plasticity, Rigid-Viscoplastic, Elastic-Plastic

Dedication

A mi Padre, José Manuel Rivera Díaz, el mejor calibrador de perfiles laminados en caliente del mundo

Acknowledgements

I would like to express my appreciation and gratitude to my thesis advisors: Dr. Robert L. West, for his fantastic guidance and the freedom he gave me, allowing me to "design" my own dream thesis, have control of it in all of its aspects, and work on it at my own pace. He always pointed me in the right direction and allowed my mind to "run wild & free". The lack of constraints he imposed on me made all the difference without a doubt. Also, his class in Mechanical Design as an undergraduate was the one that triggered my interest in the Finite Element Method applied to Machine Design, and it was back then that I decided that I should work in the field of structural mechanics & dynamics.

To Dr. John "Jack" Lesko, whose class in Strength of Materials that I took back in 1997 as a technical elective for my ISE curriculum, was such an eye opener and had such a profound impact on me, that I decided that I had to add Mechanical Engineering as a second major. His amazing lectures set the foundations of my knowledge in elasticity and mechanics of materials, and after his class it was just a matter of time before I decided to dive into the fascinating field of plasticity. And finally to Dr. Robert Sturges for his enthusiasm, his good tips, and the ones he will definitely give me during the Ph.D. portion of this wonderful project. He represents the link between my Industrial and Mechanical Engineering backgrounds that blend so well in the exciting and dynamic field of manufacturing engineering. Thanks to the three of them for their guidance throughout the course of my academic career and this Masters' thesis.

My deepest gratitude to Mrs. Jan Riess, student advisor in the Mechanical Engineering Department who when I first met her and told her I wanted to double major in ISE and ME she told me I could do it, when everybody else told me it was impossible. Thanks to her also for her great advice and help during my undergraduate years. Also to Dr. Charles Reinholtz, my faculty advisor in Mechanical Engineering who was always full of great suggestions for my career.

Many thanks to Dr. John G. Lenard, Professor Emeritus of the University of Waterloo, Canada. His books were some of my main references, and he had the kindness of replying to an email I sent asking him to please verify that I had chosen the right yield surfaces, hardening rules, and material models.

Finally, I would like to thank my parents, José Manuel Rivera and Candi Muñiz, for believing in me and letting me fulfill the dream of my life: coming to an American university and to the United States to pursue my academic career and life goals. I would also like to thank them for the effort they had to make to support me financially, working so hard all of their lives, and mostly for their encouragement, inspiration, and love. Also my brother, German Rivera Muñiz for being the bravest person I have ever met, and also for his unconditional support.

Table of Contents

Chapter 1: Introduction

1.1 Basic Definition and History of Rolling 2
1.2 The Finite Element Method (FEM), Virtual Manufacturing, and its potential impact in the hot rolling industry.....11
1.3 Objectives and Scope of this work 12
1.4 Organization of Thesis.....15

Chapter 2: Mathematical Models and Mechanics Aspects of the Rolling Problem

2.1 Introduction 18
2.2 Governing Equations of the Mechanical Problem.....20
2.3 Boundary Conditions of the Mechanical Problem & the Mechanical Initial Boundary Value Problem (M-IBVP) 23
2.4 Heat Transfer & Thermal Balance 25
2.5 Boundary Conditions of the Thermal Problem & the Thermal Initial Boundary Value Problem (M-IBVP).....31
2.6 Classic Mathematical Solution Model of Flat Rolling.....33
2.7 Mathematical aspects of the Contact Problem 38
2.8 Friction Modeling.....42
2.9 Material Model & Plasticity 46
2.10 Summary and Concluding Remarks.....51

Chapter 3: Non-linear Thermal Mechanical Finite Element Modeling in Rolling

3.1 Introduction 54
3.2 The Finite Element Formulation – Variational Approach.....55
3.3 Approaches to the Simulation of Metal Forming Processes...58
3.4 The Rigid- Plastic Flow Finite Element Model.....60
3.5 The Rigid-Viscoplastic Material Model 68
3.6 Heat Transfer Finite Element Modeling in Rolling.....70
3.7 The Elastic-Plastic Flow Formulation.....74
3.8 Coupled Thermal-Mechanical Analysis.....75
3.9 Non-Linearities in the Rolling Problem 78
3.10 Summary and Concluding Remarks.....86

Chapter 4: Results for 2-D Plane Strain Finite Element Models for the Flat Rolling Problem

4.1 Introduction 89
4.2 2-D Plane Strain Model for Flat Cold Rolling 90
4.3 2-D Plane Strain Model for Flat Hot Rolling 121
4.4 Summary and Concluding Remarks 135

Chapter 5: Summary & Concluding Remarks

5.1 Summary 139
5.2 Conclusions 145
5.3 Recommendations and Future Work 148

Bibliography & References

List of Symbols

Uppercase Symbols

A	Cross Sectional Area (m^2)
A_{rad}	Area of radiating surface (m^2)
$A_{contact}$	Contact Area
B	Contact bias factor
$\boldsymbol{C}$	Heat capacity matrix / global conductivity matrix (W/m^2 K)
C_p	Specific Heat (J/kg K)
C	Steel's carbon content (weight per cent)
$\boldsymbol{D}$	Effective strain rate tensor (s^{-1})
D	Contact distance
D	Activation energy of diffusion
E	Young's modulus of elasticity (MPa)
$\boldsymbol{E}$	Lagrangian strain tensor
E_{ij}	Components of the strain tensor
$\dot{E}_{in}$	Rate at which thermal energy enter through the control surface (W/m^3)
$\dot{E}_{out}$	Rate at which thermal energy leave through the control surface (W/m^3)
$\dot{E}_g$	Energy generation (W/m^3)
$\dot{E}_{st}$	Rate of energy stored within the control volume (W/m^3)
E''_{st}	Energy stored flux (W/m^2)
$E(\dot{\varepsilon}_{ij})$	Work function for rigid-viscoplastic materials
F	Roll force (N)
$\boldsymbol{F}$	Nodal Forces matrix (N)
F_s	Contact separation force
F_t	Tangential Force (N)
F_n	Normal Reaction (N)
G	Shear modulus (MPa)
I_1 or I_T	Linear invariant of the stress tensor
I_2 or II_T	Quadratic invariant of the stress tensor
I_3 or III_T	Cubic invariant of the stress tensor
J_1 or I_s	Linear invariant of the deviatoric stress tensor
J_2 or II_s	Quadratic invariant of the deviatoric stress tensor
J_3 or III_s	Cubic invariant of the deviatoric stress tensor
$\boldsymbol{K}$	Stiffness matrix (N/m)
$\boldsymbol{K_c}$	Heat Conduction matrix (W/m^2 K)
K	Strain hardening coefficient
L_{pw}	Length of region subject to plastic deformation

L	Roll gap/contact arc length (m)
$\boldsymbol{L}$	Velocity gradient tensor
P	Roll pressure (Pa)
Q	Heat Flux Vector (nodal) (W/m^2)
R	Roll Radius (m)
$\boldsymbol{S}$	Deviatoric Stress Tensor (MPa)
S	Constrained yield strength in rolling (MPa)
$S_{\bar{F}}$	Surface where traction $\bar{F}_i$ is prescribed
$S_{\bar{v}}$	Surface where velocity $\bar{v}_i$ is prescribed
$\boldsymbol{T}$	Cauchy Stress Tensor (MPa)
T	Nodal temperatures matrix (K)
TOL	Contact closure distance
T_R	Roll temperature (K)
T_w	Workpiece temperature (K)
T_∞	Environment temperature (K)
U	Nodal displacements matrix (m)
U_0	Strain Energy density
U	Strain Energy
U_0^v	Volumetric strain energy density
U_0^d	Distortional strain energy density
V	Volume (m^3)
V_r	Roll surface velocity (m/s)
V_o	Workpiece initial speed (m/s)
V_f	Workpiece exit speed (m/s)
V_x	Velocity of the metal being rolled at section dx (m/s)
$\boldsymbol{X}$	Back stress tensor (MPa)

Lowercase Symbols

$\boldsymbol{a}$	Acceleration vector (m/s^2)
$\boldsymbol{b}$	Body forces vector (N)
b_j	Components of body forces vector (N)
dh	Infinitesimal thickness (m)
dx	Infinitesimal length (m)
e	Dilatation
e	Elongation (m)
e	Engineering strain
f	Residual of the nodal point force vector
$f(\sigma_{ij})$	Yield function / plastic potential
f_{fr}	Friction force (N)
h	film convection heat transfer coefficient (W/m^2 K)
h_0 / h_1	Strip/workpiece entry thickness (m)
h_f / h_2	Strip/workpiece exit thickness (m)
h_a	Average workpiece thickness (m)
Δh	draft (m)

k	Shear yield stress (MPa)
k	Thermal conductivity/ conduction heat transfer coefficient (W/m^2 K)
k	Boltzmann constant = 1.380 x 10^{-23} J/K molecule
m	mass of rolled stock, workpiece, strip, etc (kg)
n	Strain hardening exponent
$\bar{n}$	Unit normal vector
P	Roll pressure (MPa)
$\boldsymbol{p}$	Hydrostatic pressure tensor (MPa)
q_{fr}	Heat transfer rate due to friction (W)
q''_{cond}	Conduction heat flux (W/m^2)
q''_{conv}	Convection heat flux (W/m^2)
q''_{rad}	Radiation heat flux (W/m^2)
q''_{pw}	Plastic work heat generation flux (W/m^2)
q''_{fr}	Friction heat flux (W/m^2)
$\dot{q}$	Rate of heat generation per unit volume (W/m^3)
s_{ij}	Components of the deviatoric stress tensor (MPa)
$\bar{t}$	Unit tangential vector
t	time (s)
$\bar{u}_A$	Position vector point A
$\bar{u}_B$	Position vector point B
$\Delta\bar{u}_A$	Incremental displacement vector of node A
$\Delta\bar{u}_{normal}$	Incremental displacement vector in the normal direction of contact
$\Delta\bar{u}_{\tan}$	Incremental displacement vector in the tangential direction of contact
v_j	Components of velocity vector (m/s)
Δv	Increment of nodal velocity
$\bar{v}$	Velocity vector (m/s)
v_r	Relative roll-workpiece sliding velocity

Greek Symbols

Γ_i	Mechanical boundary conditions corresponding to boundary *i*
Φ_i	Thermal boundary conditions corresponding to boundary *i*
α	Roll bite angle (rad)
α	Friction coefficient multiplier
α	Deceleration coefficient
β	Stick to slip transition friction region
γ	Shear strain
γ	Dislocation density
δ	Convergence criterion
σ	Stephan-Boltzmann constant = 5.67 x 10^{-8} W/m^2 K^4
σ_{fr}	Tangential friction stress
σ_n	Normal stress (MPa)
σ_{ij}	Components of the Cauchy stress tensor (MPa)

$d\sigma_{ij}$	Infinitesimal stress (MPa)
$\bar{\sigma}$	Effective/equivalent stress, flow stress (MPa)
$\bar{\sigma}_{ij}$	Components of equivalent stress tensor (MPa)
σ_m	mean normal stress (MPa)
σ_Y	Yield Strength in uniaxial tension (MPa)
$\dot{\lambda}$	Flow rule nonnegative factor of proportionality
λ	Lagrangian multiplier
ε	True strain
ε_0	Initial strain
ε_{ij}	Components of the strain tensor
ε	Emissivity
$\bar{\varepsilon}$	Effective/equivalent strain
$\bar{\varepsilon}^p$	Effective/equivalent plastic strain
ε_m	Mean normal strain
$\dot{\varepsilon}_{ij}$	Components of the strain rate tensor (s^{-1})
$\dot{\varepsilon}_v$	Volumetric strain rate (s^{-1})
$\dot{\bar{\varepsilon}}$	Effective/equivalent strain rate (s^{-1})
$\dot{\bar{\varepsilon}}^p$	Effective/equivalent plastic strain rate (s^{-1})
$\dot{\bar{\varepsilon}}_{ij}^p$	Components of equivalent plastic strain rate tensor (s^{-1})
$\dot{\varepsilon}_{ij}^{\ p}$	Plastic strain-rate (s^{-1})
$\dot{\varepsilon}_{ij}^{\ e}$	Elastic strain-rate (s^{-1})
$d\varepsilon_{ij}$	Infinitesimal strain
θ	Neutral point angle (rad)
θ_x	Angle between the tangent to the roll surface and the horizontal axis (rad)
μ	Coefficient of friction
ν	Poisson's ratio
τ	Shear stress (MPa)
τ_x, τ_y	Boundary friction tractions
τ_Y	Shear yield stress (MPa)
τ_{oct}	Octahedral shear stress (MPa)
ρ	Density (kg/m^3)
π	Functional
$\delta\pi$	Variation of functional π
η	Heat generation efficiency (fraction of the plastic strain energy that is converted to heat)
ξ	Fraction of friction energy that is converted to heat
ψ_0	Complementary strain energy density
ψ	Complementary strain energy
δ	Oil film thickness (m)
ω	Rolls angular velocity (rev/min)
υ	Energy per unit length of dislocation (J/m)

List of Figures

Figure 1.1: Flat rolling: (a) general, (b) cross section for slab rolling, (c) cross section for sheet rolling [71] 2
Figure 1.2: Schematic of a five-stand rolling mill [71] © Cambridge University Press 3
Figure 1.3: Schematic of various flat-and-shape rolling processes [41] 3
Figure 1.4: (a) Schematic Illustration of the flat-rolling process, (b) Friction forces acting on strip surfaces, (c) Roll force *F* and torque acting on the rolls [41] 4
Figure 1.5: Leonardo's Rolling Mill Designs [62] 5
Figure 1.6: John Hanbury's Mill for rolling iron sheets for the manufacture of tinplate. Source: Cold Rolling of Steel [62] 6
Figure 1.7: Rolls designed by John Payne in 1728 to produce round bars [62]…..... 6
Figure 1.8: English patent issued to John Purnell in 1766 for grooved mills driven in unison by coupling boxes and pinions [62] 7
Figure 1.9: English patent specifications filed by W. Playfield in 1783 [62]…..... 7
Figure 1.10: Typical sheet mills of the 1860's [62]..... 8
Figure 1.11: 48-inch, high-speed, five-stand tandem cold-reduction mill [62] …..... 9
Figure 1.13: Rough pass in a hot rolling mill 10
Figure 1.14: CNC manufactured rolls 10
Figure 1.15: Thesis Organization Diagram..... 16
Figure 2.1: Schematic Diagram of the Flat Rolling Process [56] 19
Figure 2.2: Mechanical boundary conditions in the deformation zone 24
Figure 2.3: Schematic of the thermal events and boundary conditions in the roll gap [56] 27
Figure 2.4: Thermal boundary conditions in the deformation zone..... 31
Figure 2.5: Schematic Representation of the deformation zone in flat rolling [32] 34

Figure 2.6: Types of frictional force and their distribution along the arc of contact according to the different theories of rolling [32] 36
Figure 2.7: Distribution of Normal Pressure and frictional force along the arc of contact according to the classical rolling theories [32] 37
Figure 2.8: Normal Gap between potentially contacting bodies [53] 38
Figure 2.9: Contact coordinate system [53] 39
Figure 2.10: Deformable to Rigid Body Contact Procedure [54] 39
Figure 2.11: Bias factor [53] 40
Figure 2.12: Bias factor comparison [53] 40
Figure 2.13: Deformable contact; Piecewise Linear Geometry Description [53]…….41
Figure 2.14:Contact constraint requirements [53] 41
Figure 2.15: Stick –Slip Friction model and parameters [54] 42
Figure 2.16: Coulomb Friction Model [54] 43
Figure 2.17: Force based Coulomb model approximation ($f_n = 1$, C=$|v_r|$) [54] 44
Figure 2.18: Shear Friction Mode [54] 45
Figure 2.19: Temperature Dependent Stress-Strain Diagrams (T_3>T_2>T_1) [53] 49
Figure 2.20: Shida Flow Stress Surfaces 51
Figure 3.1: Quadrilateral element and natural coordinate system 62
Figure 3.2: Newton-Raphson method for stiffness updates [53] 66
Figure 3.3: Modified Newton-Raphson method [53] 67
Figure 3.4: Schematic Illustration of the strip elastic recovery [32] 74
Figure 3.5: Coupled Thermo-Mechanical Analysis [54] 76
Figure 3.6: Normal gap between potentially contacting bodies [54] 82
Figure 3.7: Non-linear conductivity in hot rolling 85
Figure 3.8: Non-linear density in hot rolling 85
Figure 3.9: Non-linear Specific Heat in Hot Rolling 86
Figure 4.1: Plane strain model of the flat rolling process [49] 91
Figure 4.2: 2-D model geometry 92
Figure 4.3: Strain Hardening curve for 0.1 % Carbon Steel where K_f is the yield stress 93
Figure 4.4: True stress – true plastic strain curve for 0.1% Carbon Steel 94

Figure 4.5: Krupkowski's True stress – true plastic strain curve for 0.1% Carbon Steel input in MARC 94
Figure 4.6: Strain hardening curves for steel according to Krupkowski: 1- 0.1% Carbon steel; 2- 0.33% Carbon Steel; 3- 0.42% Carbon Steel; 4- N Steel 0.9%C; 5 – T55 Steel 0.55%C; 6 – 18-8 Steel [72] 95
Figure 4.7: Boundary Conditions on the deformable – rigid case 96
Figure 4.8: Contact definition 97
Figure 4.9: mesh detail and plane strain geometry 98
Figure 4.10: Equivalent Von Mises Stress 98
Figure 4.11: Temperature distribution 99
Figure 4.12: Velocity distribution according to FEM and to the classical theory of rolling [72] 99
Figure 4.13: Displacement distribution 101
Figure 4.14: Plasticine bar rolled between wooden rolls [72] 101
Figure 4.15: Displacement in y direction 102
Figure 4.16: Detail of the contact Friction force 102
Figure 4.17: The rolled strip comes out perfectly flat 103
Figure 4.18: Equivalent Plastic Strain Rate $\dot{\bar{\varepsilon}}^p$ 103
Figure 4.19: Equivalent Plastic Strain $\bar{\varepsilon}^p$ 104
Figure 4.20: Equivalent Total Strain $\bar{\varepsilon}$ 104
Figure 4.21: Detail of the model with the two types of elements 105
Figure 4.22: Detail of the slight increase in temperature on the outer edge of the rolls 106
Figure 4.23: contact friction force 106
Fig 4.24: contact normal force 107
Figure 4.25 a: Stress distribution in rolls and slab 108
Figure 4.25 b: Distribution of normal pressure and roll separating force in rolling [32] 109
Fig 4.26: Temperature distribution 110
Figure 4.27: Velocity Distribution and the Neutral plane 110
Figure 4.28: FE model for hertz contact stress between a disc and a flat surface 111
Figure 4.29: Hertzian Stresses in a symmetric model 112

Figure 4.30: The Hertz Contact Problem 113
Figure 4.31: Initial shape and mesh of square block model 114
Figure 4.32: Plane Strain Upsetting of a Square Block: Equivalent von Mises stress after a 10% reduction 115
Figure 4.33: Plane Strain Upsetting of a Square Block: Equivalent von Mises stress after a 20% reduction 115
Figure 4.34: Plane Strain Upsetting of a Square Block: Equivalent von Mises stress after a 25% reduction 116
Figure 4.35: Displacement in the x direction 116
Figure 4.36: Displacement y-direction 117
Figure 4.37: Temperature increase 117
Figure 4.38: Deformation of square block with no friction 118
Figure 4.39: Shida flow curves (front view). Temperature axis is perpendicular to the plane of the paper 122
Figure 4.40: perspective view of the Shida flow curves for a strain rate = 2 s^{-1} 123
Figure 4.41: Boundary conditions 124
Figure 4.42: Equivalent von Mises Stress 125
Figure 4.43: Equivalent plastic strain rate distribution 125
Figure 4.44: Detail of how the material flows in the y direction 126
Figure 4.45: Displacement distribution 126
Figure 4.46: Velocity distribution. Notice the neutral plane 127
Figure 4.47: Temperature distribution 128
Figure 4.48: Total equivalent plastic strain. The largest strains appear near the surface 128
Figure 4.49: workpiece comes out perfectly flat 129
Figure 4.50: Detail of the contact friction 129
Figure 4.51: Equivalent Plastic Strain $\bar{\varepsilon}^{p}$ 130
Figure 4.52: The mechanism of bite in rolling: workpiece as it enters the roll gap 131
Figure 4.53: Forces acting in the roll bite during initial entry of the workpiece [32] ... 132
Figure 4.54: The entry coefficient of friction μ is larger than the tangent of the roll bite angle α and the rolls bite the workpiece. 133

Figure 5.1: Homogeneous vs. Redundant Deformation [63] 146

List of Tables

Table 4.1: Results for 2-D Plane Strain Cold Rolling FE models……..119

Table 4.2: Results for 2-D Plane Strain Hot Rolling FE models……134

Table 5.1: Summary of Results for 2-D Plane Strain Cold and Hot Rolling …….142

Chapter 1
Introduction

1.1 Basic Definition and History of Rolling

According to Wagoner & Chenot, "the rolling process can be defined as a continuous process of plastic deformation for long parts of constant cross section, in which a reduction of the cross sectional area is achieved by compression between two rotating rolls (or more)" [71]. In *cold rolling* the material is deformed at room temperature (but it can be slightly higher with heat dissipation due to plastic work) and in *hot rolling* the temperature is high (more than half of the absolute melting temperature).

Another important distinction is made according to geometric considerations. *Flat rolling* is performed with cylinders: this is also the case for *sheet rolling* or *strip rolling* (in which the thickness is very small, of the order of millimeters or less), or *slab rolling* (in which the slab thickness is of the order of 0.1 m) and any intermediate situation. *Shape rolling* allows the production of more complex workpieces by using appropriate roll geometries: the cross section of the part can be a round, an oval, various beams, a rail, and so on. Figure 1.1 represents the general principle for flat rolling and two examples of geometries in a vertical cross section by a plane parallel to the rolling direction.

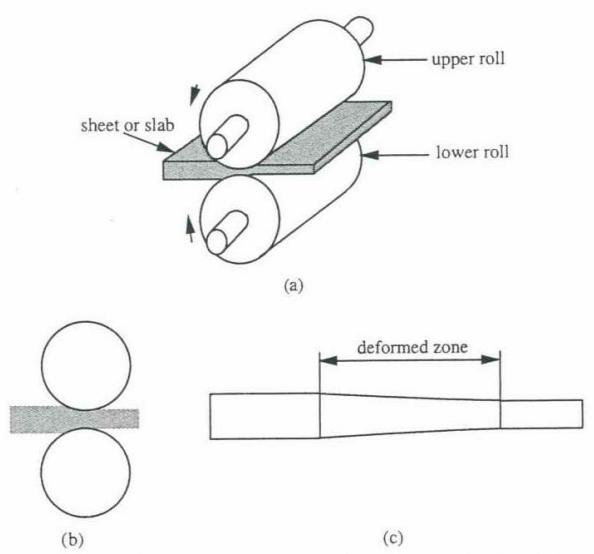

Figure 1.1: Flat rolling: (a) general, (b) cross section for slab rolling, (c) cross section for sheet rolling [71] © Cambridge University Press

For hot or cold rolling of any geometry, the desired reduction of cross-sectional area is too large to be feasible in one pass. The final deformation is progressively applied by using several stands so that several pairs of cylinders successively deform the same part as shown in Figure 1.2. There are thus interacting forces between two successive stands, which induce tension (in plane loads) either in the direction of rolling or in the opposite direction. In Figure 1.2, the smaller rolls are in contact with the sheet and produce

successive reductions of thickness. The small diameters limit the width of the deforming region and thus the roll-separating force. The larger diameter rolls are designed to prevent excessive bending of the work roll [71].

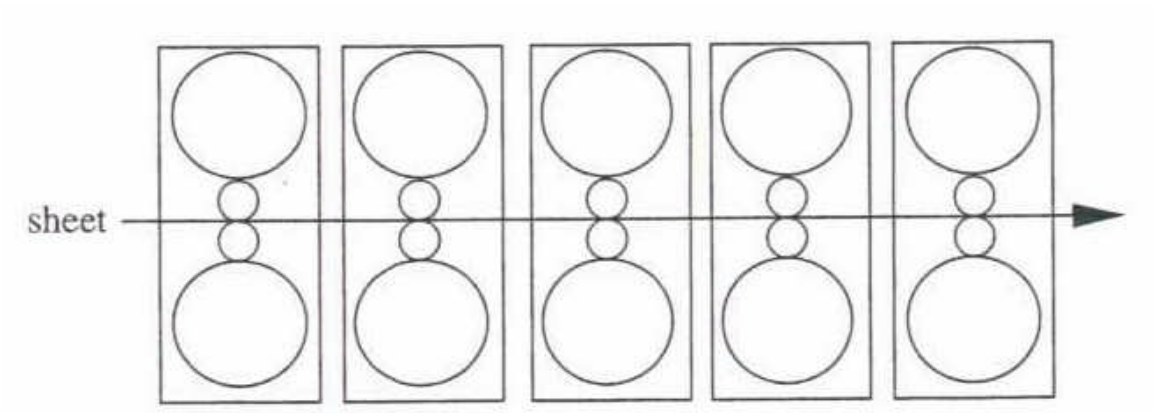

Figure 1.2: Schematic of a five-stand rolling mill [71] © Cambridge University Press

Traditionally, the initial material form for rolling is an ingot. Figure 1.3 gives a summary of the main rolling processes.

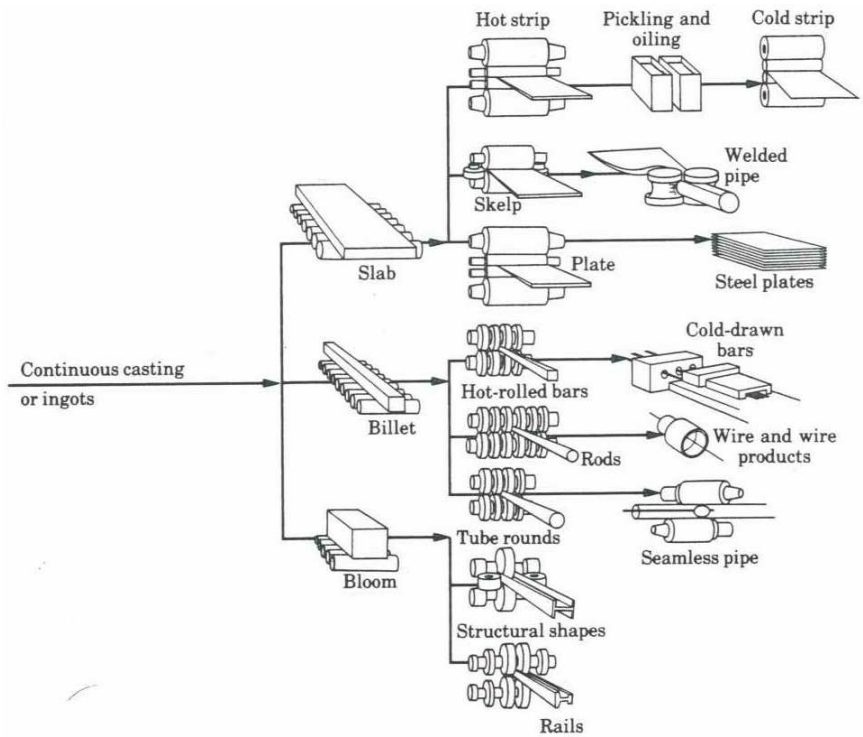

Figure 1.3: Schematic of various flat-and-shape rolling processes [41] © American Iron & Steel Institute (AISI)

A schematic illustration of the flat rolling process is shown in Figure 1.4. A strip thickness h_o enters the roll gap and is reduced to h_f by a pair of rotating rolls, each roll being powered through its own shaft by electric motors. The surface speed of the roll is V_r. The velocity of the strip increases from its initial value V_o as it moves through the roll gap, just as fluid flows faster as it moves through a converging channel. The velocity of the strip is highest at the exit of the roll gap and is denoted as V_f.

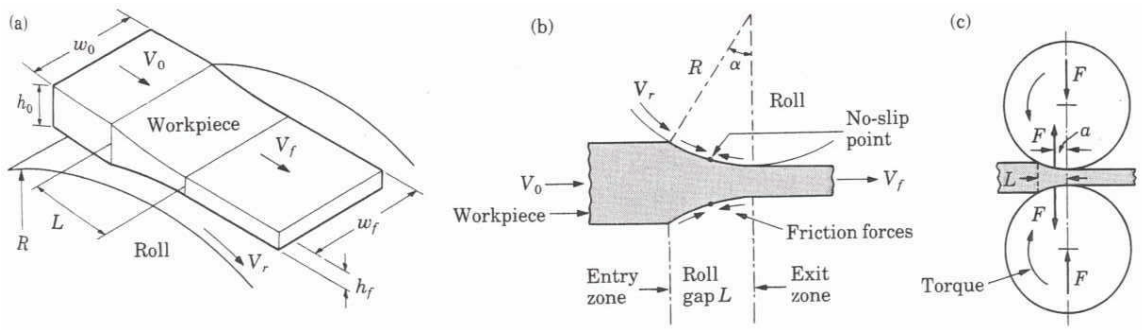

Figure 1.4: (a) Schematic Illustration of the flat-rolling process, (b) Friction forces acting on strip surfaces, (c) Roll force F and torque acting on the rolls [41] © Adisson-Wesley / Pearson Education

Since the surface speed of the roll is constant, there is relative sliding between the roll and the strip along the arc of contact in the roll gap, L. At one point along the contact length, the velocity of the strip is the same as that of the roll. This is called the neutral, or no slip, point. To the left of this point, the roll moves faster than the strip, and to the right of this point, the strip moves faster than the roll. Hence, the frictional forces, which oppose motion, act on the strip as shown in Figure 1.4b [41].

It has long been thought that rolling, which accounts for about 90% of all metals produced by metalworking processes, was first developed in the late 1500's. However, it was none other than the great *Leonardo da Vinci*, who, in the section of his notebooks dedicated to the study of mechanisms and machines, first described an exact and fully functional design of a rolling mill dedicated to the flat rolling process (Figure 1.5).

As reported by Cianchi, "Leonardo da Vinci describes in his notebooks that these two machines were intended for producing sheets of tin by making the metal pass between the principal rollers" [16]. In the sketch on the top there is however, an important addition: two smaller rollers, which keep up the pressure on the principal ones so that the sheet produced is homogeneously smooth. This method is still employed today as seen in Figure 1.2.

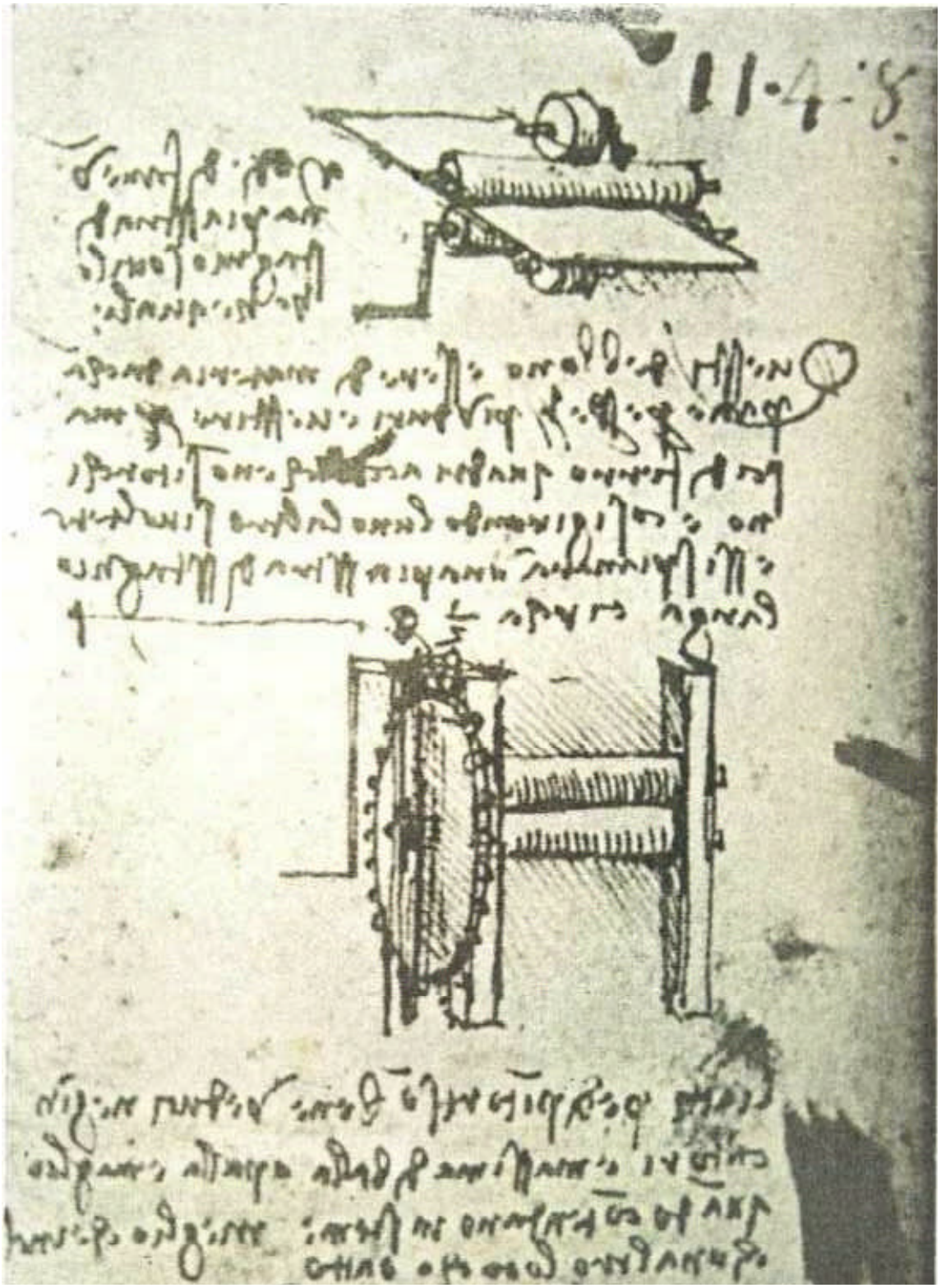

Figure 1.5: Leonardo's Rolling Mill Designs [62] © Marcel Dekker / Taylor & Francis Group

In the 1500's and 1600's very primitive mills were used to roll sheets of gold, silver, tin, and even for making coins. The use of rolls in an iron works was a German development of the 16th century. Belgium and England both started to use rolls about the same time, and so these three countries are considered as the birthplace of rolling.
By 1682 Great Britain had become the leading nation in the rolling industry and the first records of hot rolling appear, with large rolling mills for the hot rolling of ferrous materials near Newcastle, England. From that point and during the early part of the eighteenth century, rolling mills expanded to the continent.

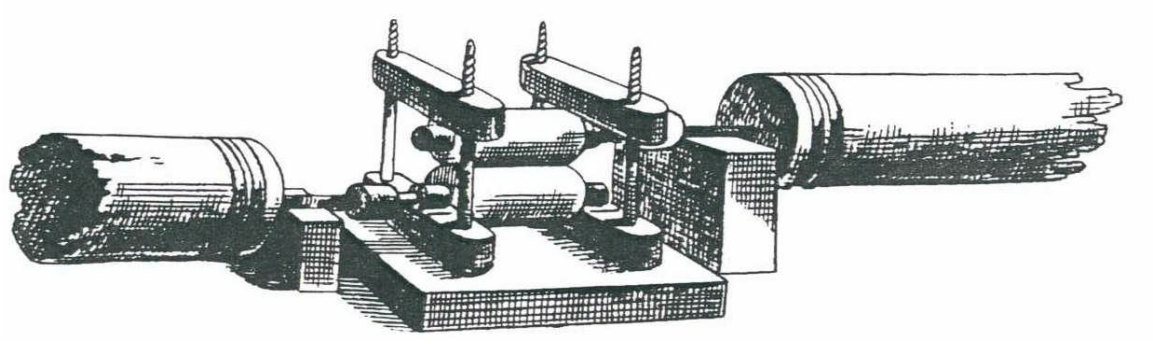

Figure 1.6: John Hanbury's Mill for rolling iron sheets for the manufacture of tinplate.
Source: Cold Rolling of Steel [62] © Marcel Dekker / Taylor & Francis Group

During the early part of the 18th century, Christopher Polhem from Sweden, designed the first mill with 4 rolls, with the backup rolls driven, in a very similar manner to how the modern Lauth mill works. In 1728 a patent for a mill to roll hammered bars was issued to John Payne in England.

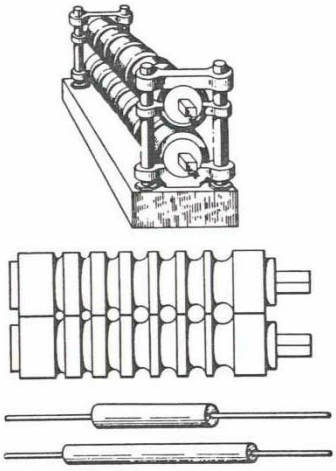

Figure 1.7: Rolls designed by John Payne in 1728 to produce round bars [62]
© Marcel Dekker / Taylor & Francis Group

Also, in 1766, another Englishman, John Purnell received a patent for grooved rolls with coupling boxes and nut pinions for turning the rolls in unison.

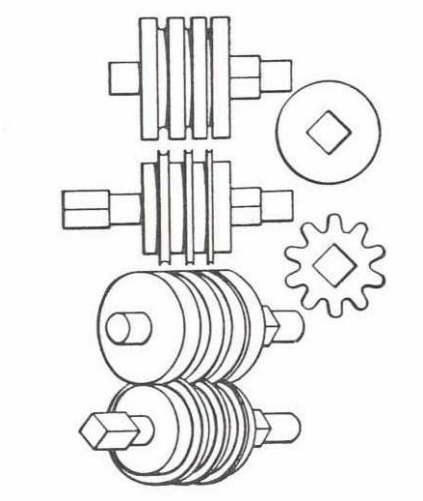

Figure 1.8: English patent issued to John Purnell in 1766 for grooved mills driven in unison by coupling boxes and pinions [62] © Marcel Dekker / Taylor & Francis Group

It is in this same period, that the general appearance of these hot mills began to change to the modern form. For example, the cast housing and the single screw on each side of the mill became a standard, as we can see in a design by William Playfield in 1782.

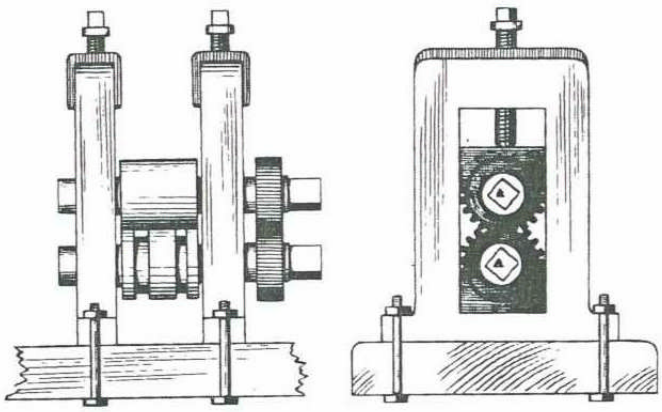

Figure 1.9: English patent specifications filed by W. Playfield in 1783 [62]
© Marcel Dekker / Taylor & Francis Group

Roberts describes how “the eighteenth century also saw the advent of the tandem mill in which the metal is rolled in successive stands. Richard Ford patented the first true tandem mill of which there is record in England in 1766, for the hot rolling of wire rods. A later patent issued in 1798, refers to a tandem mill for the rolling of hot plates and sheets and in the same year, John Hazeldine added mechanical guides to a rod mill” [62].

In the beginning of the 19th century, the industrial revolution in England was gathering momentum, creating an unprecedented demand for iron and steel. Accordingly, rolling mill developments were numerous and important. John Bikenshaw started the first rail rolling mill in 1820 producing wrought iron rails in lengths of 15 to 18 feet. In 1831 the first T rail was rolled in England and the first I beams were rolled by Zores in Paris in 1849 [62].

Three high mills were also introduced about the middle of the century. A British patent for such a mill, designed for rolling heavy sections, was granted in 1853 to R. Roden. In this mill, the middle roll was driven and fixed in the housing while the upper and lower rolls were adjustable in position. On the same mill, a steam-operated lifting table raised and lowered the material to be rolled.

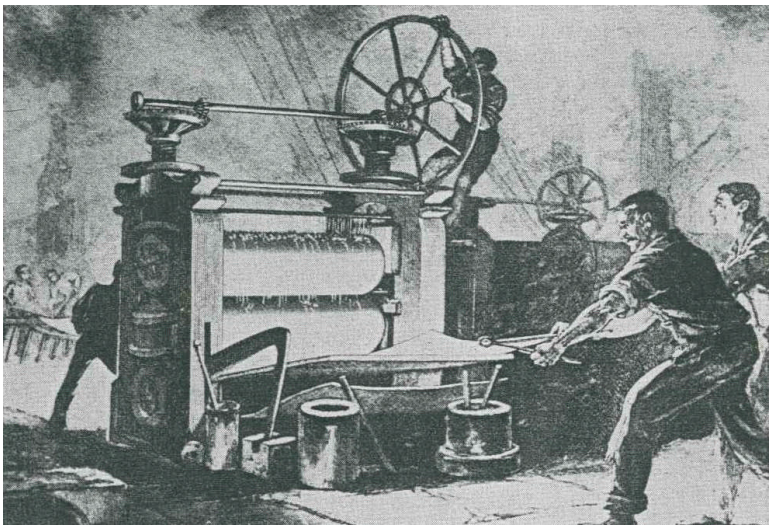

Figure 1.10: Typical sheet mills of the 1860’s [62]

© Marcel Dekker / Taylor & Francis Group

In mid century, the first reversing plate mill was put into operation at the Parkgate Works in England, and in 1854 it was used to roll the plates for the “Great Eastern” steamship. In 1848, R.M. Daelen of Lendersdorf, Germany, who also built the first mill of this type about seven years later, invented the universal mill. The first mill constructed on the continuous principle of rolling iron or steel was patented to Charles White of Wales [62].

Roberts also writes: “a British patent issued in 1862 to J.T. Newton of Wales, described a predecessor to the modern cluster mill, in as much as it used small work rolls backed up by others of large diameter. The work rolls were driven but the pressure was applied by the large backup rolls, a principle utilized in both the hot and cold mills of today” [62].
The four-high mill with its rolls in the same vertical plane was introduced in 1872 by Bleckley of England; Tandem rolling of hot steel took an upsurge around 1890, and in 1892, a semi-continuous hot strip mill, with a mechanically geared two-high tandem finishing train, was built at Bohemia. As reported by Roberts, “the first record of tandem cold rolling of steel strip goes back to about 1904, when the West Leechburg Steel Company installed and operated a 2-high 4-stand tandem mill, each stand being driven by a separate, adjustable speed dc motor. Reel tandem mill operation, with tension between stands, and a tension reel was developed around 1915, on mills in Pittsburgh, Pennsylvania” [62].

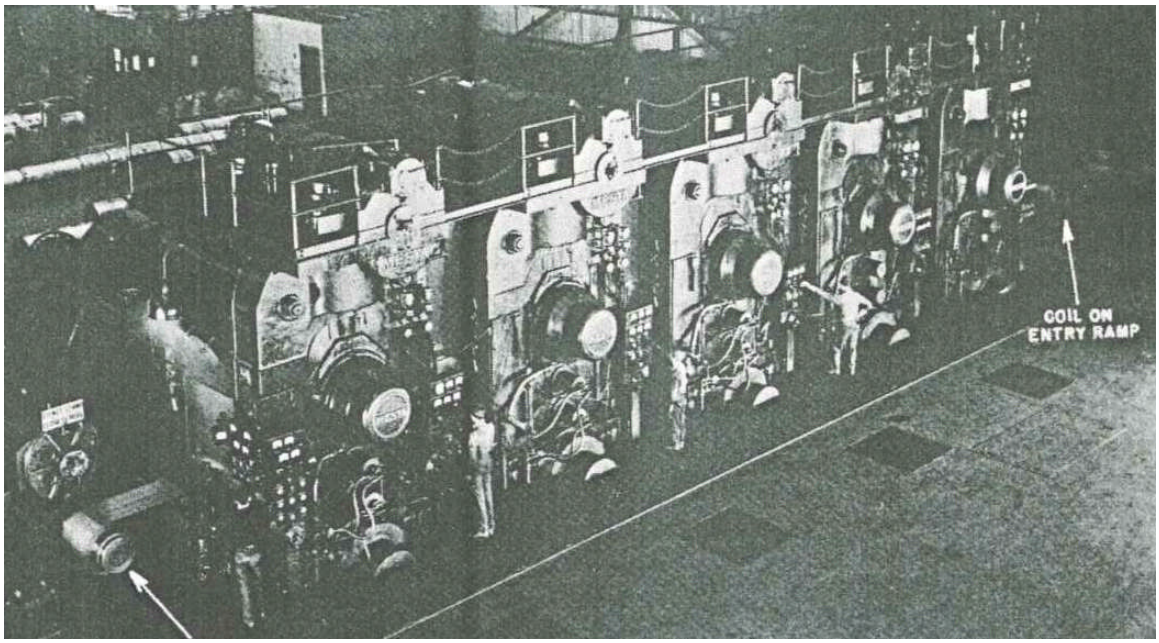

Figure 1.11: 48-inch, high-speed, five-stand tandem cold-reduction mill [62]
© Marcel Dekker / Taylor & Francis Group

Figure 1.11 shows an example of five stand tandem mills, which came into use in the 1930’s for the production of tin plate. Six stand mills were introduced in the 1960’s with still more installed horsepower and slightly larger work rolls. In the 1970’s and 1980’s new and larger fully continuous mills were put into operation.

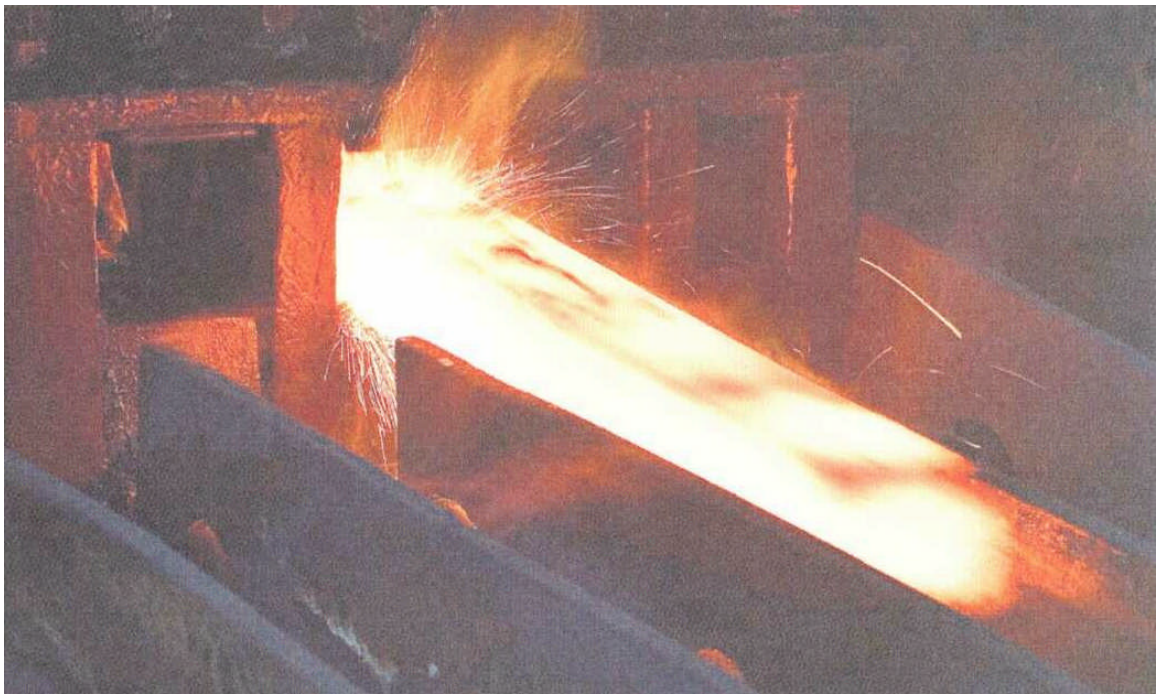

Figure 1.13: Rough pass in a hot rolling mill © INDUSLA S.A. (www.indusla.com)

Finally, in the late 80's and in the beginning of the 1990's , the rolling industry began to take advantage of the development of the CNC & CAD/CAM technology, particularly applied to the design and manufacture of rolls for hot-rolled steel special section profiles (Figure 1.14).

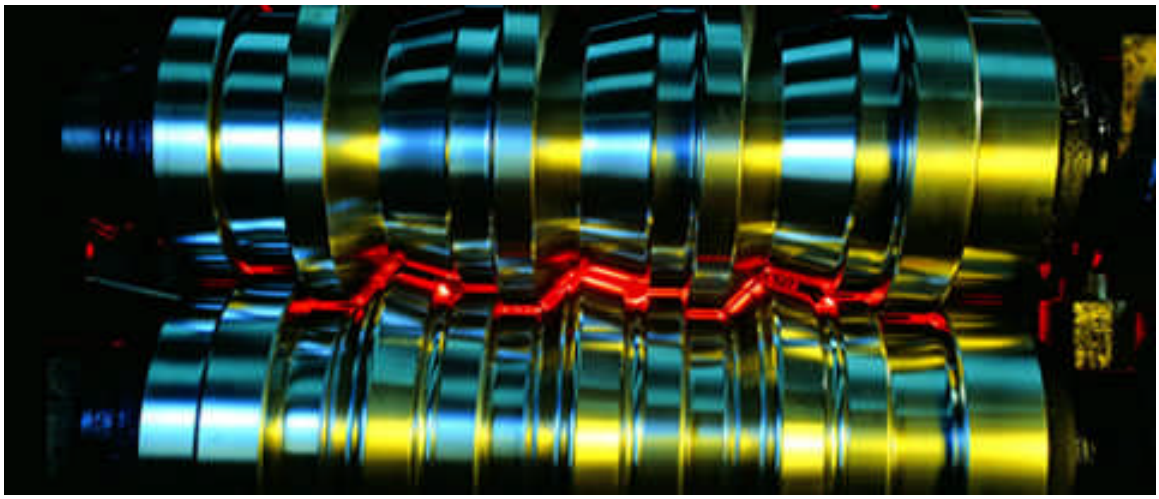

Figure 1.14: CNC manufactured rolls © INDUSLA S.A. (www.indusla.com)

1.2 The Finite Element Method (FEM), Virtual Manufacturing, and its potential impact in the hot rolling industry

The major development in the metalforming industry in the end of the 20th and the beginning of the 21st centuries has been the application of Finite Element Method (FEM) to the solution of complicated non-linear metal deformation processes.
The Finite Element Method is a numerical analysis procedure used to obtain approximate solutions to boundary value problems, which are found in every field of engineering. Most problems encountered in everyday practical applications do not have closed-form solution. The problems with closed form solutions that can be found in any textbook on strength of materials, fluid dynamics, and other fields of mechanics, correspond to usually rather basic models of reality, where a lot of simplifying assumptions have been made in order to be able to solve the governing differential equations and their associated initial and boundary conditions, that are generated when formulating the initial boundary value problem. It is then from this inability to solve many complex structural mechanics, heat transfer analysis, and fluid mechanics problems, that the Finite Element Method became an indispensable tool in the field of engineering mechanics [14, 64].

The FEM was initially applied to the structural analysis area and its associated theory of elasticity. As the structural applications of FEM were refined, the FEM expanded to the thermal & fluids areas. During the 1970s and early 1980s many papers applied the finite element method to the Navier-Stokes equations for fluids, and to the solution of the heat diffusion equation. Once these areas had been developed, researchers began to focus their attention into more complicated problems in continuum mechanics such as those that can be found in materials that do not meet the definition of elastic solid or Newtonian fluid, i.e. viscous (non-Newtonian) fluids and plastic/viscoplastic materials, whose behavior is described by the theories of plasticity, and viscoplasticity, which are used to explain the permanent deformations that occur in the metal forming processes [14,35]. These developments together with the advances in computer technology of the 1990's, when the speed of computers increased at almost the same rate as their price was decreasing, allowed the application of the Finite Element Method to non-linear problems, such as those found in metal deformation, and led to the appearance of a new field, known as virtual manufacturing.

Virtual manufacturing uses a computer to simulate the processes involved in the fabrication of a product. One approach to virtual manufacturing utilizes nonlinear finite element technologies to provide detailed analysis information about a product, which is then used for optimization of key factors affecting its profitability, such as manufacturability, final shape, residual stress, product durability and life-cycle estimations, etc. Simulation technology can also directly affect profitability by reducing the cost of production, material usage, and warranty liabilities [54].

This new field saw immediate application in the metal forming industry that realized the potential of the Finite Element Method and virtual manufacturing as a tool to optimize

their product and manufacturing process. On top of the advantages already mentioned, virtual manufacturing applied to the rolling industry also reduces the cost of tooling, eliminates the need for multiple physical prototypes, and reduces material waste. This increases the chances of getting it right the first time, thus providing the rolling manufacturers with the confidence of knowing that they can deliver quality products to the market on time and within budget. Small improvements in manufacturing have dramatic and profound effects in terms of cost and quality.

Nonlinear finite element analysis in particular, facilitates the simulation of metal forming processes in a more realistic manner than ever before, especially in the hot rolling industry where only a few people have a clear understanding of the behavior of steel at high temperatures, and where most companies need to use a trial and error approach before they obtain the desired results.
To summarize the potential benefits to the hot rolling industry:

a) Fewer trials in the design of the rolls => more time can be spent on engineering, and design,
b) Less material waste,
c) Reduced cost of tooling,
d) Confidence in the manufacturing process,
e) Improved quality,
f) Reduced time to market,
g) Lower overall manufacturing cost;

It is for the above reasons that an improvement in the rolling manufacturing process, no matter how small, can have great economic and financial implications for a company and thus the great relevance of the topic subject of this thesis.

1.3 Objectives and Scope of this work

The goal of this work is to develop a fully nonlinear finite element analysis model that can be used as a tool in order to analyze the rolling of cold and hot steel strips under a series of different parameters and scenarios. The purpose is to provide the roll designer with a tool that he can use in order to understand the behavior of the steel as it flows through the different kinds of passes in the rolls. Currently, this is a very difficult industry problem that requires skilled engineers with many years of experience. In today's practice, the correct roll design is achieved through a trial and error approach that results in very high costs and expenses to the rolling company. Many of the mechanisms that govern the hot rolling process are still not fully understood, and there exists a need to provide engineers with comprehensive tools that allow them to design the rolls right the first time, thus reducing the number of trials in the design of the rolls, the amount of material waste, the cost of tooling, and therefore increasing the time that roll designers can spend on engineering as well as the confidence in the manufacturing process and the quality of the final product. All of the above also lead to a reduced time to market, and a lower overall manufacturing cost. The main problem that is found in the industry is regarding the design of rolls for roll pass design of non-symmetric structural shapes.

This problem is of enormous difficulty due to the fact that it is yet not understood how the material at 1,200 ºC behaves when there is no symmetry with respect to the neutral axis of rolling. For flat products, both rolls are perfectly cylindrical, and the workpiece goes right through the middle of the roll gap. However, for structural shapes of complex geometry, the top roll is different from the bottom roll, and the roll designer must estimate based on his judgment and experience how much each roll will work the slab, ensuring that the amount of deformation fills the roll gap completely yet trying to minimize the number of passes that are needed in order to achieve the final desired cross section. The main problem seems to be that currently there is no material model that accurately predicts the behavior of the steel at high temperatures. Also, certain mechanisms like friction in the roll gap, and the modeling of the contact problem are not fully understood. The heat generation due to friction and work of plastic deformation are also areas of current research. The ultimate goal is to be able to model the roll passes using non linear FEM in order to allow the roll designer to do virtual tests on the computer, that will always be a lot cheaper than having to manufacture the rolls, to then test them, which requires a lot of tooling, labor, and associated costs. To get to this point however, we must make sure we have a great handle of the problem of which we know the solution of, which is the flat rolling problem, which is the simplest one, and has been extensively researched with many formulae available for the main parameters of it. Therefore, in this first phase, the basic principles of hot and cold rolling of flat products will be studied and modeled using non-linear FEM. Flat products are a good starting point since they all have a simple rectangular geometry, and there is symmetry with respect to the neutral plane of the section, which facilitates the analysis. This work will look at the cold and hot rolling problem from the following aspects: materials science, mathematical models of rolling, theory of plasticity, machine and mechanical design aspects, heat transfer issues, etc, then focusing on the Finite Element Analysis issues concerning this problem, such as coupled thermo-mechanical analysis, thermo-mechanical finite element modeling, and all the non-linear aspects of the rolling problem.

Furthermore, in this thesis I will try to demonstrate that:

a) the steel in cold rolling can be accurately modeled using the elastic-plastic material model,
b) the steel in hot rolling (at temperatures between 800 and 1200 C) can be modeled using the rigid-plastic material model with the flow stress as a function of the strain, strain rate, and the temperature,
c) in cold rolling, plane sections do not remain plane (as the classic theory assumes in the derivations of formulas for stress) and due to this, all the empirical formulas used in the classical theory of rolling can only be used as an estimate,
d) the degree of deformation, stresses and strains, strain rates, as well as other parameters of interest, on the workpiece and in the rolls can be predicted,
e) the heat transfer from the workpiece to the rolls, as well as the plastic heat generation, and the friction heat can be accurately modeled,
f) the stresses developed in the rolls are very similar to the stresses developed in the Hertzian contact problem,

g) the complicated and not well understood friction process between the roll and the workpiece can be accounted for in the FE models,
h) the Finite Element Method can be used to predict material flow.

This thesis will also examine:

a) The mechanism of bite in rolling,
b) the main heat transfer aspects present in the rolling problem,
c) the non-linear finite element approach to solving the problem,
d) the main issues from the theory of plasticity point of view, analyzing and finding the adequate yield surface and work hardening rule for both the cold and hot rolling problem, as well as studying the main constitutive equations that have been proposed for low carbon steel at low and high temperatures, and selecting the appropriate ones for the FEM models used in this thesis.

In order to examine the above, the following non-linear FEM models will be developed:

a) 2-D plane strain model for flat cold rolling,
b) 2-D plane strain model for flat hot rolling,

The models will be validated using a stepping-stone approach by which simplified versions of the problem will be first analyzed to demonstrate the results obtained. New parameters and physical phenomena will be progressively added to the initial basic models. In each case the updated models will be analyzed and verified until arriving at the full model of flat rolling for both hot and cold rolling. The validation of the models uses classical stress analysis techniques and methodology, or proofs in the existing literature via the classical theory of rolling or published data and/or photos of actual rolling tests.

In summary, for this project, the author proposes a computational method that can enhance analytical modeling of the flat cold and hot rolling processes by consideration of all the physical phenomena mentioned above. These models will allow us to fully understand all the issues involved with non linear FEM modeling applied to flat rolling, namely, the modeling of the material, the types of plastic models used, hardening rules, yield surfaces, the types of FEM elements needed to model the problem in 2-D plane strain case, the setup of the contact parameters within the software in order to achieve convergence (the contact problem is extremely complicated), etc. If we are successful, we will then be in a good situation to try to move into the more complicated problem of shape rolling, which is the one that the industry is really interested in.

1.4 Organization of Thesis

This thesis is divided into three parts. The first part deals with the Mathematical aspects of the rolling problem as well as the plasticity concepts needed to develop the models. In this section, the equations of equilibrium roll-work piece are developed, the governing equations for both the mechanical and thermal problems are shown, together with their appropriate boundary conditions. At this point it is shown that mathematically, the rolling problem consists of a pair of very large and complicated Initial Boundary Value Problems, one mechanical, and one thermal. These two IBVPs need to be solved simultaneously due to the strong coupling between the thermal and the mechanical parts of the problem, thus the designation of coupled thermal-mechanical problem.

Once the engineering mechanics of the rolling problem have been explained, the second part of this thesis will explain how the mathematics, physics and mechanics of the problem are implemented into the finite element method. The Rigid-Plastic Flow, the Elastic-Plastic Flow finite element methods and the Rigid-Viscoplastic material models will then be analyzed in detail. Finally, the different types of non-linearities present in the rolling problem, material, geometric, boundary, and heat transfer, are explained.

The third part of the thesis deals with the creation of the different FEM models that are needed in order to meet the goals of this thesis. This section is further subdivided into two sets, one for the 2-D plane strain cold rolling models and the other for the 2-D plane strain hot rolling cases. All of the features of the models, i.e., initial conditions, boundary conditions, contact problems, material properties, etc are addressed. Also, results are presented showing the answers and conclusions to which we arrived after studying the solutions provided by the FE models. One by one, the different models will be used to demonstrate the goals listed in this Chapter in Section 1.2.

The fourth and final section deals with the discussion of the results obtained from the FE models, and conclusions obtained from this study, as well as the discussion of the future work that needs to be accomplished in order to advance in the research of this challenging and at the same time fascinating problem.

The following flow chart is meant to be a basic “roadmap” for this thesis

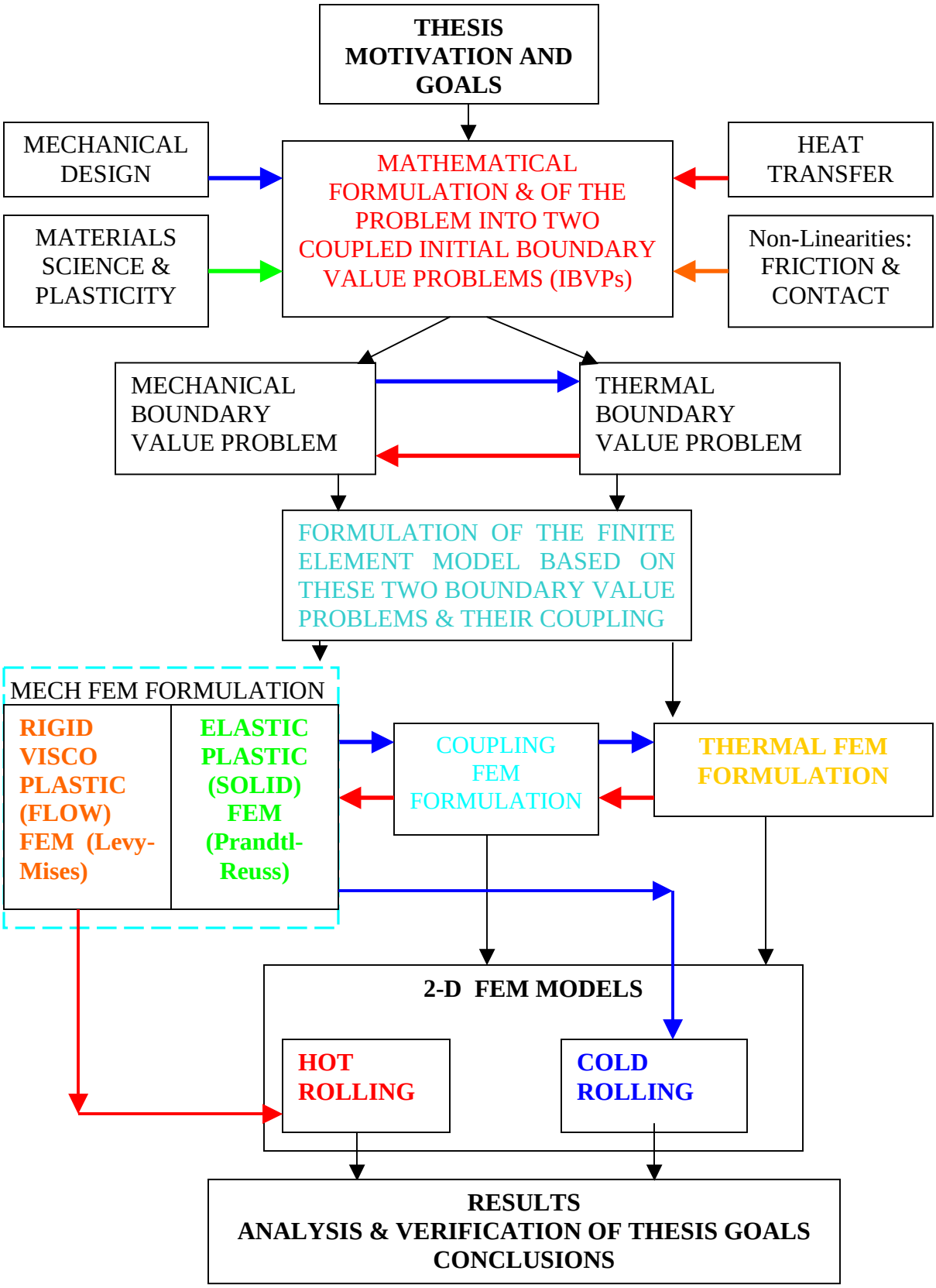

Figure 1.15: Thesis Organization Diagram

Chapter 2
Mathematical Models and Mechanics Aspects of the Rolling Problem

2.1 Introduction

Mathematical models of the flat rolling process are numerous. In each, the equations of motion, thermal balance, material properties and roll deformation are used to calculate the stress, strain, strain rate, velocity and temperature fields, the roll pressure distribution, roll separating forces and roll torques [56,49].
The accuracy of these models depends on the quality of the assumptions made. In the conventional models, most researchers assume the existence of homogeneous compression of the strip, considered to be made of an isotropic and homogeneous material that is incompressible in the plastic state. Further, plane strain conditions are assumed to exist and either a constant friction factor or Coulomb friction conditions apply at the roll-strip interface. Assumptions and simplifications vary broadly when finite element methods are employed. The same applies to the material models the main models used being the elastic plastic and rigid plastic ones [56].

A general mathematical model of the flat rolling process should include [56]:

a) Equations of motion of the deformed metal,
b) Heat balance of the roll/strip system,
c) Equations of equilibrium of the work roll,
d) Description of the frictional forces between the work roll and the metal,
e) Description of the material properties.

As the strip enters the roll gap it is first deformed elastically. It speeds up; the relative velocity between the roll and the strip is such that friction draws the metal in. The criterion of plastic flow governs the manner in which the transformation from elastic to plastic happens in what is known as the elastic-plastic interface. The strip proceeds through the roll gap and more plastic flow occurs until finally at the exit roll pressure is removed. The strip is unloaded and it returns, through an elastic state to the original, load free condition. It is observed that during rolling, the relative velocities of the roll and the strip change and as the strip is accelerating forward it reaches the roll surface velocity at the no-slip or neutral point. From then on, as further compression occurs, the strip speeds up and the direction of friction changes in such a way that it now retards motion. Exit velocity of the strip is often larger than that of the roll and the difference between the two velocities is determined by the forward slip [56,49].

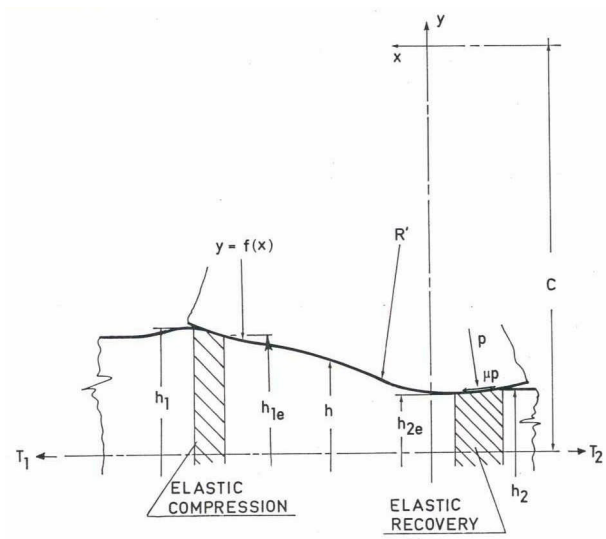

Figure 2.1: Schematic Diagram of the Flat Rolling Process [56] © Springer-Verlag

Thermal events occurring during the strip's passage through the roll gap are also of importance. In fact, it is the thermal events that contribute most to the metallurgical developments of the final structure of the rolled material. Surface conditions, roll wear and thus roll life are also affected by thermal conditions. Heat is generated because of the work done on the strip, increasing its temperature. Interfacial friction forces also cause the temperature to rise. Contact with the cold and often water-cooled rolls also causes heat losses. Metallurgical transformations also contribute to temperature changes. A complete mathematical model should account for both thermal and mechanical events, which occur in the deformation zone during the rolling process [56,49].

Several assumptions regarding material behavior must be made. The material is usually assumed to be, and to remain, isotropic and homogeneous; it is considered to be elastic-plastic even though as gross plastic straining takes place, elastic deformations may be quite small in comparison to plastic strains. During forming the volume of the plastic region is taken to remain constant, and finally, a plane state of strain is assumed to exit [56,49].

In this chapter we will study the governing equations and boundary conditions for the mechanical problem portion of the rolling problem. Then, we will study the heat transfer and thermal balance problem looking at the five sources of heat transfer as well as the heat transfer boundary conditions involved in both the cold and hot rolling problems.

Finally, we will take a look at the main classical mathematical rolling model, developed by von Karman. We will study the mathematical aspects of the complicated contact problem, paying attention to both the rigid-deformable, and the deformable-deformable cases. The friction problem and its influence in the rolling problem will then be

examined. Later in this chapter, we will take a look at the main theory of plasticity issues, and the material model used in this thesis for both the cold and hot rolling problems.

This chapter sets up the theoretical mathematical and engineering mechanics foundations upon which we can build on our FE models. By having a great understanding of the physics of the problem we can then model these physics into our finite element model. After all, the results the model will produce are only as good as the mechanics of the model created. As we will see in chapter 3, the physics of this problem will lead to a second order linear homogeneous partial differential equation for the thermal portion of the problem, that together with the boundary and initial conditions constitutes a thermal Initial Boundary Value Problem (T-IBVP) which we will solve using a variational approach that will be implemented into the finite element formulation. The mechanical portion of the problem leads to another set of PDEs given by the equilibrium conditions, the compatibility conditions, the constitutive equations, and the yield criterion, which together with the boundary conditions, lead to a Mechanical Initial Boundary Value Problem (M-IBVP) whose solution is obtained through a variational approach that requires that among the admissible velocities v_i that satisfy the conditions of compatibility and incompressibility, as well as the velocity boundary conditions, the actual solution gives the mechanical functional a stationary value .
The final solution to our problem will be determined by the simultaneous solutions of these two IBVPs due to the strong coupling between the mechanical and the thermal problems. There are two primary causes of coupling. First, coupling occurs when deformations result in a change in the associated heat transfer problem. Such a change can be due to either large deformation or contact. The second cause of coupling is heat generated due to inelastic deformation. The irreversibility of plastic flow causes an increase in the amount of entropy in the body, which in turns results in changes to the associated mechanical problem.

2.2 Governing Equations of the Mechanical Problem

The equation that governs the conditions of equilibrium of both the plastically deforming strip and the elastically loaded rolls is the following

$$\frac{\partial \sigma_{ij}}{\partial x_j} + \rho \cdot b_j = \rho \frac{\partial v_j}{\partial t} \tag{2.1a}$$

where

$\sigma_{ij} =$ components of the Cauchy stress tensor

$b_j =$ components of body forces vector

v_j = components of velocity vector

ρ = density of material

In the rectangular Cartesian coordinate system, if the body force is neglected, the equilibrium equations, are given by [9,35,51]

$$\begin{aligned} \frac{\partial \sigma_x}{\partial x} + \frac{\partial \tau_{yx}}{\partial y} + \frac{\partial \tau_{zx}}{\partial z} &= 0 \\ \frac{\partial \tau_{xy}}{\partial x} + \frac{\partial \sigma_y}{\partial y} + \frac{\partial \tau_{yz}}{\partial z} &= 0 \\ \frac{\partial \tau_{xz}}{\partial x} + \frac{\partial \tau_{yz}}{\partial y} + \frac{\partial \sigma_z}{\partial z} &= 0 \end{aligned} \tag{2.1b}$$

Plastic flow occurs according to the *von Mises yield criterion*, given by the alternative forms of Equation (2.2)

$$\bar{\sigma} = f(\sigma_{ij}) = \sqrt{\frac{1}{2}(\sigma_x - \sigma_y)^2 + (\sigma_y - \sigma_z)^2 + (\sigma_z - \sigma_x)^2 + 6(\tau_{xy}^2 + \tau_{yz}^2 + \tau_{zx}^2)} = \sigma_Y \tag{2.2a}$$

$$\bar{\sigma} = f(\sigma_{ij}) = \sqrt{(\sigma_1 - \sigma_2)^2 + (\sigma_2 - \sigma_3)^2 + (\sigma_3 - \sigma_1)^2} = \sigma_Y \tag{2.2b}$$

$$\bar{\sigma} = f(\sigma_{ij}) = \sqrt{J_2} = \sqrt{s_1^2 + s_2^2 + s_3^2} = \frac{1}{2} s_{ij} s_{ij} = \frac{\sigma_Y^2}{3} \tag{2.2c}$$

and it says "yield occurs when the equivalent stress (Mises stress) equals the yield stress in uniaxial tension σ_Y, i.e., $\bar{\sigma} = \sigma_Y$" [1,35,48,54,58]

The *Constitutive Equations* can be given by the *Levy-Mises flow rule* (used for the rigid-plastic flow formulation) [37,40]

$$\dot{\varepsilon}_{ij} = \dot{\lambda} \frac{\partial f(\sigma_{ij})}{\partial \sigma_{ij}} = \frac{3}{2} \frac{\dot{\bar{\varepsilon}}}{\bar{\sigma}} s_{ij} \tag{2.3a}$$

$$\dot{\lambda} = \frac{3}{2} \frac{\dot{\bar{\varepsilon}}}{\bar{\sigma}} \tag{2.3b}$$

$$\dot{\bar{\varepsilon}} = \sqrt{\frac{2}{3} \dot{\varepsilon}_{ij} \dot{\varepsilon}_{ij}} \tag{2.3c}$$

$$\bar{\sigma} = \sqrt{\frac{3}{2} s_{ij} s_{ij}} \tag{2.3d}$$

or by the *Prandtl-Reuss flow rule* (used for the elastic plastic solid formulation) [35,44,48]

$$\dot{\varepsilon}_{ij}^p = \dot{\lambda} \frac{\partial f(\sigma_{ij})}{\partial \sigma_{ij}} = \dot{\lambda} s_{ij} \tag{2.3e}$$

$$\dot{\lambda} = \frac{1}{\tau_Y}\sqrt{\frac{1}{2}\dot{\varepsilon}_{ij}\dot{\varepsilon}_{ij}} \tag{2.3f}$$

where

s_{ij} = components of the deviatoric stress tensor

$\dot{\varepsilon}_{ij}$ = components of the strain rate tensor

$\dot{\varepsilon}_{ij}^{p}$ = components of the plastic strain rate tensor

$\dot{\bar{\varepsilon}}$ = effective/equivalent strain rate

$\bar{\sigma}$ = effective/equivalent stress, flow stress

$\dot{\lambda}$ = flow rule nonnegative factor of proportionality

$f(\sigma_{ij})$ = Yield function / plastic potential

σ_Y = Yield strength in uniaxial tension

$\tau_Y = 0.577\sigma_Y$ = yield strength of the rolled material in pure shear

Finally we have the *compatibility conditions* given by the *strain rate* tensor [1,44]

$$\dot{\varepsilon}_{ij} = \frac{1}{2}\left(\frac{\partial v_i}{\partial x_j} + \frac{\partial v_j}{\partial x_i}\right) \tag{2.4}$$

The unknowns for the solution of a quasi-static plastic deformation process are six stress components and three velocity components. The governing equations are the three equilibrium equations, the yield condition, and five strain-rate ratios derived from the flow rule. The boundary conditions are prescribed in terms of velocity and traction. Along the roll-workpiece interface, the velocity component is prescribed in the direction normal to the interface and the traction is specified by the frictional stress in the tangential direction. One possibility is to assume that Coulomb friction is present and that the interfacial shear stress equals the roll pressure P multiplied by a constant coefficient of friction μ.

` $$\tau = \sigma_{fr} = \mu P \tag{2.5}$$

Equations (2.1) through (2.5) are the governing equations of the mechanical problem and form the basis of the mathematical model for flat rolling.

2.3 Boundary Conditions of the Mechanical Problem & the Mechanical Initial Boundary Value Problem (M-IBVP)

Realistic analysis of the flat rolling processes means that the events taking place during a pass should be looked at as a coupled thermal-mechanical problem that, on top of the mechanical events seen in the previous section, will be able to properly take into account the following combined phenomena:

a) heat generation due to plastic work,
b) heat generation due to friction forces,
c) accumulation of the deformation work connected with an increase of dislocation density,
d) thermal events connected with metallurgical transformations,
e) cooling by air or by water spray on free surfaces,
f) cooling due to contact with the roll,
g) radiation from the slab at 1200 °C to the environment in the hot rolling case.

In order to obtain a solution for stress, strain, strain rate, velocity and temperature fields within the rolled strip, appropriate boundary and initial conditions have to be introduced. Both steady-state and non steady-state solutions have to satisfy the thermal boundary conditions which we will see later in this chapter, and the mechanical boundary conditions which are given by the prescribed velocities and tractions along the boundary of the roll-workpiece interface:

a) Tension & compression tractions T_i,
b) Friction tractions along the contact surface τ_i,
c) Velocity constraints.

Schematic illustration of the *mechanical boundary conditions* Γ_i, in the deformation zone for the cold rolling case is presented in Figure 2.2.

- Γ_1: Tension tractions $\overline{T}_x = 0$ & $\overline{T}_y = 0$ for rolling without tensions or $\overline{T}_x = T_1$ and $\overline{T}_y = 0$ for rolling with tensions,
- Γ_2: Symmetry $\overline{T}_x = 0$ & $v_y = 0$,
- Γ_3: Tension tractions $\overline{T}_x = 0$ & $\overline{T}_y = 0$ for rolling without tensions or $\overline{T}_x = T_2$ and $\overline{T}_y = 0$ for rolling with tensions,
- Γ_4: Zero traction, $\overline{T}_x = 0$ & $\overline{T}_y = 0$, and zero mass flow $\overline{v} \cdot \overline{n} = 0$,
- Γ_5: Friction tractions $\tau_x = \mu \cdot P \cdot \cos\theta_x$, & $\tau_y = \mu \cdot P \cdot \sin\theta_x$
  Compression tractions $\overline{T}_x = P \cdot \cos\theta_x$, & $\overline{T}_y = P \cdot \sin\theta_x$
  Velocity vectors $v_x > 0$, & $v_y = -v_x \tan\theta_x$
- Γ_6: Zero traction, $\overline{T}_x = 0$ & $\overline{T}_y = 0$, and zero mass flow $\overline{v} \cdot \overline{n} = 0$.

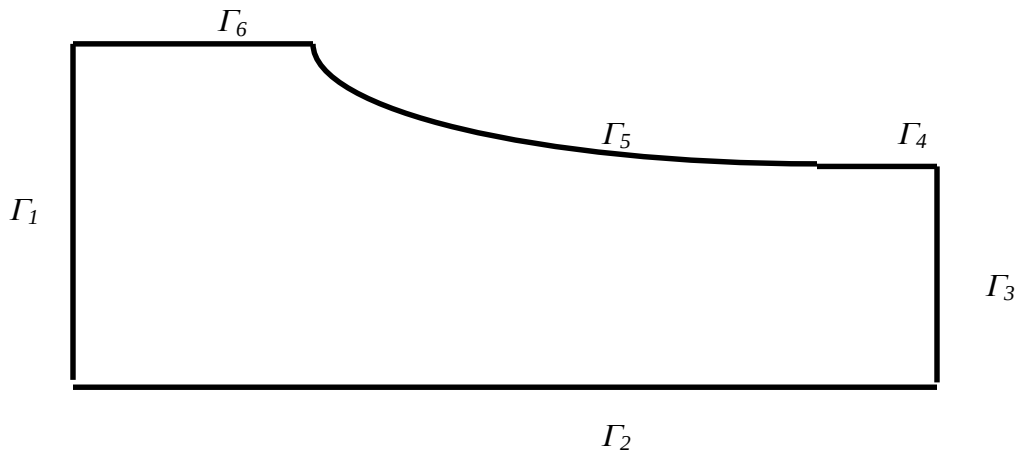

Figure 2.2: Mechanical boundary conditions in the deformation zone

θ_x = angle between the tangent to the roll surface and the horizontal axis
τ_x, τ_y = boundary friction tractions
$\overline{T}_x, \overline{T}_y$ = tension or compression tractions
v_x, v_y = velocity vector components
μ = friction coefficient

The governing equations seen in Section 2.2, the boundary conditions we have just seen, and the initial conditions are part of the Mechanical Initial Boundary Value Problem (M-IBVP), which is summarized as follows:

Governing Equations:
a) Equilibrium Equations
b) Mises Yield Condition
c) Flow Rule (constitutive equations)
d) Constitutive equations

Boundary Conditions:
a) Velocities
b) Tractions (frictional stresses in tangential direction)

Initial Conditions
a) Initial Velocities
b) Initial Tractions

This Mechanical Initial Boundary Value Problem (M-IBVP) constitutes one half of the overall problem in rolling, the Thermal IBVP being the second half, as we will see in the next section.

2.4 Heat Transfer & Thermal Balance

Heat transfer plays a very important role in the rolling process. In cold rolling there is heat arising from the work of friction forces on the contact surface and also heat gain arising from the work of plastic deformation. In the hot rolling case, on top of these, there is additional heat loss to the environment due to radiation and convection, heat loss by conduction to the rolls, and temperature change due to the energy accumulated during the metallurgical transformations. In some cases, there is also heat loss due to water-cooling. All of these physical phenomena are a key part of our Initial Boundary Value Problem, which as we will see consists of a linear and homogeneous Partial Differential Equation (heat equation), and a set of boundary and initial conditions.

2.4.1 Thermal Balance Equations

The various contributions to the overall heat balance for a particular cross section in a billet, slab or strip can be summarized as:

a) heat loss to the environment by radiation and convection along the free surfaces,
b) heat gain arising from the work of friction forces on the contact surface,
c) heat gain arising from the work of plastic deformation,
d) heat loss by the conduction transfer to the roll,
e) temperature change due to the energy accumulated or realized during the metallurgical transformations.

The heat conduction within the material is described by the general heat diffusion equation [28,39]

$$\frac{\partial}{\partial x}\left(k\frac{\partial T}{\partial x}\right)+\frac{\partial}{\partial y}\left(k\frac{\partial T}{\partial y}\right)+\frac{\partial}{\partial z}\left(k\frac{\partial T}{\partial z}\right)+\dot{q}=C_p\rho\frac{\partial T}{\partial t} \tag{2.6}$$

where

k = heat conduction coefficient
T = temperature (K)
$\dot{q}$ = rate of heat generation (W/m^3)
C_p=specific heat (J/kg K)
ρ = material's density (kg / m^3)
t = time (s)

The rate of heat generation takes into account the plastic work done, energy accumulated in the material due to the increase of dislocation density and heat produced during the softening process. It is described by the equation [56]

$$\dot{q}=\int_V\left[\eta\bar{\sigma}_i\dot{\bar{\varepsilon}}_i^p-\upsilon A\dot{\bar{\varepsilon}}_i+\upsilon B\gamma e^{\left(-\frac{D}{kT}\right)}\right]dV \tag{2.7}$$

where V = volume of the body (m^3)

$\bar{\sigma}_i$ = equivalent stress (MPa)
$\dot{\bar{\varepsilon}}_i^p$ = equivalent strain rate (s^{-1})
$\bar{\sigma}_i \dot{\bar{\varepsilon}}_i^p$ = rate of heat generation due to plastic work (W/m^3)
υ = energy per unit length of dislocation (J/m)
A, *B* = material constants
D= activation energy of diffusion
γ = dislocation density
k= 1.380 x 10^{-23} J/K molecule (Boltzmann constant)

The non-steady state temperature model, with a time-dependent term in Equation (2.6), should be applied to all cases of hot rolling of ingots and billets. During continuous rolling of strips however, a steady state temperature field may be assumed in the roll gap and an additional term connected with heat convection due to the motion of the strip needs to be introduced. A typical steady-state convective-diffusion equation is then written as [39]

$$\frac{\partial}{\partial x}\left(k\frac{\partial T}{\partial x}\right)+\frac{\partial}{\partial y}\left(k\frac{\partial T}{\partial y}\right)+\frac{\partial}{\partial z}\left(k\frac{\partial T}{\partial z}\right)+\dot{q}-C_p\rho\frac{\partial T}{\partial t}=0 \tag{2.8}$$

In order to obtain a solution for the stress, strain, rate of strain, velocity and temperature fields within the rolled strip, appropriate boundary and initial conditions have to be introduced. Both steady-state and non-steady-state solutions have to satisfy the thermal boundary conditions, which may be of the following types [28]:

a) the temperature is prescribed along the boundary surface

$$T(x,t)=T_S \tag{2.9}$$

b) the heat flux normal to the surface is prescribed along the boundary

Finite heat flux $$-k\frac{\partial T}{\partial n}=q''_S \tag{2.10}$$

Adiabatic or insulated surface $$\frac{\partial T}{\partial n}=0 \tag{2.11}$$

c) convective heat transfer to the environment:

$$-K\frac{\partial T}{\partial n}=h(T-T_\infty) \tag{2.12}$$

h = film convection coefficient
T_∞ = environment temperature

d) radiative heat transfer to the environment

$$-K\frac{\partial T}{\partial n}=\sigma\varepsilon\left(T_w^4-T_\infty^4\right) \tag{2.13}$$

Schematic illustration of the thermal events including the boundary conditions in the deformation zone is presented in Figure 2.3. As explained by Lenard [49], main sources

of heat losses include air cooling of the free surfaces and heat transfer to the cooler roll. In modeling, the axis of symmetry and the exit plane from the control volume are treated as insulated surfaces. Finally, constant temperature is prescribed along the vertical plane at the entry to the control volume. The temperature across the contact surface is allowed to be discontinuous, to account for the discontinuity created by the relative velocity between the two surfaces, and also that caused by the resistance to heat transfer across an interface. This latter effect can be specified as a function of the normal stress between the two surfaces in contact or by means of a constant heat transfer coefficient. Finally, interfacial frictional forces at the roll-strip interface and the shape of that interface need to be accounted for as well [49].

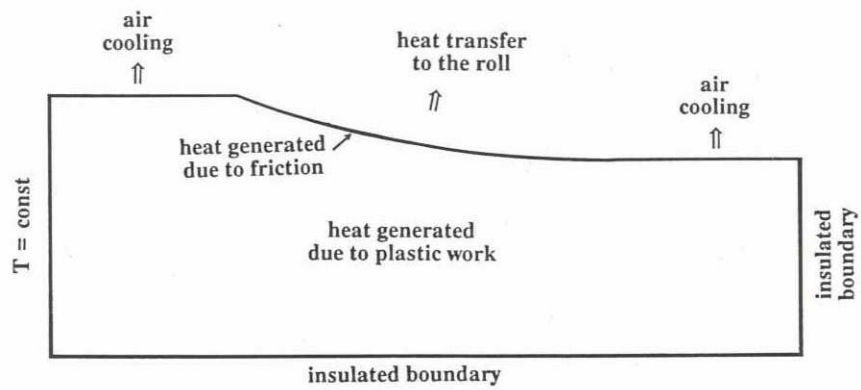

Figure 2.3: Schematic of the thermal events and boundary conditions in the roll gap [56] © Springer-Verlag

Lastly we have the initial boundary conditions, which in our case is given by the prescribed initial temperatures on the boundaries of the roll gap, and which are given by Equation 2.9 for time $t = 0$.

2.4.2 Heat Transfer from Mechanical Sources: Friction & Plastic Deformation

During the rolling process, the temperature rise due to mechanical work is very significant, especially in cold rolling. This temperature rise is due to two factors:

a) friction derived mechanical work dissipated to the interface between the material being rolled and the work roll

b) plastic deformation derived mechanical work absorbed by the material being rolled during deformation. This energy is not completely transformed into heat: as the deformation process progresses, the displacement of dislocations are being counteracted which causes internal stresses to appear at different points of the grains.

The heat rate generated due to plastic deformation is determined by [44,54]

$$\dot{q} = \eta \bar{\sigma}_{ij} \dot{\bar{\varepsilon}}_{ij}^{p} \qquad (\mathrm{W/m^3}) \tag{2.14}$$

where

$\eta =$ heat generation efficiency (fraction of the plastic strain energy that is converted to heat ~ 0.9) , $0 < \eta < 1$

$\bar{\sigma}_{ij} =$ components of equivalent stress tensor (MPa)

$\dot{\bar{\varepsilon}}_{ij}^{p} =$ components of equivalent plastic strain rate tensor (s^{-1})

The heat transfer rate due to friction is expressed by [44,54]

$$q''_{fr} = \sigma_{fr} \cdot v_r \cdot \xi \qquad (\mathrm{W/m^2}) \tag{2.15}$$

where

$\sigma_{fr} =$ friction stress (MPa)

$v_r =$ relative sliding velocity between the roll and the workpiece (m/s)

$\xi =$ fraction of friction energy that is converted to heat, $0 < \xi < 1$

2.4.3 Heat Transfer due to Conduction to the Rolls

The way we will model the heat flux at the heat roll interface is by using Fourier's law [39].

$$q''_{cond} = k(T_w - T_R) \tag{2.16}$$

where

q''_{cond} = conduction heat flux (W/m^2)

k = conduction heat transfer coefficient (W/m^2K)

T_w = Workpiece temperature (K)

T_R = Roll temperature (K)

k is not constant along the arc of contact and it is a function of:

a) Roll pressure distribution,

b) Interface oxide layer,

c) Surface roughness,
d) Surface chemistry (if lubricant used).

The conduction heat transfer coefficient in the contact area between the roll and the stock is very high and has values typically between 6000 and 10000 $\frac{W}{m^2K}$ [56].

2.4.4 Convection Cooling Heat Transfer

Convection in the hot strip mill is due to the motion of air surrounding the workpiece. Depending upon whether the air motion is forced or free, the heat transfer is referred to as either forced or free convection, the later being usually the case in hot strip mills. A key factor in the calculation of temperature losses due to convection is to determine the heat transfer coefficient, which depends on the material temperature, ambient temperature, material specific heat and density, and the dynamic viscosity of the air flow and its characteristics, i.e., free, laminar, turbulent, etc.

In this thesis, the formula that will be used to study convection is the well-known Newton's law of cooling [39].

$$q''_{conv} = h(T_w - T_\infty) \tag{2.17}$$

q''_{conv}= convective heat flux (W/m^2)
h = film convection heat transfer coefficient (W/m^{2}K)
T_w = workpiece temperature (K)
T_∞ = temperature of surrounding air or water (K)

In the hot rolling process we encounter two types of convection. The first one is the convection due to the air that surrounds the hot strip. The thermal transfer/film coefficient h in this case is very low with values that range between 15 and 50 $\frac{W}{m^2K}$. If we have force air convection, then the film coefficient becomes larger in the order of 500 $\frac{W}{m^2K}$. The second type of convection occurs in some hot rolling processes that use water in order to de-scale the workpiece and also to cool the rolls that otherwise after several hours of continued rolling, begin to get too hot. The film coefficient in the case of water convection cooling reaches values ranging between 500 and 4000 $\frac{W}{m^2K}$ [49,56].

2.4.5 Radiation Heat Transfer

Apart from the thermal flow due to convection, rolling stock heat is lost also due to radiation. The heat losses due to radiation can be determined from the Stefan-Boltzmann law [39].

$$q''_{rad} = \varepsilon\sigma\left[(T_w)^4 - (T_\infty)^4\right] \tag{2.18}$$

where

q''_{rad} = radiation heat flux (W/m^2)
$\varepsilon \cong 0.8$ = emissivity of the workpiece at a temperature around 1000˚C
σ = Stefan-Boltzmann radiation constant of black body
T_w= absolute temperature of the workpiece
T_∞ = absolute ambient temperature ~ 20˚C+273 K = 293 K

Since

$$q''_{rad} = \frac{mC_p \Delta T_{rad}}{A_{rad} t} \tag{2.19}$$

where

m = mass of the rolled stock (kg)
C_p= specific heat of stock (J/kg K)
ΔT_{rad} = change in temperature (K)
t = radiation time (s)
A_{rad} = surface of radiating workpiece (m^2)

therefore

$$\Delta T_{rad} = \frac{q''_{rad}\, At}{mC_p} = \frac{\varepsilon\sigma A_{rad} t}{mC_p}\left[(T_w)^4 - (T_a)^4\right] \tag{2.20}$$

This formula can be used to find the drop in temperature in each pass due to radiation.

2.4.6 Surface Thermal Balance

Applying the energy balance for conservation of energy at the surface of the workpiece,

$$\dot{E}_{in} + \dot{E}_g - \dot{E}_{out} = \dot{E}_{st} \tag{2.21}$$

where

$\dot{E}_{in}$ = rate at which thermal energy enter through the control surface

$\dot{E}_{out}$ = rate at which thermal energy leave through the control surface

$\dot{E}_g$ = energy generation (thermal energy created within the control volume due to conversion from other energy forms, in our case plastic deformation and friction)

$\dot{E}_{st}$ = rate of energy stored within the control volume

In Figure 2.3, five heat transfer terms are shown for the control surface. On a unit area basis they are the conduction within the workpiece to its surface, and from the workpiece to the rolls (q''_{cond}), the convection from the surface of the workpiece to the surrounding fluid, air or water (q''_{conv}), the net radiation exchange from the surface to the surroundings (q''_{rad}), and finally, the energy generation terms due to work of plastic deformation (q''_{pw}), and friction (q''_{fr})

The energy balance then takes the form,

$$E''_{st} = q''_{pw} + q''_{fr} \pm q''_{cond} - q''_{conv} - q''_{rad} \tag{2.22}$$

and we can express each of the terms using the appropriate rate equations,

$$E''_{st} = \eta \cdot \overline{\sigma}_{ij} \cdot \dot{\overline{\varepsilon}}_{ij}^{\,p} L_{pw} + \sigma_{fr} v_r \xi - k(T_w - T_R) - h(T_w - T_\infty) - \varepsilon \cdot \sigma \cdot \left(T_w^4 - T_\infty^4\right) \tag{2.23}$$

2.5 Boundary Conditions of the Thermal Problem & the Thermal Initial Boundary Value Problem (M-IBVP)

Likewise, the *thermal boundary conditions* Φ_i, in the deformation zone for the cold rolling case are presented in Figure 2.2

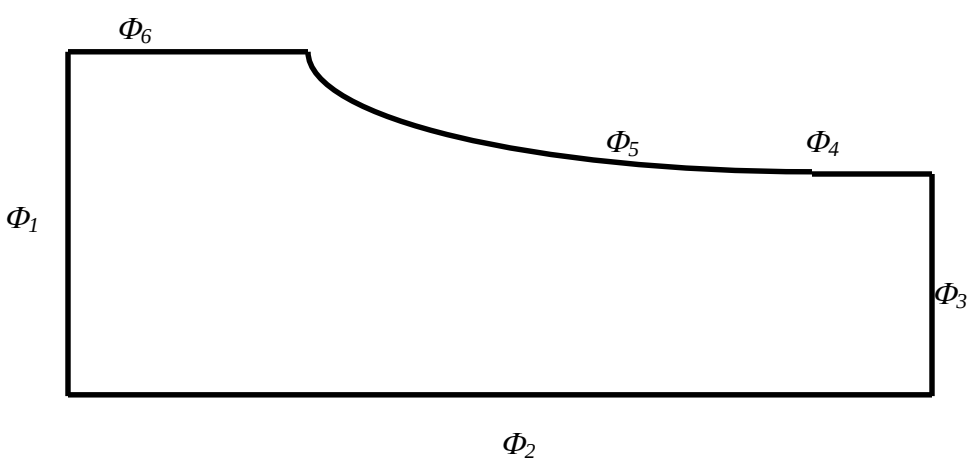

Figure 2.4: Thermal boundary conditions in the deformation zone

Φ_1 : Constant temperature $T(x,t) = T_S$

Φ_2 : insulated boundary $\frac{\partial T}{\partial n} = 0$

Φ_3 : insulated boundary $\frac{\partial T}{\partial n} = 0$

Φ_4 : convection air cooling $-k\frac{\partial T}{\partial n} = h(T - T_\infty)$

plastic work generated heat conducted to surface $-k\frac{\partial T}{\partial n} = q''_{pw}$

radiation in the case of hot rolling $-k\frac{\partial T}{\partial n} = \sigma\varepsilon\left(T_w^4 - T_\infty^4\right)$

Φ_5 : plastic work generated heat conducted to boundary $-k\frac{\partial T}{\partial n} = q''_{pw}$

conduction from workpiece to rolls $-k\frac{\partial T}{\partial n} = q''_{cond}$

heat generated due to friction $q''_{fr} = f_{fr} \cdot v_r \cdot \xi$

Φ_6 : convection air cooling $-k\frac{\partial T}{\partial n} = h(T - T_\infty)$

plastic work generated heat conducted to surface $-k\frac{\partial T}{\partial n} = q''_{pw}$

radiation in the case of hot rolling $-k\frac{\partial T}{\partial n} = \sigma\varepsilon\left(T_w^4 - T_\infty^4\right)$

We now have all the information necessary to set up our second Boundary Value Problem corresponding to the thermal portion of the rolling problem.

The T-IBVP is given by

Governing Partial Differential Equation

a) Heat Diffusion Equation

Boundary Conditions:

b) Conduction
c) Convection
d) Radiation
e) Friction heat
f) Plastic work heat

Initial Conditions

c) Initial Temperature of workpiece

This Thermal Initial Boundary Value Problem (T-IBVP) constitutes the second of the overall problem in rolling. As we will see later, the mechanical and thermal parts of this problem are coupled. In order to handle a coupled thermo-mechanical deformation problem, it is necessary to solve simultaneously the mechanical material-flow problem (mechanical portion) for a given temperature distribution and the heat transfer equations (thermal portion).

There are two primary causes of coupling:

a) the body undergoes large deformations such that there is a change in the boundary conditions associated with the heat transfer problem;
b) deformation converts mechanical work into heat through an irreversible process, which is large relative to other heat sources.

Therefore, the overall solution of our rolling problem lies in the simultaneous solution of both the mechanical and the thermal initial boundary value problems. This is one of the reasons that makes this such a complicated, challenging, and at the same time fascinating problem.

In the next section of this chapter we will take a look at the main classical mathematical solution of the flat rolling problem, developed by one of the main plasticians of the 20th century, vonKarman. We will also take a look at the mathematical aspects of two of the critical problems that make rolling a highly non-linear problem: the contact and the friction problems. Finally, we will take a look at the material models used for this thesis for both the cold and hot rolling cases.

2.6 Classic Mathematical Solution Model of Flat Rolling

The derivation of this solution can be found in any textbook on classic rolling theory such as [32,33,34,49,56,62,63]. The one presented in this section is Ginzburg's [32]. Figure 2.5 illustrates the stresses acting upon a differential elemental vertical section of the flat workpiece between the rolls. To analyze the plastic deformation of the workpiece an infinitesimal element in the workpiece of thickness *dx* has been selected, and all normal and friction forces acting on the element have been identified. Then the appropriate differential equation can be derived from which a solution is obtained by integration of the equation using appropriate boundary conditions.

In this analysis the following assumptions are made [32,33,34]

a) The direction of the applied load and planes perpendicular to this direction define principal directions,
b) The principal stresses do not vary on these planes,
c) The frictional forces do not produce the internal distortion of the metal and do not change the orientation of the principal directions,
d) Plane vertical sections remain plane and therefore, the deformation is homogeneous in regard to determination of induced strain,

e) Elastic deformation of the workpiece is negligible in comparison with the plastic deformation,
f) There is no elastic deformation of the tool in the contact zone,
g) The compressive strength is constant throughout the contact length,
h) The workpiece does not spread laterally as we assume a state of plane strain,
i) There is no roll flattening in the arc of contact,
j) The peripheral velocity of the rolls is constant,
k) Material does not undergo work-hardening during its passage between the rolls,
l) The compression rate from point along the arc of contact does not have any effect on the magnitude of the compression strength.
m) The vertical component of the friction force is negligible

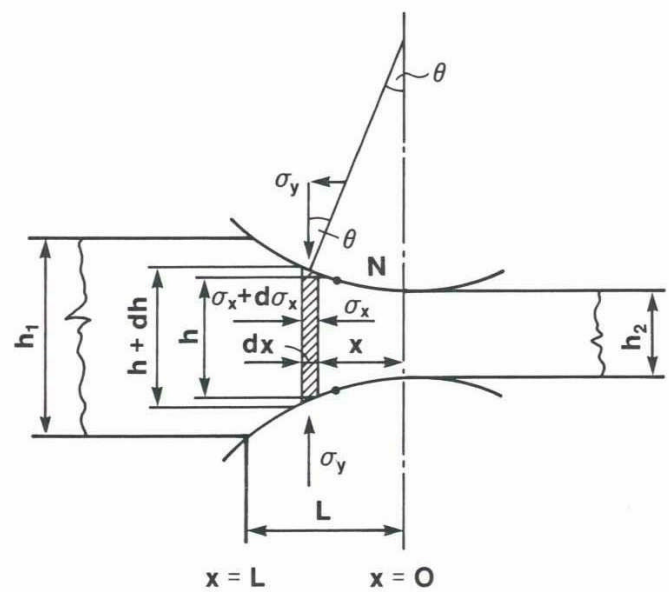

Figure 2.5: Schematic Representation of the deformation zone in flat rolling [32]
© Marcel Dekker / Taylor & Francis Group

The nomenclature that will be used throughout the rest of this thesis for the flat rolling problem parameters is the following:

h_1=Strip/workpiece entry thickness (m)
h_2 =Strip/workpiece exit thickness (m)
h_a=Average workpiece thickness (m)
w = angular velocity of the rolls (rpm or rad/s)
L=Roll gap/contact arc length (m)
V_r=Roll surface velocity (m/s)
V_o=Workpiece initial speed (m/s)
V_f=Workpiece exit speed (m/s)
V_x=Velocity of the metal being rolled at section dx (m/s)
F=Roll force (N)

P=Roll pressure (Pa)
α=Roll bite angle (rad)
θ=Neutral point angle (rad)
θ_x =Angle between the tangent to the roll surface and the horizontal axis (rad)

The horizontal forces acting on vertical faces of the section *dx* produce compressive stresses $\sigma_x + d\sigma_x$ acting on the face of the section of height *h* + *dh* and compressive stresses σ_x acting on the face of height *h*.
The equilibrium of the horizontal forces acting on section *dx* may be expressed as

$$(\sigma_x + d\sigma_x)(h + dh) \pm 2\mu\sigma_y dx - 2\sigma_y \tan\theta dx - \sigma_x h = 0 \tag{2.24}$$

or

$$2\sigma_y(\tan\theta \mp \mu)dx = d(h\sigma_x) \tag{2.25}$$

where the (-) sign before μ corresponds to the sections dx located between the entry and neutral planes and sign (+) corresponds to the sections dx located between the neutral and exit planes.
Since, $\tan\theta = \frac{1}{2}\frac{dh}{dx}$, Equation (2.25) can be rewritten as

$$\sigma_y \frac{dh}{dx} \mp 2\mu\sigma_y = \frac{d(h\sigma_x)}{dx} \tag{2.26}$$

Taking into account the yield criterion given by Equation (2.25) for the case of plain strain, $\sigma_y - \sigma_x = 2\tau_y$, and that $P = \sigma_y$ we obtain the differential Equation (2.26) in its final form

$$P\frac{dh}{dx} \mp 2\mu P = \frac{d[h(P - 2\tau_y)]}{dx} \tag{2.27}$$

Equation (2.27) was derived by Von Karman in 1925 and is the starting point in the analysis known as the theory of homogeneous deformation [32].
A number of solutions to this equation have been proposed. These solutions differ mainly in respect to the assumed nature of the frictional forces in the contact zone as shown in Figure 2.6.

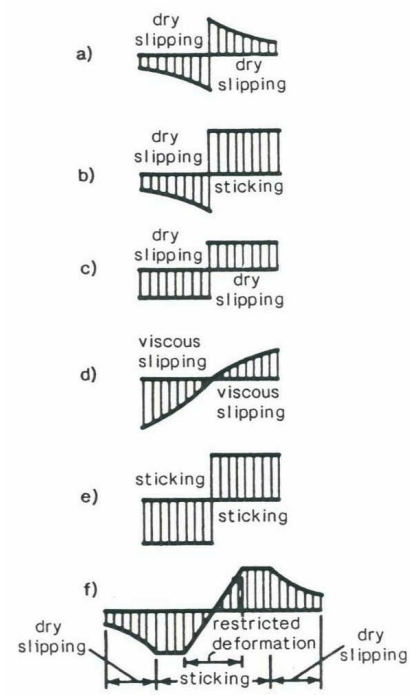

Figure 2.6: Types of frictional force and their distribution along the arc of contact according to the different theories of rolling [32]

© Marcel Dekker / Taylor & Francis Group

According to Ginzburg, Von Karman's solution is based on the assumption that dry slipping would occur over the whole arc of the contact between the rolls and the rolled material (Figure 2.6a). Also the frictional shear stress is directly proportional to the value of local normal pressure, i.e.

$$\tau = \sigma_{fr} = \mu\sigma_y = \mu P \tag{2.28}$$

Ekelund's solution is based on the assumption that the dry slipping would occur over the whole entry side, and sticking over the whole exit side of the arc of contact (Figure 2.6b) Siebel's solution is obtained for the case when the dry slipping occurs over the whole arc of contact between the rolls and the rolled material (Figure 2.6c) and it is assumed that the frictional force is constant along the arc of contact $(f_{fr} = cons\tan t)$

Nadai's solution is based on the assumption that viscous slipping exists in the roll contact zones (Figure 2.6d), and that the frictional force is proportional to the relative velocity of the slip. Thus,

$$\tau_x = \mu \frac{(V_x - V_r)}{\delta} \tag{2.29}$$

where

V_x= velocity of the metal being rolled at the section *dx* (Figure 2.5)
V_r= peripheral roll velocity
δ = oil-film thickness

Orowan and Pascoe's solution is derived for the case when sticking occurs over the whole arc of the contact (Figure 2.6e). Sims and Alexander make a similar assumption. Tselikov's solution is provided for the case when there is a zone of restricted plastic deformation in the middle of the sticking zone. It is also assumed that dry slipping occurs at the entry and the exit of the arc of contact as shown in Figure 2.6f.
Figure 2.7 shows the distribution of normal pressure and frictional force along the arc of contact as calculated by Tselikov according to the four theories discussed.

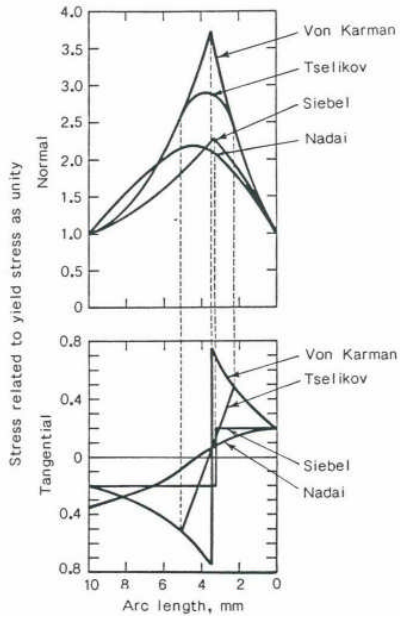

Figure 2.7: Distribution of Normal Pressure and frictional force along the arc of contact according to the classical rolling theories [32]

© Marcel Dekker / Taylor & Francis Group

The theories we have just looked at have a lot of limitations because they are based on the erroneous assumption that a plane vertical section of the rolled material remains plane during rolling. However, this contradicts the facts obtained from numerous experiments and even FEM simulations, as we will see later. Another limitation of the theories of homogeneous deformation arises from the assumptions that the yield stress of the material and the coefficient of friction remain constant. In most cases in cold rolling, the constrained yield strength, $S = 2\tau_Y = 1.15\sigma_Y$, increases due to work-hardening and there is a strong possibility that the coefficient of friction is not constant in all points in the arc of contact especially in dry rolling. Further, the homogeneous theories of rolling give a simplistic description of the deformation zone that can be improved if such factors as roll flattening and elastic recovery of the rolled strip are taken into consideration.

2.7 Mathematical aspects of the Contact Problem

Contact, by nature, is a non-linear boundary value problem. During contact, mechanical loads and sometimes heat are transmitted across the area of contact. If friction is present, shear forces are also transmitted.
Boundary contact conditions cause huge difficulties and make the convergence of the model extremely difficult. It is necessary to match the initial geometric shape as well as possible, but also to introduce test to determine when a node comes into contact with a rigid or elastic tool. This can be done geometrically, and the node then restored to the surface if it has apparently crossed the boundary. It is then necessary to determine whether the normal force has become tensile, before re-sitting the node [19,53,64].

Contact can be defined as finding the displacement of points A and B such that

$$\left(\bar{u}_A - \bar{u}_B\right) \bullet \bar{n} < TOL \tag{2.30}$$

where $\bar{u}_A$ is the position vector for the first body, $\bar{u}_B$ is the position vector on the second body, $\bar{n}$ is the direction cosine of a vector between the two points, and *TOL* is the closure distance

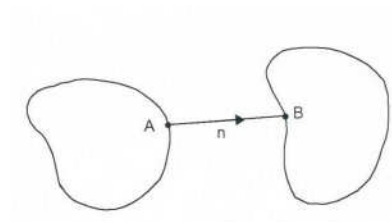

Figure 2.8: Normal Gap between potentially contacting bodies [53]

© MSC Software Corporation

Contact problems are commonly divided into two domains [19,53]:

a) A deformable body makes contact with a rigid surface,
b) A deformable body makes contact with another deformable body or itself.

2.7.1 Deformable-Rigid Contact

In such a problem, a target node on the deformable body has no constraint while contact does not occur. Once contact is detected, the degrees of freedom are transformed to a local system and a constraint is imposed such that

$$\Delta\bar{u}_{normal} = \bar{v} \cdot \bar{n} \tag{2.31}$$

where $\bar{v}$ is the prescribed velocity of the rigid surface. This local transformation is continuously updated to reflect sliding of point A along the rigid surface. If the contact is glue contact, an additional displacement constraint is activated

$$\Delta\bar{u}_{\tan} = \bar{v} \cdot \bar{t} \tag{2.32}$$

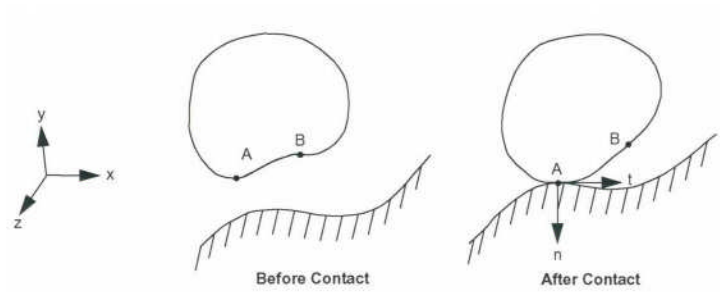

Figure 2.9: Contact coordinate system [53] © MSC Software Corporation

The determination of when contact occurs and the calculation of the normal vector are critical to the numerical simulation. The procedure used by MSC Marc is as follows:
In the deformable to rigid body contact case, the contact procedure has three cases:
Case 1: Contact not detected when

$$\Delta\bar{u}_A \cdot \bar{n} < |D - d| \tag{2.33}$$

In this case node A does not touch the rigid surface so no constraint is applied
Case 2: Contact detected when

$$|\Delta\bar{u}_A \cdot \bar{n} - d| \le D \tag{2.34}$$

In case 2a node A is near the rigid body within tolerance and contact constraint pulls node A to contact surface if $F < F_s$
In case 2b node A penetrates within tolerance and the contact constraint pushes node A to contact surface.

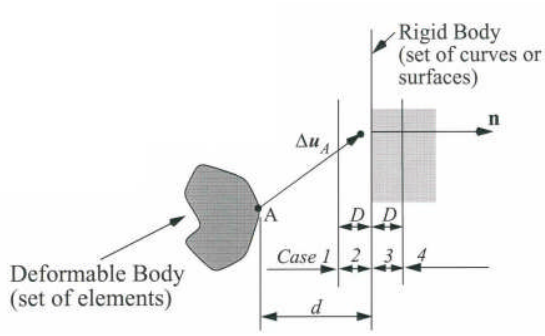

Figure 2.10: Deformable to Rigid Body Contact Procedure [54]

© MSC Software Corporation

where
v = the prescribed velocity of the rigid surface
$\Delta\bar{u}_A$ = incremental displacement vector of node A
$\bar{n}$ = unit normal vector with proper orientation

$\bar{t}$ = unit tangential vector
D = contact distance
F_s = separation force
TOL = contact closure distance

Case 3: Penetration detected when

$$\Delta\bar{u}_A \cdot \bar{n} > |D + d| \tag{2.35}$$

In this case node A penetrates out of tolerance and increment gets split (loads reduced) until no penetration occurs.

By default, in most models, the contact tolerance is equally applied to both sides of a segment. This can be changed by introducing a bias factor B such that $0 \le B \le 1$

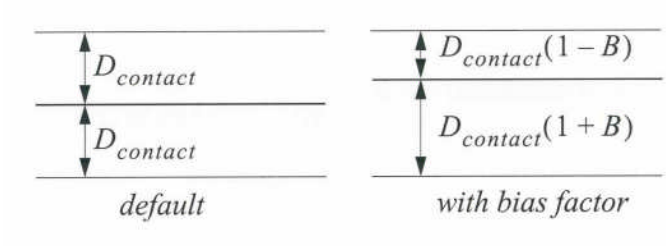

Figure 2.11: Bias factor [53] © MSC Software Corporation

Choosing a bias factor > 0 may be useful to reduce increment splitting since the distance to cause penetration is increased, and to improve accuracy, since the distance below which a node comes into contact is reduced.

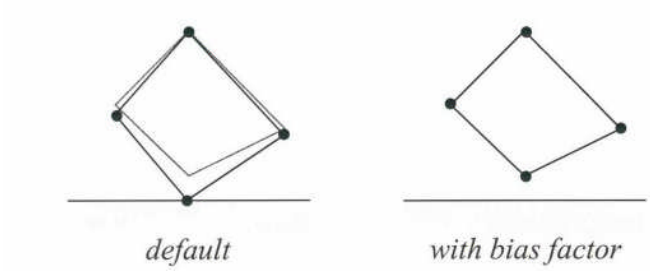

Figure 2.12: Bias factor comparison [53] © MSC Software Corporation

2.7.2 Deformable-Deformable Contact

When a node contacts a deformable body, a tying relation is formed between the contacting nodes and the nodes on the other body (Figure 2.10). This constraint relationship uses information regarding the normal to the surface. For lower-order elements, this normal is calculated based upon the piecewise linear representation of the element face. This has the consequences that the constraint relation is not accurate because it is constant over the complete segment. As a node slides from once face to

another, there is a discontinuity in the normal, which leads to potential numerical difficulties. When higher-order elements are used, a normal is created based upon the true quadratic surface.

Discrete deformable contact is based on a piecewise linear geometry description of either 2-node edges in 2 dimensions or 4-node faces in 3 dimensions on the outer surface of all contacting meshes.

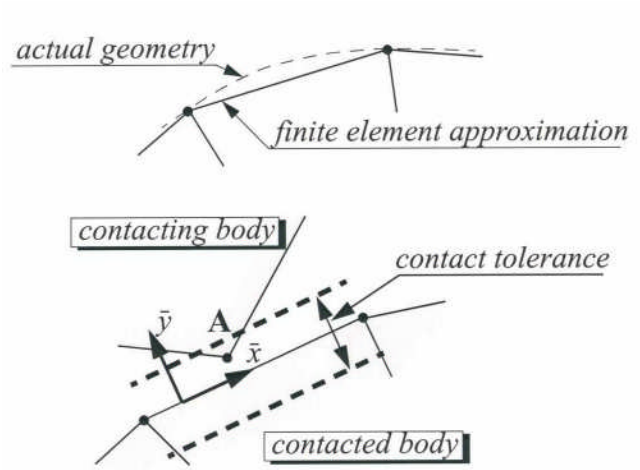

Figure 2.13: Deformable contact; Piecewise Linear Geometry Description [53] © MSC Software Corporation

The constant constraint defines the tying relation for the displacement of the contacting node in local $\bar{y}$ direction, and also, applies a correction on the position in the local $\bar{y}$ direction.

Potential errors due to piecewise linear descriptions of geometry include:

a) the tying relation may not be completely correct due to the assumption that the normal direction is constant for a complete segment,

b) if contacting node slides from one segment to another, a discontinuity in the normal direction may occur,

c) the correction on the position of the contacting node may not be completely correct.

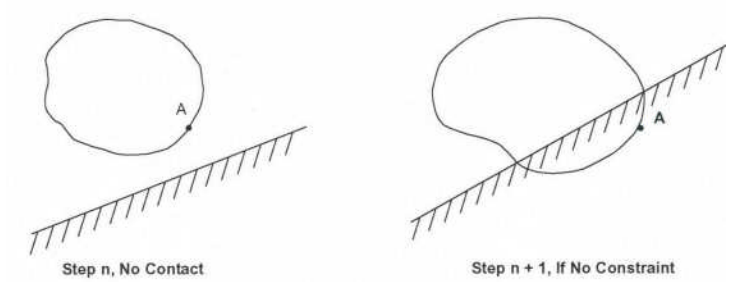

Figure 2.14:Contact constraint requirements [53] © MSC Software Corporation

2.8 Friction Modeling

Friction is a complex physical phenomenon that involves the characteristics of the surface such as surface roughness, temperature, normal stress, and relative velocity. The actual physics of friction continues to be a topic of research. Hence, the numerical modeling of friction has been simplified to three idealistic models [19,54,64].

a) Stick-Slip: based on the Coulomb model of friction, it models the transition from stick to slip,
b) Adhesive or Coulomb friction: an adhesive model of friction in which the friction stress is based upon the coefficient of friction and the equivalent normal stress at the surface,
c) Shear Friction: a cohesive model of friction in which the friction stress is based upon the coefficient of friction and the equivalent von Mises stress in the material.

2.8.1 Stick-Slip Friction Model

Discovered by Leonardo da Vinci in the 15th century, and verified by experiments by Charles A. Coulomb in the 18th century, this stick slip friction model uses a penalty method to describe the step function of Coulomb's Law.

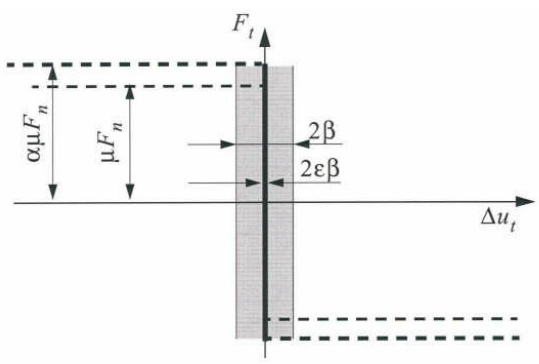

Figure 2.15: Stick –Slip Friction model and parameters [54] © MSC Software Corporation

with $F_t \leq \mu F_n$ static and $F_t \leq \alpha\mu F_n$ kinetic
where

F_t = tangential force
F_n = normal reaction
Δu_t = incremental tangential displacement
β = stick to slip transition region
α = coefficient multiplier
ε = small constant ~ 10^{-6} so that $\varepsilon\beta \approx 0$

2.8.2 Adhesive Friction or Coulomb Sliding Friction Model

This model is the most commonly used and the one used in this thesis to model the friction between the workpiece and the rolls. The Coulomb sliding friction model is:

$$\sigma_{fr} \leq -\mu\sigma_n \cdot t \tag{2.36}$$

where

σ_n = normal stress

σ_{fr} = tangential/shear friction stress

μ = friction coefficient

t = tangential vector in the direction of the relative velocity

$$t = \frac{v_r}{|v_r|} \tag{2.37}$$

v_r = relative sliding velocity

The Coulomb model is also often written with respect to forces

$$f_t \leq -\mu f_n \cdot t \tag{2.38}$$

where

f_t = tangential force

f_n = normal reaction

For a given normal stress, the friction stress has a step function behavior based upon the value of v_r or Δu

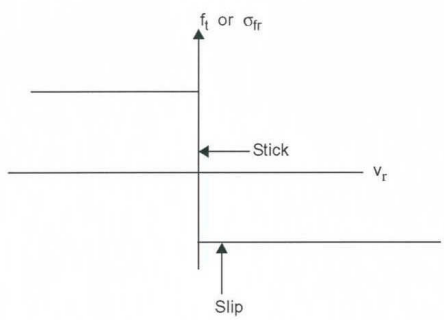

Figure 2.16: Coulomb Friction Model [54] © MSC Software Corporation

The discontinuity in the value of σ_{fr} can result in numerical difficulties so a modified Coulomb friction model is implemented [19,49]:

$$\sigma_{fr} \leq -\mu\sigma_n \frac{2}{\pi}\arctan\left(\frac{v_r}{|v_r|}\right) \cdot t \tag{2.39}$$

Physically, the value of $|v_r|$ is the value of the relative velocity when sliding occurs. This value is very important when determining how closely the mathematical model represents the step function. Note: a very large value of $|v_r|$ results in poor convergence.

In terms of the tangential and normal forces

$$f_t = -\mu f_n \frac{2}{\pi} \arctan\left(\frac{v_r}{|v_r|}\right) \cdot t \tag{2.40}$$

This is actually equivalent to a nonlinear dashpot whose damping depends on the relative sliding velocity as:

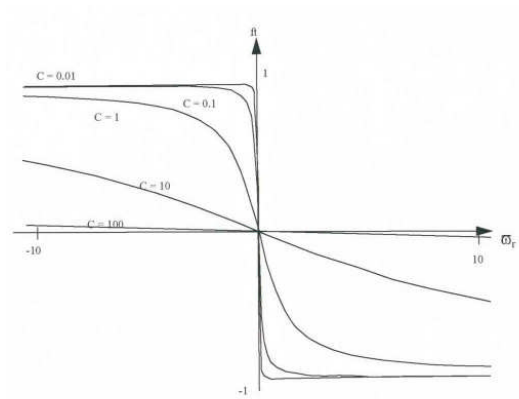

Figure 2.17: Force based Coulomb model approximation ($f_n = 1$, C=$|v_r|$) [54] © MSC Software Corporation

Coulomb friction is a highly nonlinear phenomenon dependent upon both the normal force and relative velocity.
Incidentally, this is the model used by Chen and Kobayashi in which the frictional forces are dependent on the velocity and also the one used in this thesis. Therefore, for the finite element models shown in this work, $\sigma_{fr} = \frac{2}{\pi} \mu \sigma_n \arctan \frac{v_r}{|v_r|}$ is the friction stress.

2.8.3 Shear (Sliding) Friction Model

The Coulomb friction model sometimes does not correlate well with experimental observations when the normal force/stress becomes large. If the normal stress becomes large, the Coulomb model might predict that the frictional shear stresses increase to a level that can exceed the flow stress or the failure stress of the material. As this is not physically possible, the choices are either to have a nonlinear coefficient of friction or to use the cohesive, shear based friction model.
The shear-based model states that the frictional stress is a fraction of the Mises equivalent stress in the material:

$$\sigma_{fr} \le -\mu \frac{\bar{\sigma}}{\sqrt{3}} t \tag{2.41}$$

Again, this model is implemented using an arctangent function to smooth out the step function:

$$\sigma_{fr} \leq -\mu \frac{\bar{\sigma}}{\sqrt{3}} \frac{2}{\pi} \arctan\left(\frac{v_r}{|v_r|}\right) \cdot t \tag{2.42}$$

with $\mu = \mu(x, f_n, T, v_r, \bar{\sigma})$ = friction coefficient, where:

x = position of the point at which friction is being calculated

f_n = normal force at the point at which friction is being calculated

T = temperature at the point at which friction is being calculated

v_r = relative sliding velocity between point at which friction is being calculated and a surface

$\bar{\sigma}$ = flow stress of the material

The heat rate generated due to friction is expressed by [19]

$$q_{fr} = f_{fr} \cdot v_r \cdot \xi \tag{2.43}$$

where

f_{fr} = friction force

v_r = relative roll-workpiece sliding velocity

ξ = fraction of friction energy that is converted to heat

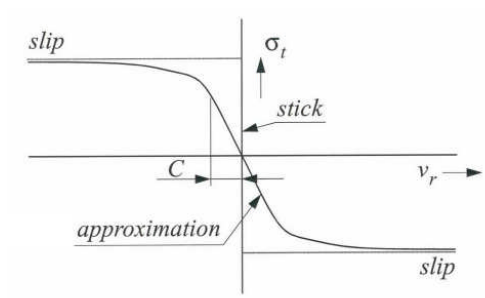

Figure 2.18: Shear Friction Mode [54] © MSC Software Corporation

2.9 Material Model & Plasticity

The equations relating stress, strain, stress rate (increase of stress per unit time), and strain rate are called the constitutive equations, since they depend upon the material properties of the medium under discussion. In the case of elastic solids, the constitutive equations take the form of generalized Hooke's law, which involves only stress and strain and is independent of the stress rate or strain rate.

In plasticity however, the constitutive equations have a more difficult formulation, as they need to describe more complex phenomena. According to Lenard & Pietrzyk, functions describing the constitutive behavior of metals at high temperatures can be divided into several groups [49,56].

a) Group I: functions $\sigma = f(\varepsilon)$, which account for the current strain (ε), and in some cases, for the initial stress (σ_Y) or initial strain (ε_0),
b) Group II: functions $\sigma = f(\varepsilon, \dot{\varepsilon}, T)$, which account for an influence of the current temperature (T), strain rate $(\dot{\varepsilon})$ and strain (ε),
c) Group III: functions $\sigma = f(\varepsilon, \dot{\varepsilon}, T, \sigma_w)$, which in addition to the temperature, strain, and strain rate, account for the influence of an internal state variable of the material (σ_w),
d) Group IV: functions $\sigma = f(\varepsilon, \dot{\varepsilon}, T, t)$, which also account for the time in addition to the Group II independent variables,
e) Group V: functions, which account for an influence of strain directions.

The basic factors that affect the magnitude of yield stress are the temperature and the rate of deformation. Their influence is different in cold and hot working [71]:
Cold Working: metal undergoes strain hardening and the yield stress increases with the amount of cold work. The rate of increase falls off as the degree of cold work increases. Finally, a degree of cold work is reached, beyond which no increase in strain hardening can be observed.
Hot Working: the phenomena of strain hardening and re-crystallization take place simultaneously. Therefore, the effects of strain hardening are not apparent. Assuming that the working temperature is constant, it can be concluded that the yield stress should also remain constant. The determination of the yield stress at temperatures above 700 ºC is a challenge. The stress-strain curve does not show any great change of direction on reaching the yield stress. Some researchers make the assumption that at these high working temperatures the yield stress differs very little from the ultimate tensile stress, and this value is sometimes defined as the constrained yield stress, $S = 2\tau_Y = 1.15\sigma_Y$.
The temperature of the workpiece has great influence on the strain rate. In order to study it, we will distinguish the following temperature ranges [33,49,71]:

1. Lower temperature range: brittleness can occur on applying large strain rates to metals which are ductile at low strain rates,
2. The cold working range (below recrystallization temperature): the influence of strain rate is very small but the mechanical factors introduced due to the increase of strain rate can be of importance,

3. Higher temperature range (above recrystallization temperature): while the phenomena of cold work occurs at high strain rates, hot working takes place at low strain rates,
4. Hot working range: The strain rate has an important influence. The higher the strain rate, the higher the yield stress. At very high temperatures, as the strain rate increases the heat has no time to be dissipated and remains in the metal, causing a rise in temperature. This results in lowering the temperature of fusion of the metal at high strain rates => the permissible temperature range for hot working becomes narrower. Therefore, low strain rates are necessary in hot rolling.

The basic factor that decides the degree of plastic deformation of metal is the yield stress, which is dependent on the condition of the metal at the moment of deformation.

a) For deformation and forming problems under conditions insufficient for recrystallization – cold working, the yield stress depends on:
    - the kind of metal,
    - the amount of cold work or initial strain hardening,
    - the strain
    - the strain rate to a very small degree which is almost negligible
b) Deformation above the temperature of recrystallization processes (hot working), the yield stress depends on:
    - the kind of metal
    - the strain
    - the strain Rate
    - the temperature of working

Therefore functions in group I are effective in the simulation of cold working processes, and functions in groups II, III, IV, and V are the ones used to simulate hot forming processes.

For cold rolling, the most common and at the same time accurate constitutive equation is given by the well known power law:

$$\sigma = K\varepsilon^{n} \tag{2.44}$$

where

n = strain hardening exponent , 0(perfectly plastic) < n < 1 (perfectly elastic)

K = strain hardening coefficient

In the literature we find some variations of the power law such as:

Dasko
$$\sigma = K(\varepsilon_0 + \varepsilon)^{n} \tag{2.45}$$

ε_0 = pre-existing amount of strain hardening

Ramberg-Osgood
$$\sigma = \sigma_Y + K\varepsilon^{n} \tag{2.46}$$

σ_Y = yield stress

According to Haslach & Armstrong, "the larger the hardening exponent, the easier the metal is to cold work. Experiments have shown that the strain hardening coefficient, *K*, is proportional to the square root of the density of dislocations in the material γ, i.e., $K \sim \sqrt{\gamma}$ " [35].

These three constitutive equations all belong to group I of stress-strain relationships. The Ramberg-Osgood version of the power law is the one used in the FEM modeling of the cold rolling process in this thesis.

The determination of the right stress-strain equation to accurately model the flow stress of steel at high temperatures is an extremely difficult problem that is still not fully understood. The constitutive equation for the hot rolling problem is somewhat of a "holy grail" that every hot rolling company would like to discover. Many models that use group III functions $\sigma = f(\varepsilon, \dot{\varepsilon}, T, \sigma_w)$ have been proposed. We will focus on the Shida constitutive equation that is recognized as one of the most accurate ones in the existing literature.

<u>Shida's model for high temperature behavior of carbon steels</u>

As reported by Pietrzik & Lenard, Shida in 1974, using a cam-plastometer, tested about 200 low, medium and high carbon steels and developed a comprehensive set of empirical equations, which describe the metal resistance to deformation as a function of the temperature, strain rate, strain, and the carbon content. The equations also take into account the behavior of the steels in the austenitic, ferritic and in the two-phase regions [49].

Shida's model is given by the relations:

$$\sigma = \sigma_f \, f\left(\frac{\dot{\varepsilon}}{10}\right)^m \left(\frac{kg}{mm^2}\right) \tag{2.47}$$

where for

$$\overline{T} \geq 0.95\frac{C+0.41}{C+0.32} \Rightarrow \sigma_f = 0.28e^{\left(\frac{5}{\overline{T}} - \frac{0.01}{C+0.05}\right)}$$

$$m = \left(-0.019C + 0.126\right)\overline{T} + \left(0.075C - 0.05\right)$$

$$\overline{T} \leq 0.95\frac{C+0.41}{C+0.32} \Rightarrow \sigma_f = 0.28q(C,\overline{T})e^{\left[\frac{C+0.32}{0.19(C+0.41)} - \frac{0.01}{C+0.05}\right]}$$

with $$q(C,\overline{T}) = 30(C+0.9)\left[\overline{T} - 0.95\frac{C+0.49}{C+0.42}\right]^2 + \frac{C+0.06}{C+0.09}$$

and $$m = (0.081C - 0.154)\overline{T} - 0.019C + 0.207 + \frac{0.027}{C+0.32}$$

The other parameters are defined as

$$f = 1.3(5\varepsilon)^n - 1.5\varepsilon$$
$$n = 0.41 - 0.07C$$
$$\overline{T} = \frac{T + 273}{1000}$$

T = temperature in ºC, 700 < T < 1200
C = carbon content in weight per cent, C<1.2%
$\dot{\varepsilon}$ = strain rate, 0.1< $\dot{\varepsilon}$ <100 s^{-1}
ε = strain < 70 %

Shida's model was the constitutive model used in the hot rolling FEM simulation subject of this thesis work.

All constitutive equations that are dependent on the temperature are part of what is known as temperature dependent plasticity. As seen in Figure 2.19, as the temperature increases, the stress-strain curve becomes more relaxed, i.e. the slope of the elastic and plastic part decreases.

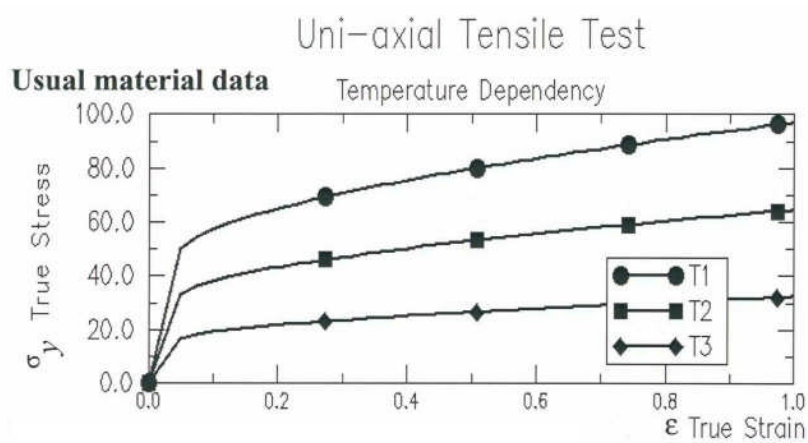

Figure 2.19: Temperature Dependent Stress-Strain Diagrams (T_3>T_2>T_1) [53] © MSC Software Corporation

The above behavior is perfectly captured by Shida's model for high temperature steel. The graphical representation of this equation is obtained by plotting the flow stress versus the strain, the strain rate and the temperature for the following ranges for each of the three independent variables:

$$0 \le \varepsilon \le 1$$
$$1 \le \dot{\varepsilon} \le 50(s^{-1})$$
$$700°C \le T \le 1200°C$$

The following plots show the Shida flow stress surfaces for strain rates of 1, 5 and 10 s^{-1} For each strain rate we obtain a different Shida flow stress surface, and within that particular surface, for every value of strain and temperature we obtain a value of flow stress. Therefore, within the ranges for each of the three independent variables, each set of three values uniquely determines a value of the flow stress. This model is particularly convenient for the hot rolling process where as the workpiece deforms, the strain, strain rate, and temperature all change simultaneously.

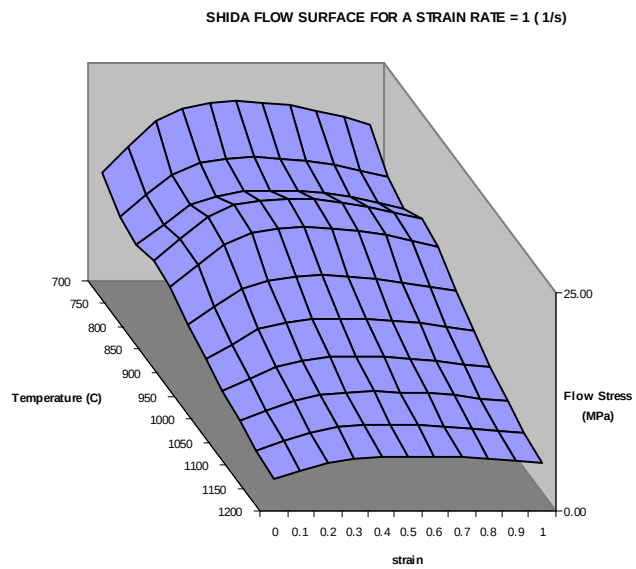

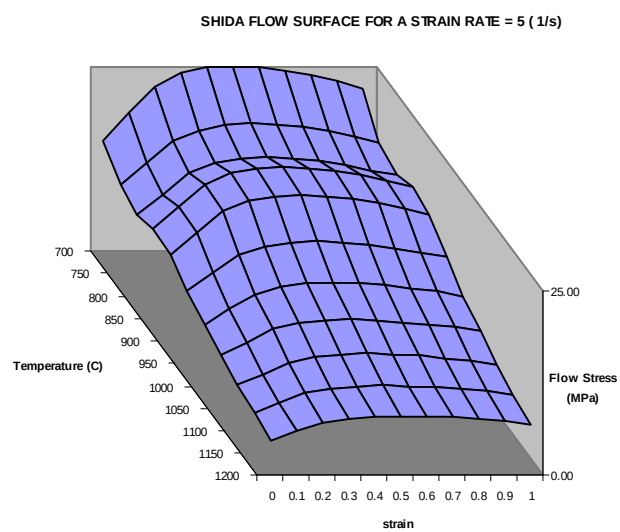

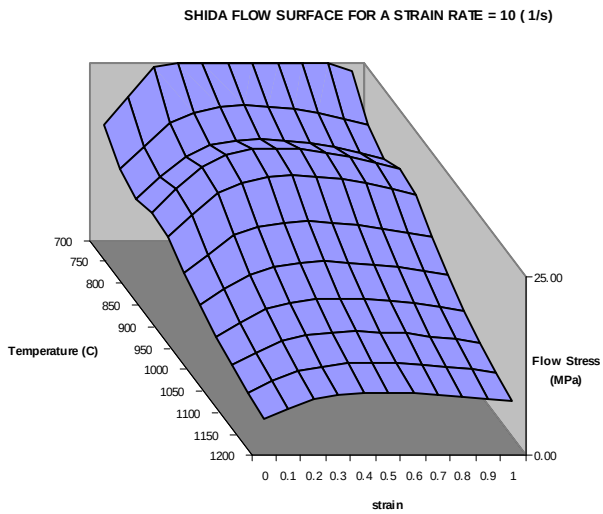

Figure 2.20: Shida Flow Stress Surfaces

2.10 Summary and Concluding Remarks

In this chapter we looked at the mathematical models and mechanical aspects of the rolling problem. Mathematical models of the flat rolling process are numerous. In each, the equations of motion, thermal balance, material properties and roll deformation are used to calculate the stress, strain, strain rate, velocity and temperature fields, the roll pressure distribution, roll separating forces and roll torques. As we saw, our mathematical model described the equations of motion of the deformed metal, the equilibrium equations of the work roll, the heat balance of the roll/strip system, the description of the frictional forces between the work roll and the metal, and the description of the material properties used to model the workpiece.

In this chapter we also took a look at the main classical mathematical rolling model, developed by von Karman. We studied the mathematical aspects of the complicated contact problem, paying attention to both the rigid-deformable, and the deformable-deformable cases and its interaction with the challenging friction that has such great influence in the rolling problem. Later in the chapter, we studied the main theory of plasticity issues, as well as the material models used in this thesis for both the cold (Ramberg-Osgood) and hot rolling (Shida) problems. Finally we studied the heat transfer and thermal balance problem looking at the five sources of heat transfer.

This chapter set up the theoretical mathematical and engineering mechanics foundations upon which we can build our FEM model on. By having a great understanding of the physics of the problem we can then model these physics into our finite element model. After all, the results the model will produce are only as good as the mechanics of the

model created. The mathematical physics of this problem lead to a second order homogeneous partial differential equation (PDE), for the thermal portion of the problem, that together with the boundary and initial conditions constitutes a thermal Initial Boundary Value Problem (T-IBVP) which we will solve using a variational approach that will be implemented into the finite element formulation. The mechanical portion of the problem leads to another set of PDEs given by the equilibrium conditions, the compatibility conditions, the constitutive equations, and the yield criterion, which together with the boundary conditions leads to another Initial Boundary Value Problem (M-IBVP) whose solution is obtained through a variational approach that requires that among the admissible velocities v_i that satisfy the conditions of compatibility and incompressibility, as well as the velocity and traction boundary conditions, the actual solution gives the mechanical functional a stationary value.

In summary, the Initial Boundary Value Problem (IBVP) we are dealing with from the thermal point of view is determined by a Partial Differential Equation (PDE) given by he heat Equation (2.8), the boundary conditions given by Equations (2.9) through (2.13).
The Mechanical IBVP is determined by Equations (2.1), (2.2), (2.3), and (2.4). The overall solution of the problem is obtained by the simultaneous solution of these two IBVPs due to the strong coupling between the mechanical and the thermal problems. There are two primary causes of coupling. First, coupling occurs when deformations result in a change in the associated heat transfer problem. Such a change can be due to either large deformation or contact. The second cause of coupling is heat generated due to inelastic deformation. The irreversibility of plastic flow causes an increase in the amount of entropy in the body, which in turns results in changes to the associated mechanical problem.

As it will be shown in chapter 3, the solution of these two IBVP will be done using numerical & variational methods. As explained by Farlow, S.J., "a partial differential equation can be changed to a system of algebraic equations by replacing the partial derivatives in the differential equation with their finite-difference approximations. The system of algebraic equations can then be solved numerically by an iterative process in order to obtain an approximate solution to the PDEs"[28]. In our case, the solution to this IBVP is found using the finite element method. Consequently, in the next chapter we will take a look at how all of this is implemented into the Finite Element Model by interpreting our PDE as the Euler-Lagrange equation of some functional, and then finding the minimizing function of the functional. The minimizing function will then be the solution of the PDE.

Chapter 3
Non-Linear Thermal Mechanical Finite Element Modeling in Rolling

3.1 Introduction

The use of the Finite Element Method (FEM) in the simulation of metal forming processes originated in the late 1960's. Fast development of finite-element simulations of metal forming processes has been observed since then. This development has been parallel to the development of supercomputers. With today's supercomputers, the application of the FEM to the simulation of manufacturing processes is becoming more and more popular. Finite element analyses of non-linear problems such as those found in metal deformation are common nowadays. The Finite Element Method allows the solution of complex Initial Boundary Value Problems (IBVPs) by combining the best of numerical methods and super computing, which allows the fast solution of the millions of equations that are generated by a finite element model.

As explained by Kobayashi, Oh, & Altan, the basic concept of the finite element method is one of *discretization*. The finite element model is constructed in the following manner. A number of finite points are identified in the domain of the function, and the values of the function and its derivatives, when appropriate, are specified at these points. The points are called *nodal points*. The domain of the function is represented approximately by a finite collection of subdomains called *finite elements*. The domain is then an assemblage of elements connected together appropriately on their boundaries. The function is approximated locally within each element by continuous functions that are uniquely described in terms of the nodal-point values associated with the particular element[44].
The path to the solution of a finite element problem consists of five specific steps:

a) identification of the problem,
b) definition of the element,
c) establishment of the element equation,
d) assemblage of the element equations,
e) numerical solution of the global equations.

The formation of element equations is accomplished by one of four approaches:

a) direct approach
b) variational methods
c) method of weighted residuals
d) energy balance approach

The basis of finite element metal flow modeling, for example, using the variational approach, is to formulate proper functionals, depending upon specific constitutive equations. The solution of the initial boundary value problem (IBVP) is obtained by the solution of the dual variational problem in which the first order variation of the functional vanishes. Choosing an approximate interpolation function (or shape function) for the field variable in the elements, the functional is expressed locally within each element in terms of the nodal-point values. The local equations are then assembled into the overall problem. Thus, the functional is approximated by a function of global nodal-point values. The condition for this function to be stationary results in the stiffness equations. These stiffness equations are then solved under appropriate boundary conditions. The

basic mathematical description of the methods, as well as the solution techniques, are given in many excellent books on the subject such as those written by Bathe, K.J.[5], Zienkiewicz, O.C.[73,74], Reddy, J.N.[60,61], Cook, R.D. [20,21], or Hughes, T.J.R. [38], as well as others that are listed in the bibliography section of this thesis.

The main advantages of the finite element method are [44]:

a) the capability of obtaining detailed solutions of the mechanics of a deforming body, namely, velocities, shapes, strains, stresses, temperatures, or contact pressure distributions,
b) the fact that a computer code, once written, can be used for a large variety of problems by simply changing the input data.

In the remainder of this chapter we will take an in depth look at the flow formulation (rigid-plastic & rigid-viscoplastic) finite element model, and a less rigorous look at the elastic-plastic finite element model corresponding to the solid formulation. We will also study the finite element model for the heat transfer part of this problem, as well as examine how the finite element model handles the coupling between the mechanical and thermal portions of this complex problem. Finally, we will study the main non-linearities present in this highly non-linear problem.

3.2 The Finite Element Formulation – Variational Approach

Out of the 4 approaches for the derivation of the basic equations for the finite-element analysis we have just stated in section 3.1, the variational method and the weighted residual method are the most commonly used for finite element flow modeling.

The duality of the boundary value problem and the variational problem can be seen clearly by considering the use of the functional [47,35]

$$\pi(u) = \int_a^b F(x,u,u')dx \text{, a} \leq \text{x} \leq \text{b} \tag{3.1}$$

where x is the coordinate, u is the field variable, and u' is the derivative of u with respect to x. Then using the theory of calculus of variations, $\delta\pi(u)= 0$, breaks down into two parts, that of the domain, and that of the boundary as follows:

$$\delta\pi(u) = \int_a^b \delta F dx = \int_a^b \left[\frac{\partial F}{\partial u}\delta u + \frac{\partial F}{\partial u'}\frac{'d(\delta u)}{dx} \right] dx \tag{3.2}$$

Integrating the second term by parts, we have

$$\delta\pi(u) = \int_a^b \left[\frac{\partial F}{\partial u} - \frac{d}{dx}\left(\frac{\partial F}{\partial u'} \right) \right] \delta u dx + \left[\frac{\partial F}{\partial u'} \delta u \right]_a^b \tag{3.3}$$

Thus,

$$\delta\pi(u) = \int_v \{Euler\ Equation\}\ \delta u dV + \{\text{the boundary term}\} \tag{3.4}$$

The Euler equation is a differential equation taken over the domain V that is argued to be zero because of the arbitrariness of δu. Given the differential equations, the functional π and the boundary terms can often be constructed by manipulation.

For our boundary value problem, the *variational approach* is based on one of two variational principles. It requires that "among admissible velocities v_i that satisfy the conditions of compatibility and incompressibility, as well as the velocity boundary conditions, the actual solution give the following functional (function of functions) a stationary value:

$$\pi = \int_V \bar{\sigma}\dot{\bar{\varepsilon}} dV - \int_{S_F} F_i v_i dS \tag{3.5a}$$

for rigid-plastic materials, and

$$\pi = \int_V E(\dot{\varepsilon}_{ij}) dV - \int_{S_F} F_i v_i dS \tag{3.5b}$$

for rigid-viscoplastic materials, where $\bar{\sigma}$ is the effective stress, $\dot{\bar{\varepsilon}}$ is the effective strain rate, F_i represents the surface tractions, and $E(\dot{\varepsilon}_{ij})$ is the work function, such that, $s_{ij} = \dfrac{\partial E}{\partial \dot{\varepsilon}_{ij}}$, where s_{ij} denote the deviatoric stresses" [44].

The solution of the original boundary value problem is then obtained from the solution of the dual variational problem, where the first-order variation of the functional vanishes, namely,

$$\delta\pi = \int_V \bar{\sigma}\delta\dot{\bar{\varepsilon}} dV - \int_{S_F} F_i \delta v_i dS = 0 \tag{3.6}$$

where $\bar{\sigma} = \bar{\sigma}(\bar{\varepsilon})$ and $\bar{\sigma} = \bar{\sigma}(\bar{\varepsilon}, \dot{\bar{\varepsilon}})$ for rigid-plastic and rigid viscoplastic materials, respectively. The incompressibility constraint on admissible velocity fields in Equation

(3.6) may be removed by introducing a Lagrange multiplier λ and modifying the functional (3.5a) by adding the term $\int \lambda \dot{\varepsilon}_v dV$, where $\dot{\varepsilon}_v = \dot{\varepsilon}_{ii}$, is the volumetric strain rate. Then,

$$\delta\pi = \int_V \bar{\sigma}\delta\dot{\bar{\varepsilon}}dV + \int_V \lambda\delta\dot{\varepsilon}_v dV + \int_V \dot{\varepsilon}_v\delta\lambda dV - \int_{S_F} F_i\delta v_i dS = 0 \tag{3.7}$$

Another way of removing the constraint is to use the penalized form of the incompressibility [73,47] as

$$\delta\pi = \int_V \bar{\sigma}\delta\dot{\bar{\varepsilon}}dV + K\int_V \dot{\varepsilon}_v\delta\dot{\varepsilon}_v dV - \int_{S_F} F_i\delta v_i dS = 0 \tag{3.8}$$

where K, a penalty constant, is a very large positive constant, δv_i and $\delta\lambda$ are arbitrary variations, and $\delta\dot{\bar{\varepsilon}}$ and $\delta\dot{\varepsilon}_v$ are the variations in strain rate derived from δv_i. Equation (3.7) or (3.8) is the basic equation for finite element formulation.

An alternative approach to Equation (3.7) is to begin with a weak form of the equilibrium equations, namely [44,61]

$$\int_V \frac{\partial\sigma_{ij}}{\partial x_j}\delta v_i dV = 0 \tag{3.9}$$

where δv_i is an arbitrary variation in v_i. Equation (3.9) becomes

$$\int_V \sigma_{ij}\frac{\partial(\delta v_i)}{\partial x_j}dV - \int_V \frac{\partial}{\partial x_j}(\sigma_{ij}\delta v_i)dV = 0 \tag{3.10}$$

which is the expression of the virtual-work principle, if δv_i is considered to be the virtual motion. Using the symmetry of the stress tensor and the divergence theorem, we have

$$\int_V \sigma_{ij}\delta\dot{\varepsilon}_{ij}dV - \int_{S_F} F_i\delta v_i dS = 0 \tag{3.11}$$

For the surface integral term in (3.11), the boundary conditions that δv_i=0 on S_v (essential boundary condition) and the tractions $F_i = \sigma_{ij}n_j$ on S_F (suppressible boundary condition), are imposed.

Substituting the expression for the Cauchy stress $\sigma_{ij} = s_{ij} + \delta_{ij}\sigma_m$, where $\sigma_m = \frac{1}{3}\sigma_{kk}$ is the hydrostatic or mean stress, into Equation (3.11) gives

$$\int_V s_{ij}\delta\dot{\varepsilon}_{ij}dV + \int_V \sigma_m \delta\dot{\varepsilon}_v dV - \int_{S_F} F_i \delta v_i dS = 0 \tag{3.12}$$

From the constitutive equation and the definition of $\dot{\bar{\varepsilon}}$, it is seen that, $s_{ij}\delta\dot{\varepsilon}_{ij} = \bar{\sigma}\delta\dot{\bar{\varepsilon}}$, and the final form of Equation (3.12) suitable for finite element formulation becomes

$$\int_V \bar{\sigma}\delta\dot{\bar{\varepsilon}}dV + \int_V \sigma_m \delta\dot{\varepsilon}_v dV - \int_{S_F} F_i \delta v_i dS = 0 \tag{3.13a}$$

with the incompressibility constraint given by $\dot{\varepsilon}_v = 0$ in V. The incompressibility constraint is removed by modifying Equation (3.13a) as

$$\int_V \bar{\sigma}\delta\dot{\bar{\varepsilon}}dV + \int_V \sigma_m \delta\dot{\varepsilon}_v dV + \int_V \delta\sigma_m \dot{\varepsilon}_v dV - \int_{S_F} F_i \delta v_i dS = 0 \tag{3.13b}$$

By comparison of Equations (3.7) and (3.8) to Equation (3.13b), the Lagrangian multiplier λ in Equation (3.7) is identified as the mean or hydrostatic stress σ_m, where $\sigma_m = \frac{K}{2}\dot{\varepsilon}_v$, thus providing the interpretation of K as a constant similar to the bulk modulus.

Equation (3.7) or (3.8) is the basic equation for the finite element discretization. Once the solution of the velocity field that satisfies the basic equation is obtained, then corresponding stresses can be calculated using the flow rule and the known mean stress distribution [44].

We will now look at the two main formulations used in the application of FEM to metal forming, namely, the flow formulation and the solid formulation. Flow formulation assumes that the deforming material has negligible elastic response, while solid formulation includes elasticity. Then we will develop the finite element equations for each of these two formulations, solid and flow, starting from Equation (3.7) or (3.8) which as we have just seen is the basic equation for finite element formulation.

3.3 Approaches to the Simulation of Metal Forming Processes

As observed by Lenard, Pietrzyk, & Cser, there are two major and distinct approaches to the simulation of metal forming processes.

The first is the *solid-state incremental approach*, also known as *solid formulation* (considers finite deformation), which usually employs elastic-plastic or elastic-viscoplastic material models. This approach uses a Lagrangian description of motion.

The nodal displacements are the basic unknowns, which are related to the strains by the standard kinematic expressions or strain-displacement relationships [73]. The constitutive model used relates the stresses and the strains through stress-strain or constitutive relationships expressed in incremental form. The equilibrium equations can be written either as differential equations, to be satisfied in the volume and on the boundary of the body, or in a variational form as done by the principle of virtual work.

The second approach, the *flow formulation* (based on infinitesimal deformation theory), uses the *rigid-plastic* or *rigid-viscoplastic* material models [44]. Since in metal forming operations, the non-linear plastic strains are much larger than the elastic strains, these last ones are usually neglected allowing the use of a simpler rigid-plastic model in the analysis. The resulting constitutive equations in this approach are identical to those of a non-Newtonian fluid. The constitutive equations now relate the stresses and the strain rates. Various constitutive models are used in the flow formulation. These include the Levy-Mises model used in rigid-plastic solutions, as well as visco-plastic models such as the *Norton-Hoff law* or the *Sellars-Tegart law* [49,56].
The main advantage of the flow formulation (rigid-plastic method) is that the power of deformation is calculated as a product of the invariants of the stress tensor and the strain rate tensor, making the solution insensitive to rotations. Also, the resistance of the material to deformation can be introduced as a function of the strain rate, strain and temperature, and essentially any type of approximating function can be used. The rigid-plastic method is more suitable for the large, non-linear plastic deformations found in the hot rolling process [49].

As explained in Chapter 2, the original problem associated with the deformation process, of materials, is a *boundary value problem*. For the deformation process of rigid-viscoplastic materials, *flow formulation*, the boundary-value problem is stated as follows: at a certain stage in the process of quasistatic distortion, the shape of the body, the internal distribution of temperature, and the current values of material parameters are supposed to be given or to have been determined already. The velocity vector v_i is prescribed on a part of the surface S_v together with traction F_i on the remainder of the surface, S_F. Solutions to this problem are the stress and velocity distributions that satisfy the governing equations and the boundary conditions.

In the *solid formulation* approach, the boundary value problem is stated such that, in addition to the current states of the body, the internal distribution of the stress also is supposed to be known and the boundary conditions are prescribed in terms of velocity and traction-rate. Distributions of velocity and stress-rate (or displacement and stress-increment) are the solutions to this problem. The solid formulations of the finite element method for metal forming problems have been based on the use of the *Prandtl-Reuss* equations for elastic-plastic materials. The formulation is given in the rate form and assumes the infinitesimal theory of deformation. In analyzing metal-forming processes, however, the elastic-plastic finite element method with infinitesimal formulation has severe drawbacks. The large amount of rotation involved in metal forming rules out infinitesimal analysis. Furthermore, the nature of elastic-plastic constitutive equations

requires short time steps in nonsteady-state analysis, a requirement that is severe when the body goes from elastic to plastic deformations.

A simplified solution to this problem is given by the *flow formulation* where the elastic portion of deformation is neglected all plastic deformation is treated as a *flow problem*. The flow formulation of the finite element method for metal forming processes is based on the *Levy-Misses* plasticity model for rigid plastic materials, which assumes that work hardening is negligible. A very important improvement was the inclusion of the effects of strain-rate and temperature in material properties and of thermal-mechanical coupling, in the solution. This development has extended the finite element analysis into the warm and hot working range and allowed us to successfully model the hot rolling process as we will see in Chapter 4.

3.4 The Rigid- Plastic Flow Finite Element Model

The rigid-plastic flow analysis is an approach to large deformation analysis, which can be used for metal forming problems such as hot rolling. The rigid-plastic formulation takes into account only the plastic contribution to the total strain rate, ignoring the elastic part:

$$\dot{\varepsilon} = \dot{\varepsilon}^{p} \tag{3.14}$$

According to Lenard & Pietrzyk, two formulations are available: Eulerian (steady state) and Lagrangian (transient). The effects of elasticity are not included in the R-P formulation, and if they are important, such as in cold rolling, the elastic-plastic formulation must be used.
The rigid-plastic formulation needs to enforce the incompressibility condition, which is inherent to the strictly plastic type of material response being considered. Incompressibility may be imposed in three ways:

1. Lagrange Multipliers
2. Penalty functions $\rightarrow K = \dfrac{E}{6(1-2\nu)}$ (one half of the bulk modulus)
3. Updating the thickness (for plane stress analysis)

The *rigid-plastic flow formulation* is based on iteration for the velocity field in an incompressible, non-Newtonian fluid. The normal flow condition for a nonzero strain rate is given by the Levy-Mises flow rule that can be expressed as [35]

$$\dot{\varepsilon}_{ij} = \frac{3}{2}\frac{\dot{\bar{\varepsilon}}}{\bar{\sigma}} \tag{3.15}$$

where $\dot{\bar{\varepsilon}} = \sqrt{\frac{2}{3}\dot{\varepsilon}_{ij}\dot{\varepsilon}_{ij}}$ is the equivalent strain rate, and $\bar{\sigma} = \sqrt{\frac{3}{2}s_{ij}s_{ij}}$ is the equivalent stress (which may be rate dependent) and $s_{ij} = \sigma_{ij} - \frac{1}{3}\delta_{ij}\sigma_{kk}$ gives the deviatoric stress.

The effective viscosity is evaluated as $\mu = \frac{2}{3}\frac{\bar{\sigma}}{\dot{\bar{\varepsilon}}}$ and so when $\dot{\bar{\varepsilon}} \to 0, \mu \to \infty$ and we then have rigid plasticity.

In rigid plastic flow analysis, several iterations are required at any given increment, the greatest number occurring in the first increment. Subsequent increments require fewer iterations, since the initial iteration can make use of the solution from the previous increment. Due to the simplicity of the rigid plastic formulation, it is possible to bypass stress recovery for all iterations but the last in each increment, provided that the displacement control is used. In such cases, considerable savings in execution time are achieved [56].

The Steady-State rigid-plastic flow formulation is based on a Eulerian reference system. The nodal coordinates are updated at the end of a step according to the relation

$$x_i^n = x_i^{n-1} + \dot{u}_i^n \Delta t \tag{3.16}$$

where n refers to the step number, $\dot{u}_i^n$ is the nodal velocity component, and Δt is an arbitrary time step. Δt is selected in such a way as to allow only a reasonable change in mesh shape while ensuring stability with each step. Updating the mesh requires judicious selection for a time step. This requires some knowledge of the magnitude of the nodal velocities that will be encountered. The time step should be selected such that the strain increment is never more than one per cent for any given increment.

In the transient (Lagrangian) analysis procedure, there is an automatic updating of the mesh at the end of each increment. During the analysis, the updated mesh may exhibit severe distortion and the solution may be unable to converge. Mesh rezoning must be used in that case to overcome this difficulty.

With respect to the hot rolling problem, the development of computational techniques allowed the finite element method to simulate both thermal and mechanical events in the deformation zone. The first application of the finite element method to analyze the temperature distribution in a strip during hot rolling appears to be due to Zienkiewicz in 1981.

The rigid-plastic flow FEM model described here is based on the work by Kobayashi et al., and by Pietrzyk and Lenard and contains two parts. The first part determines the velocity field, the strain rate and the strain fields using the rigid plastic FE approach. The second part deals with heat transfer and heat generation within the strip.

Rigid-Plastic finite element models are the most efficient tools in the simulation of metal forming processes and it gives very accurate results for hot rolling. They combine the

accuracy of the finite-element technique with reasonable computing times and memory requirements.

The rigid plastic approach is based on an extremum principle which states that for a plastically deforming body of volume V, under traction F_i, prescribed on a part of the surface S_F, and the velocity $\bar{v}$ prescribed on the remainder of the surface S_v, under the constraint $\dot{\varepsilon}_v = 0$ the actual solution minimizes the functional previously seen in Section 3.2 and given by Equation (3.5),

$$\pi = \int_V \bar{\sigma}\dot{\bar{\varepsilon}} dV + \int_V \lambda \dot{\varepsilon}_v dV - \int_{S_F} F_i v_i dS \tag{3.17}$$

where

$\lambda =$ Lagrange multiplier (equal to the mean stress σ_m)
$\bar{\sigma} =$ equivalent or effective stress

$\dot{\bar{\varepsilon}} = \sqrt{\frac{2}{3}\dot{\varepsilon}_{ij}\dot{\varepsilon}_{ij}}$ = equivalent or effective strain rate

$\dot{\varepsilon}_v =$ volumetric strain rate

In the flow theory of plasticity, strain rates are related to stresses by the flow rule associated with the criterion of Levy-Mises,

$$s_{ij} = \frac{2}{3}\frac{\bar{\sigma}}{\dot{\bar{\varepsilon}}}\dot{\varepsilon}_{ij} \tag{3.18}$$

For the 2-D Plane-Strain problem, the discretization of the functional π is performed in a typical finite element manner using four node quadrilateral elements (linear isoparametric element) for discretization as shown in Figure 3.1

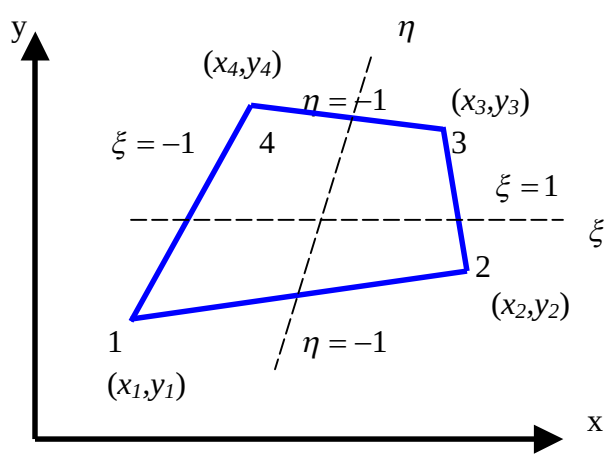

Figure 3.1: Quadrilateral element and natural coordinate system

The velocity field $\bar{v}$ inside the element is approximated by shape functions in terms of nodal point velocity values as

$$\bar{v} = \begin{bmatrix} v_x \\ v_y \end{bmatrix} = N^T v \tag{3.19}$$

where

$v = \{v_1, v_2, ..., v_8\}^T$ is the vector of nodal velocities (4 nodes x 2 DOF/node)

N is the matrix of shape functions N_1, N_2, N_3, N_4, which for four node elements and plane strain is

$$N = \begin{bmatrix} N_1 & 0 & N_2 & 0 & N_3 & 0 & N_4 & 0 \\ 0 & N_1 & 0 & N_2 & 0 & N_3 & 0 & N_4 \end{bmatrix} \tag{3.20}$$

with

$$N_1 = \frac{1}{4}(1-\xi)(1-\eta), \quad N_2 = \frac{1}{4}(1+\xi)(1-\eta)$$

$$N_3 = \frac{1}{4}(1+\xi)(1+\eta), \quad N_4 = \frac{1}{4}(1-\xi)(1+\eta) \tag{3.21}$$

Similarly, a discretization of the external traction yields

$$\bar{F} = \begin{bmatrix} T_x \\ T_y \end{bmatrix} = N^T F \tag{3.22}$$

where

F = vector of the nodal values of the friction stress

It is convenient to arrange the strain-rate components in a vector form. For plane strain $\dot{\varepsilon}_z = 0$

$$\dot{\varepsilon} = \begin{bmatrix} \dot{\varepsilon}_x \\ \dot{\varepsilon}_y \\ \dot{\gamma}_{xy} \end{bmatrix} = \begin{bmatrix} \dfrac{\partial v_x}{\partial x} \\ \dfrac{\partial v_y}{\partial y} \\ \dfrac{\partial v_y}{\partial x} + \dfrac{\partial v_x}{\partial y} \end{bmatrix} = Bv \tag{3.23}$$

which gives us a relationship between the strain rate field inside the element and the nodal velocities and where B is the matrix of the derivatives of shape functions given by [74]

$$B = \begin{bmatrix} \dfrac{\partial N_1}{\partial x} & 0 & \dfrac{\partial N_2}{\partial x} & 0 & \dfrac{\partial N_3}{\partial x} & 0 & \dfrac{\partial N_4}{\partial x} & 0 \\ 0 & \dfrac{\partial N_1}{\partial y} & 0 & \dfrac{\partial N_2}{\partial y} & 0 & \dfrac{\partial N_3}{\partial y} & 0 & \dfrac{\partial N_4}{\partial y} \\ \dfrac{\partial N_1}{\partial y} & \dfrac{\partial N_1}{\partial x} & \dfrac{\partial N_2}{\partial y} & \dfrac{\partial N_2}{\partial x} & \dfrac{\partial N_3}{\partial y} & \dfrac{\partial N_3}{\partial x} & \dfrac{\partial N_4}{\partial y} & \dfrac{\partial N_4}{\partial x} \end{bmatrix} \tag{3.24}$$

The volumetric strain rate $\dot{\varepsilon}_v$ is expressed by

$$\dot{\varepsilon}_v = \dot{\varepsilon}_x + \dot{\varepsilon}_y = C^T v \tag{3.25}$$

where

$$C^T = \{1\ 1\ 0\} B \tag{3.26}$$

The effective strain rate, $\dot{\bar{\varepsilon}}$, in a discrete form is expressed by

$$\dot{\bar{\varepsilon}} = \sqrt{\dot{\varepsilon}^T D \dot{\varepsilon}} = \sqrt{v^T B^T D B v} = \{P = B^T D B\} = \sqrt{v^T P v} \tag{3.27}$$

The matrix D is given by

$$D = \begin{bmatrix} \dfrac{2}{3} & 0 & 0 \\ 0 & \dfrac{2}{3} & 0 \\ 0 & 0 & \dfrac{2}{3} \end{bmatrix} \tag{3.28}$$

During discretization, the volume V of the body is divided into n_e elements connected at n_n nodes.

The functional for a single element is given by Equation (3.17). Substituting components and expressing in matrix form,

$$\pi = \int_V \bar{\sigma}\sqrt{v^T P v}\,dV + \int_V \lambda C^T v\,dV - \int_{S_F} N^T F N v\,dS \tag{3.29}$$

The functional for the whole deforming domain is the sum of the functionals for the elements. This functional is discretized and a set of nonlinear simultaneous equations (stiffness equations) is obtained from the arbitrariness of δv and $\delta\lambda$ as follows.

$$\frac{\partial \pi}{\partial v} = 0 \quad \& \quad \frac{\partial \pi}{\partial \lambda} = 0 \tag{3.30}$$

Differentiation of the functional π with respect to the nodal velocities and to the Lagrange multiplier at the elemental level and assembling them into the global equation under appropriate constraints yields the stiffness equations:

$$\frac{\partial \pi}{\partial v} = \sum_j \left[\int_{V_j} \frac{\bar{\sigma}}{\dot{\bar{\varepsilon}}} P v\,dV + \int_{V_j} \lambda C^T dV - \int_{S_{Fj}} N^T F N\,dS \right] = 0 \tag{3.31}$$

$$\frac{\partial \pi}{\partial \lambda} = \sum_j \left[\int_{V_j} C^T v\,dV \right] = 0 \tag{3.32}$$

These last two equations form a set of non-linear equations with nodal velocities v and Lagrange multiplier λ as unknowns, where j indicates the quantity at the jth element.
The solution is obtained iteratively by using the Newton-Raphson method. The method consists of linearization and application of convergence criteria to obtain the final solution. Linearization is achieved by Taylor expansion near an assumed solution point $v = v_0$ (initial guess), namely

$$\left[\frac{\partial \pi}{\partial v_i}\right]_{v=v_0} + \left[\frac{\partial^2 \pi}{\partial v_j}\right]_{v=v_0} \Delta v_j = 0 \tag{3.33}$$

where Δv_j is the first-order correction of the velocity v_0. Equation (3.31) can be written in the form

$$K\Delta v = f \tag{3.34}$$

where K is called the stiffness matrix, and f is the residual of the nodal point force vector. Once the solution of Equation (3.34) for the velocity correction Δv is obtained, the assumed velocity is updated according to $v_0 + \alpha\Delta v$, where α is a constant between 0 and 1 called deceleration coefficient. Iteration is continued until the velocity correction terms become negligibly small. There are two primary methods for iterating through the solution of changing material stiffnesses. At each load step, the iterative process can progress in one of two ways: a Newton-Raphson solution or a modified Newton-Raphson solution. Figures 3.2 and 3.3 illustrate these methods on a load versus displacement curve. Each peak represents separate stiffness update iteration within a load step. The solver has a limit that can be adjusted for the maximum number of iterations within a load step.

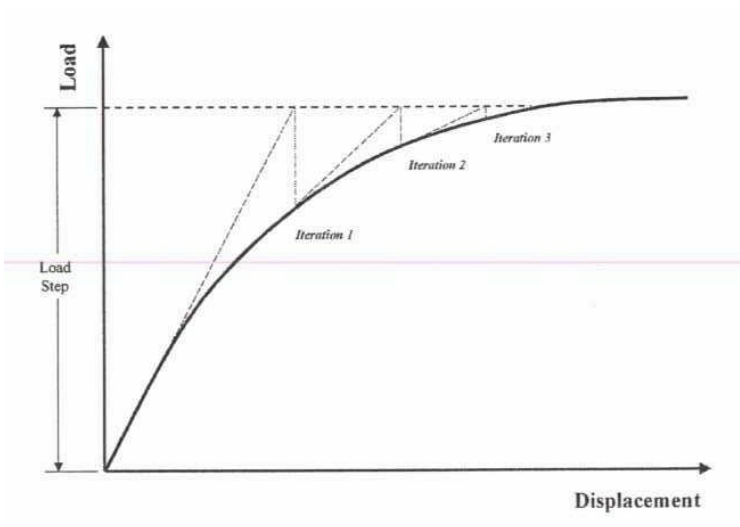

Figure 3.2: Newton-Raphson method for stiffness updates [53] © MSC Software Corporation

The *Newton-Raphson solution* uses the tangent modulus corresponding to the previous iteration to calculate the next deformed position. The calculated displacement is projected back onto the load displacement curve parallel to the load axis. The difference in load between the load step force and the projected position is subtracted from the load step and the next displacement is calculated at the tangent modulus of the projected position. The stiffness continues to update until the difference between the load step magnitude and the projected position is within some tolerance [2,73].

An alternative to the straight Newton-Raphson method is the *modified Newton-Raphson method*. In this method, the stiffness update uses the tangent modulus of the previously converged load step for each iteration. Hence, many more iterations are required to

complete a load step but the solution is much more likely to converge under many more conditions.

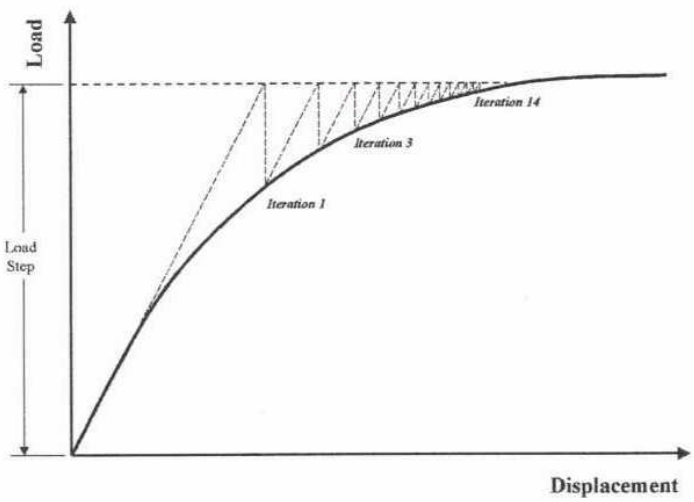

Figure 3.3: Modified Newton-Raphson method [53] © MSC Software Corporation

Two convergence criteria may be used. One measures the error norm of the velocities

$$\left|\frac{\Delta v}{v}\right| = \sqrt{\frac{\sum_{i=1}^{n}(\Delta v_i)^2}{\sum_{i=1}^{n}(v_i)^2}} < \delta \tag{3.35}$$

where

n is the number of degrees of freedom,

Δv is the increment of nodal velocity and

δ is the convergence criterion, which is usually taken to be between 0.001 and 0.0001.

The convergence criteria require such an error norm to decrease from iteration to iteration until the final convergence criterion δ is achieved. The other criterion requires the norm of the residual equations, $\left|\frac{\partial \pi}{\partial v}\right|$, to decrease.

In general terms, the first criterion is most useful in the early stages of iteration, when the velocity field is still far from the solution. The second test is most useful when slightly ill conditioned systems reach the final stage of iterations. The final solution is achieved when the error norm reaches a specified value, usually around 5×10^{-5}

The finite element method procedures outlined above are implemented in a computer program in the following way according to Kobayashi et al.:

a) Generate an assumed solution velocity,

b) Evaluate the elemental stiffness matrix for the velocity correction term Δv in Equation (3.34),
c) Impose the velocity conditions to the elemental stiffness matrix, and repeat step b) over all elements defined in the workpiece,
d) Assemble elemental stiffness matrix to form a global stiffness equation,
e) Obtain the velocity correction terms by solving the global stiffness equation,
f) Update the assumed velocity by adding the correctional term to the assumed velocity. Repeat steps b) through f) until the velocity solution converges,
g) When the converged velocity solution is obtained, update the geometry of the workpiece using the velocity of nodes during a time increment. Steps b) through g) are repeated until the desired degree of deformation is achieved.

3.5 The Rigid-Viscoplastic Material Model

Most of the common constitutive laws for idealizing materials are obtained from experimental tests. The tests show that the deformed metals exhibit temperature, strain and strain rate sensitivity. A material behavior that exhibits rate sensitivity is called viscoplastic [48].
There are a number of materials that exhibit viscoplastic behavior. They include most metals at high temperature, superplastic materials, heated glass, and polymers. When the deformation is large, most of them can be considered to be rigid-viscoplastic. This is the case of the hot rolling problem.
Because of the importance of the application of viscoplastic behavior to the metal-forming processes, several researchers have examined the treatment of time-dependent material behavior within the framework of the theory of viscoplasticity. Zienkiewicz has shown the feasibility of the finite element approach in the deformation analysis of rigid-viscoplatic materials by treating them as non-Newtonian viscous fluids [73]. Others have applied this formulation to creep forming.

In cold forming processes, the strain is the major factor affecting the yield stress, while the influence of the other two parameters is negligible. Thus, a typical elastic-plastic description of the material's resistance to deformation is the most suitable for these processes. The yield stress σ_Y in the Levy-Mises flow rule is given in the form of a strain-hardening curve.

In hot deformation processes, the majority of metals are also sensitive to changes of temperature and strain rate, and the influence of these parameters is often much stronger than the influence of strain. The behavior of these materials is well described by rigid-plastic flow and also by the visco-plastic flow rule, which is expressed by a visco-plastic potential. Two commonly used visco-plastic laws are the Norton-Hoff law and the Sellars-Teggart law [56].

The *Norton-Hoff Law*, also known as *viscoplastic power law*, was first used for uniaxial creep analysis by Norton in 1929 and extended to three dimensions by Hoff in 1953. It is generally written in the form:

$$\bar{\sigma} = 2K(\sqrt{3}\dot{\varepsilon}_i)^{m-1}\dot{\bar{\varepsilon}} \tag{3.36}$$

- m=1 corresponds to the Newtonian fluid with a viscosity $\eta = K$
- m=0 is the plastic flow rule for a material obeying the Levy-Mises yield criterion with a yield stress $\sigma_y = \sqrt{3K}$
- 0<m<1 is the first approximation for hot forming of metals

For most common metals m lies between 0.1 and 0.2 but for a superplastic material it can reach values between 0.5 and 0.7.

The *Sellars-Teggart Law* for three-dimensional problems is written as (Sellars & Teggart, 1972):

$$\bar{\sigma} = \frac{2}{3\alpha}\sinh^{-1}\left(\frac{\dot{\varepsilon}_i}{A}\right)\frac{\dot{\bar{\varepsilon}}}{\dot{\varepsilon}_i} \tag{3.37}$$

Analysis of both laws shows that the second derivative of the viscoplastic potential tends to infinity when the strain rate tends to zero. Therefore, a normalized Norton-Hoff law is suggested:

$$\bar{\sigma} = 2K\left(\sqrt{3}\right)^{m-1}\left(\dot{\varepsilon}_0^2 + \dot{\varepsilon}_i^2\right)^{\frac{m-1}{2}}\dot{\bar{\varepsilon}} \tag{3.38}$$

where

$\dot{\varepsilon}_0$ = small constant such that if $\dot{\varepsilon}_i >> \dot{\varepsilon}_0$ Equation (3.38) becomes nearly identical to Equation (3.36) and when $\dot{\varepsilon}_i << \dot{\varepsilon}_0$, the constitutive law tends to become purely Newtonian [56].

Visco-plastic material models are commonly used in the finite element simulations of metal forming processes. The domain V is discretized into finite elements in the usual way. The unknown velocity field is discretized and an analytical description of this field within an element is obtained by the interpolation $\bar{v} = Nv$. The general form of the visco-plastic functional for the Norton-Hoff law, after discretization is:

$$\pi = \int_V \frac{K}{m+1}\left(\sqrt{3}\dot{\varepsilon}_i\right)^{m+1} dV + \int_V \lambda\dot{\varepsilon}_v dV - \int_{S_F} F_i v_i dS \tag{3.39}$$

Differentiation of the functional π with respect to the nodal velocities yields a set of nonlinear equations, which is usually solved by the Newton-Raphson method.

3.6 Heat Transfer Finite Element Modeling in Rolling

A complete analysis of the rolling process also requires the simulation of heat transfer in the roll gap, making it necessary to couple the solution for the flow formulation with the thermal model. Temperatures are calculated, accounting for heat conduction in the material, heat generation due to plastic work, friction, and heat losses due to transfer to the surrounding medium.

According to Kobayashi, Oh, & Altan, "the importance of temperature calculations during a metal forming process has been recognized for a long time. Until recently, the majority of the work had been based on procedures that uncoupled the problem of heat transfer from the metal transformation problem. Several researchers have used this approach. They determined the flow velocity fields in the problem either experimentally or by calculations, and then they used these fields to calculate heat generation" [44].
In order to handle a coupled thermo-viscoplastic deformation problem, it is necessary to solve simultaneously the material-flow problem for a given temperature distribution and the heat transfer equations. Zienkiewicz et al discussed numerical solutions of such forming problems, with examples of steady flow in extrusion, drawing, rolling, and sheet metal forming. Kobayashi developed the method for a coupled analysis of transient viscoplastic deformation and heat transfer applied to solid cylinder compression and ring compression.

As seen in Chapter 2, Section 2.7.1, the general diffusion equation is [39]

$$\frac{\partial}{\partial x}\left(k\frac{\partial T}{\partial x}\right)+\frac{\partial}{\partial y}\left(k\frac{\partial T}{\partial y}\right)+\frac{\partial}{\partial z}\left(k\frac{\partial T}{\partial z}\right)+\dot{q}-C_p\rho\frac{\partial T}{\partial t}=0 \tag{3.40}$$

where

k = heat conduction coefficient
T = temperature (K)
$\dot{q} = \eta\bar{\sigma}_{ij}\dot{\bar{\varepsilon}}_{ij} =$ rate of heat generation (W/m^3)
C_p=specific heat (J/kg K)
ρ = material's density (kg / m^3)
t = time (s)

Solution of the diffusion equation must satisfy the specified boundary conditions that were mentioned in Section 2.5. Along the boundaries of the deforming material, either

the temperature T is prescribed or a heat flux is given. As explained by Kobayashi, Oh, & Altan in their derivation, the energy balance Equation (3.40) can be written in the form

$$\int_V k\frac{\partial^2 T}{\partial x_i}\delta T dV - \int_V C_p \rho \frac{\partial T}{\partial t}\delta T dV + \int_v \eta \bar{\sigma}_{ij}\dot{\bar{\varepsilon}}_{ij}\delta T dV = 0 \tag{3.41}$$

for arbitrary variation in temperature δT. By using the divergence theorem, Equation (3.41) becomes

$$\int_V k\frac{\partial T}{\partial x_i}\delta\left(\frac{\partial T}{\partial x_i}\right)dV + \int_V \rho C_p \frac{\partial T}{\partial t}\delta T dV - \int_V \eta \bar{\sigma}_{ij}\dot{\bar{\varepsilon}}_{ij}\delta T dV - \int_{S_q} q_n \delta T dS = 0 \tag{3.42}$$

where q_n is the heat flux across the boundary surface S_q, n denotes the unit normal to the boundary surface and

$$q_n = k\frac{\partial T}{\partial n} \tag{3.43}$$

Solutions to problems of this nature require the temperature field to satisfy the prescribed boundary temperatures and Equation (3.7.4) for arbitrary perturbation δT.

For the finite element formulation the temperature field in Equation (3.42) is approximated by

$$T = \sum_\alpha q_\alpha T_\alpha = N^T T \tag{3.44a}$$

where q_α is the shape function and T_α is the temperature at α^{th} . With the quadrilateral element shown in Figure 3.3,

$$N^T = \{N_1, N_2, N_3, N_4\} \tag{3.44b}$$

$$T^T = \{T_1, T_2, T_3, T_4\} \tag{3.44c}$$

where N_1, N_2, N_3, N_4 are given by Equations (3.21)

$$M = \begin{bmatrix} \frac{\partial N_1}{\partial x} & \frac{\partial N_1}{\partial y} \\ \frac{\partial N_2}{\partial x} & \frac{\partial N_2}{\partial y} \\ \frac{\partial N_3}{\partial x} & \frac{\partial N_3}{\partial y} \\ \frac{\partial N_4}{\partial x} & \frac{\partial N_4}{\partial y} \end{bmatrix} \tag{3.45}$$

and substituting Equation (3.44) into Equation (3.42)

$$\sum_j \left[\int_{V_j} k\delta T^T MM^T T dV + \int_{Vj} \rho C_p \delta T^T NN^T \frac{\partial T}{\partial t} dV - \int_{V_j} \eta(\overline{\sigma}\dot{\varepsilon})\delta T^T N dV - \int_{S_{q_j}} q_n \delta T^T N dS = 0 \right]$$

(3.46)

Because of the arbitrariness of δT, the following system of equations is obtained,

$$\sum_j \left[\int_{V_j} kMM^T dVT + \int_{V_j} \rho C_p NN^T dV \frac{\partial T}{\partial t} - \int_{V_j} \eta(\overline{\sigma}\dot{\varepsilon}) N dV - \int_{S_{q_j}} q_n N dS \right] = 0 \tag{3.47}$$

The set of equations given by (3.47) can be expressed in the form

$$C\dot{T} + K_c T = Q \tag{3.48}$$

where C is the heat capacity matrix, K_c is the heat conduction matrix, Q is the heat flux vector, T is the vector of nodal point temperatures, and $\dot{T}$ the vector of nodal point temperature-rates. The heat flux vector Q in Equation (3.48) has several components and is expressed with the interpolation function N by

$$Q = \int_V \eta\overline{\sigma}\dot{\varepsilon} N dV + \int_{S_{rad}} \sigma\varepsilon\left(T_w^4 - T_\infty^4\right) N dS + \int_{S_{conv}} h(T_w - T_\infty) N dS + \int_{S_{cond}} k\left(T_w - T_R\right) N dS + \int_{S_{cond}} q_{fr} N dS$$

(3.49)

The first term on the left is the heat, generated by plastic deformation inside the deforming body. The second term defines the contribution of the heat radiated from the workpiece to the environment, where σ is the Stefan-Boltzmann constant, ε is the emissivity, and T_w and T_∞ are the workpiece and the environment temperatures respectively which for hot rolling is approximately 0.8. The third term describes the heat convected from the body surface to the environment fluid (air or water) with heat convection coefficient h. The fourth term represents the contribution of the heat conducted from the workpiece to the rolls through their interface and k is the workpiece-roll heat transfer conduction coefficient. The last term is the contribution of the heat

generated by friction along the roll-workpiece interface, q_f being the surface heat generation rate due to friction.

The theory necessary to integrate (3.49) can be found in numerical analysis books. See for instance [4]. The convergence of a scheme requires consistency and stability. Consistency is satisfied by an approximation of the type

$$T_{t+\Delta t} = T_t + \Delta t\left[(1-\beta)\dot{T}_t + \beta\dot{T}_{t+\Delta t}\right] \tag{3.50}$$

where β is a parameter varying between 0 and 1, and t denotes time. For unconditional stability, β should be greater than 0.5. Selection of a proper value of β is an important factor in situations where it is desirable for the time step to be as large as possible, provided that the increments in strain are compatible with an infinitesimal analysis [44].

With respect to the computational procedures for thermo-plastic/viscoplastic analysis, we will treat the workpiece and the rolls separately, assuming that the die properties do not change. Thus we greatly reduce the number of equations to be solved simultaneously, which, in turn, reduces the cost of the solution. There is no internal heat generation in the die and therefore, the deformation calculations are not necessary.

The heat generated through friction, q''_{fr}, is evenly distributed between the die and the deforming material, and is calculated as

$$q''_{fr} = \sigma_{fr} \cdot v_r \cdot \xi \qquad (\mathrm{W/m^2}) \tag{3.51}$$

where

σ_{fr} = friction stress (MPa)

v_r = relative sliding velocity between the roll and the workpiece (m/s)

ξ = fraction of friction energy that is converted to heat

It should be noted that the nodes on the die do not generally coincide with those on the deforming material along the interface, and that the calculation of nodal point temperatures requires interpolation. When boundary conditions such as the convection term in Equation (3.49) apply, they are split into two parts: one containing the unknown temperatures is added to the heat conduction matrix K_c. Boundary conditions such as the radiation term in Equation (3.49) are applied using previous iteration values for body temperatures [44].

The model just described can be used to calculate the temperature distribution as well as the velocity, strain rate, strain and stress fields in the deformation zone during hot and cold rolling. Plane strain state is assumed in the velocity field and four node quadrilateral elements are used in the Non-linear FEM model.

3.7 The Elastic-Plastic Flow Formulation

The elastic-plastic or elastoplastic solid formulation is more realistic than the rigid-plastic approximation, as it takes into account the elastic contribution to the total strain rate

$$\dot{\varepsilon} = \dot{\varepsilon}^{e} + \dot{\varepsilon}^{p} \tag{3.52}$$

where the upper index is e for the elastic contribution and p for the plastic (or the viscoplastic) one.

This approach is necessary when we analyze processes in which the elastic effects play a significant role. Such is the case of the cold rolling process. As we have already seen, in cold rolling, as the strip enters the roll gap it is first deformed elastically. As the strip proceeds through the roll gap plastic flow occurs until finally at the exit the roll pressure is removed. The strip is, at that time, unloaded and it returns through an elastic state to the original load free condition.

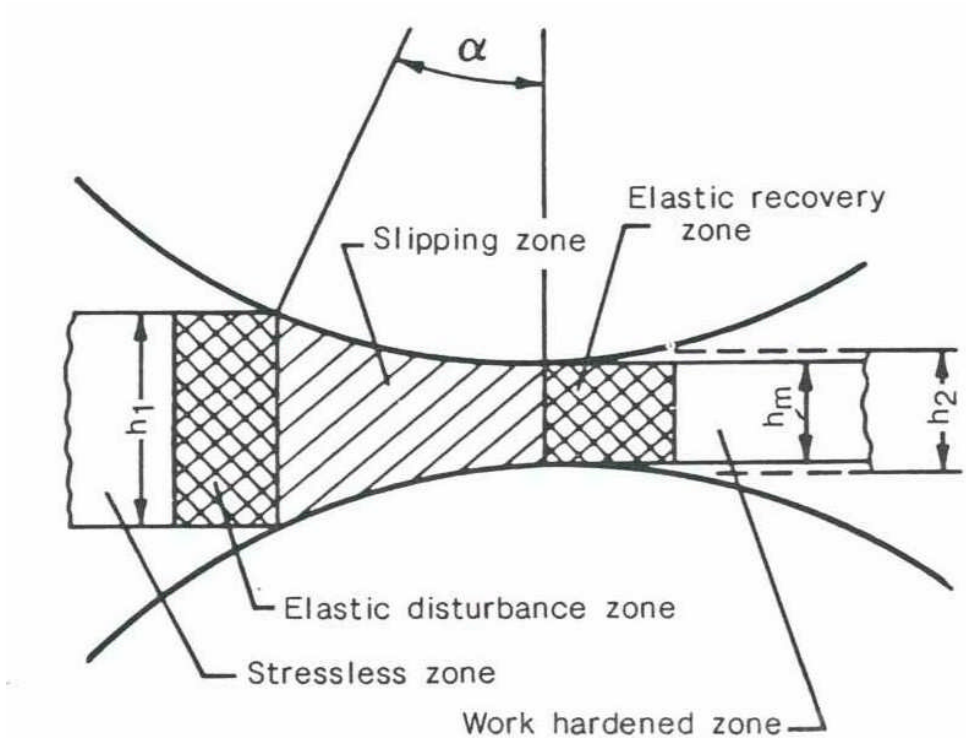

Figure 3.4: Schematic Illustration of the strip elastic recovery [32] © Marcel Dekker / Taylor & Francis Group

The elastoplastic approach is also necessary for processes where residual stresses are present and again, this is the case of the cold rolling process.
The solid formulations of the finite element method for metal forming problems are based on the use of the *Prandtl-Reuss* equations for elastic-plastic materials. The formulation is given in the rate form and assumes the infinitesimal theory of deformation

$$\dot{\varepsilon}_{ij}^{p} = \dot{\lambda} s_{ij} \tag{3.53}$$
$$\dot{\lambda} = \frac{1}{\tau_Y}\sqrt{\frac{1}{2}\dot{\varepsilon}_{ij}\dot{\varepsilon}_{ij}}$$

As explained by Lenard & Pietrzyk, "the elastoplastic formulation is more complicated, even when the small strain approximation is used, as the stress tensor is not an explicit function of the strain increment. Moreover, if large rotations occur in the process, the small strain formulation, derived from the material derivative of the stress tensor, is no longer appropriate because it violates the mechanical principle of objectivity. A new form of stress tensor differentiation must be introduced to satisfy objectivity. For isotropic solid materials, the Jauman derivative is the more often used. Finally, despite the fact that in theory no indeterminate form of the stress tensor can arise for elastoplastic material, a regularization in the form suggested by the von Mises flow rule can be utilized to improve the numerical behavior when both elastic and plastic strain-rate tensors are small" [44,56]. The derivation of the elastoplastic formulation therefore will not be included as it exceeds the scope and purpose of this thesis.

From the following, it is clear that however more approximate, the rigid-plastic or purely viscoplastic approaches are simpler to implement in computer codes, and often they are more economical with respect to computer time, as the constitutive law is explicit and therefore requires no iteration at the element level. Often much larger steps can be solved in a stable manner, and the equilibrium equation can in some formulations be solved directly, rather than solving for balance update forces. Another advantage of the rigid-plastic formulation is clear when stationary processes are considered. With the flow formulation the equations of a steady-state processes are easy to write and to solve iteratively, only one time. When elastoplastic or elasto-viscoplastic processes are investigated, the solution of the stationary state is not easy and very few references are available in the literature for a direct procedure. Most works use an incremental approach to reach the steady state as a limit case, but the nonlinear equations are to be solved a rather large number of times, that is, for each increment [44,56]

3.8 Coupled Thermal-Mechanical Analysis

From the physical point of view, the rolling process is a coupled thermal-mechanical problem. The coupling between the mechanical and thermal phenomena results from the pressure-dependent thermal contact resistance between the steel strip and the rolls.

Many operations performed in the metal forming industry (such as casting, extrusion, rolling, and stamping) can require a coupled thermo-mechanical analysis. The observed phenomena must be modeled by a coupled analysis if the following conditions pertain:
First, coupling occurs when deformations result in a change in the associated heat transfer problem. Such a change can be due to either large deformation or contact. The second

cause of coupling is heat generated due to inelastic deformation. The irreversibility of plastic flow causes an increase in the amount of entropy in the body, which in turns results in changes to the associated mechanical problem.

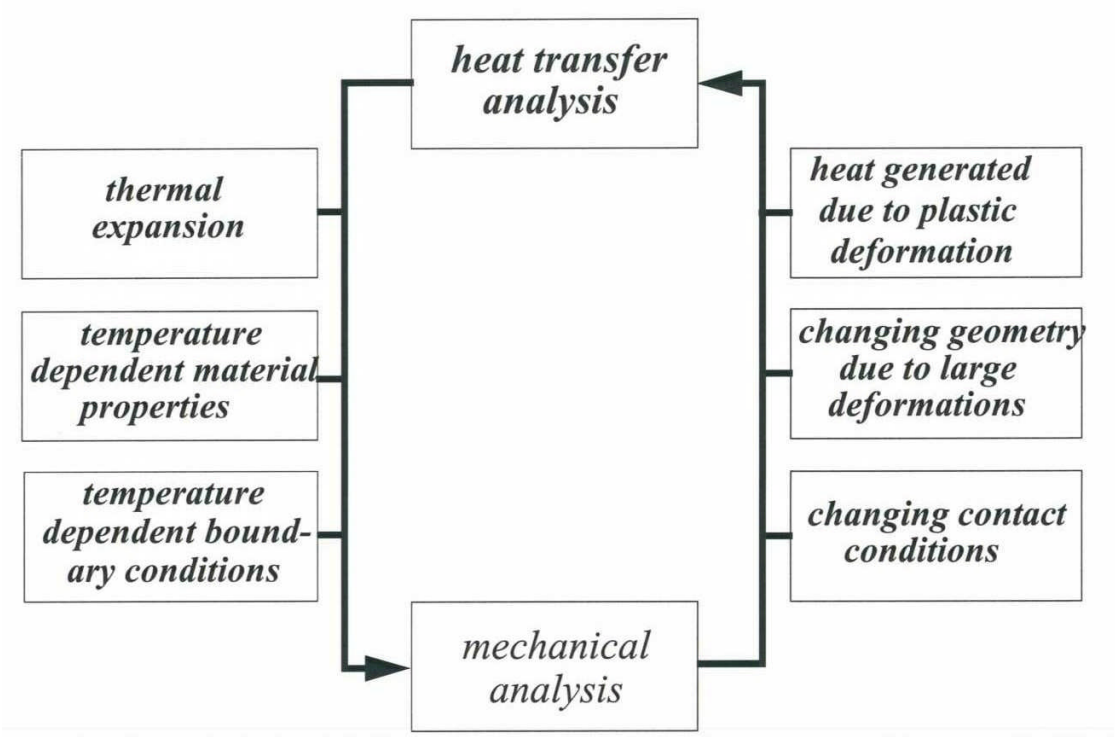

Figure 3.5: Coupled Thermo-Mechanical Analysis [54] © MSC Software Corporation

To determine the heat generated from mechanical sources such as the work done by plastic deformation (volumetric heat generation) or friction heating (surface heat generation), it is necessary to specify how much mechanical energy is converted into thermal energy. This is done by means of the heat generation factor η that takes values between 0 and 1. Work by Warren & Taylor suggests that for metal plasticity a value of $\eta = 0.9$ is appropriate.

In particular, the heat rate generated due to plastic deformation is determined by

$$\dot{q} = \eta \bar{\sigma}_{ij} \dot{\bar{\varepsilon}}_{ij}^{p} \qquad (\mathrm{W/m^3}) \tag{3.54}$$

where

$\eta =$ heat generation efficiency (fraction of the plastic strain energy that is converted to heat ~ 0.9) , $0 < \eta < 1$

$\bar{\sigma}_{ij} =$ components of equivalent stress tensor (MPa)

$\dot{\bar{\varepsilon}}_{ij}^{p} =$ components of equivalent plastic strain rate tensor ($\mathrm{s^{-1}}$)

The heat transfer rate due to friction is expressed by

$$q''_{fr} = \sigma_{fr} \cdot v_r \cdot \xi \qquad (\mathrm{W/m^2}) \tag{3.55}$$

where

$\sigma_{fr} =$ friction stress (MPa)

$v_r =$ relative sliding velocity between the roll and the workpiece (m/s)

$\xi =$ fraction of friction energy that is converted to heat, $0 < \xi < 1$

In order to handle a coupled thermo-viscoplastic deformation problem, it is necessary to solve simultaneously the material-flow problem for a given temperature distribution and the heat transfer equations. The equations for the flow analysis and the temperature calculation are strongly coupled, making a simultaneous solution of their finite element counterparts necessary.

Considering $T_{t+\Delta t}$ as a primary dependent variable, we have from Equation (3.50), with t=0 initially,

$$\dot{T}_{\Delta t} = \frac{T_{\Delta t}}{\beta \Delta t} - \frac{T_0}{\beta \Delta t} - \left(\frac{1-\beta}{\beta}\right)\dot{T}_0 = \frac{T_{\Delta t}}{\beta \Delta t} + \hat{\dot{T}} \tag{3.56}$$

where $\hat{\dot{T}} = -\frac{T_0}{\beta \Delta t} - \left(\frac{1-\beta}{\beta}\right)\dot{T}_0$. Substituting Equation (3.56) into Equation (3.48) $C\dot{T} + K_c T = Q$, yields,

$$\left(K_c + \frac{C}{\beta \Delta t}\right) T_{\Delta t} = Q_{\Delta t} - C\hat{\dot{T}} \tag{3.57}$$

The coupling procedure makes use of Equation (3.57) through the following sequence:

a) assume the initial temperature field T_0,
b) Calculate the initial velocity field ***v*** corresponding to the temperature field T_0,
c) Calculate the initial temperature-rate field $\dot{T}_0$ from Equation (3.48) using values from a) and b)
d) Calculate the quantity $\hat{\dot{T}}$
e) Update the nodal point positions and the effective strain of elements for the next step
f) Use the velocity field at the previous step to calculate the first approximate temperature T such as $\left(K_c + \frac{C}{\beta \Delta t}\right) T^{(1)}_{\Delta t} = Q^{(1)}_{\Delta t} - C\hat{\dot{T}}$ for $T^{(1)}_{\Delta t}$
g) Calculate a new velocity field with the solution of f)
h) Use the new velocity field to calculate the second temperature field such as

$$\left(K_c + \frac{C}{\beta \Delta t}\right) T_{\Delta t}^{(2)} = Q_{\Delta t}^{(2)} - C\hat{\dot{T}} \text{ for } T_{\Delta t}^{(2)}$$

i) Repeat steps g) and h) until both have converged
j) Calculate the new temperature rate field $\dot{T}_{\Delta t}$
k) Repeat steps e) through j) until the desired deformation state is reached

The iteration process for temperature calculations is not likely to require much computing time, because only the heat input vector Q is changed during iterations and, as a result triangularization of the matrix is necessary only once. Moreover, additional iterations necessary to obtain a velocity field after a new temperature field is obtained should be relatively few, because the velocity field does not show much sensitivity to small variations of the temperature field [44].

The model just described can be used to calculate the temperature distribution as well as the velocity, strain rate, strain and stress fields in the deformation zone during hot and cold rolling. Plane strain state is assumed in the velocity field and four node quadrilateral elements are used in the Non-linear FEM model.

3.9 Non-Linearities in the Rolling Problem

In this section we will take a look at the sources of nonlinearity and study how they affect the cold and hot rolling problems.

There are three types of nonlinearities: material, geometric, and nonlinear boundary conditions [73]

a) **Material nonlinearity** results from the nonlinear relationship between stresses and strains. Elastoplastic, elasto-viscoplasticity, and creep behavior are the most common material nonlinearities
b) **Geometric nonlinearity** results from the nonlinear relationship between strains and displacements on the one hand and the nonlinear relation between stresses and forces on the other hand, e.g. buckling/snap-through, as well as large strain problems such as manufacturing, crash, and impact problems
c) **Boundary conditions** and/or loads can also cause nonlinearity. Contact and friction problems lead to nonlinear boundary conditions. This type of nonlinearity manifests itself in several real life situations; for example, metal forming, gears, interference of mechanical components, pneumatic tire contact, and crash

In the hot and cold rolling problem we have to deal with these three sources of nonlinearities with permanent deformations and gross changes in geometry that the

workpiece acquires as it is rolled; stress values which exceed the elastic limits of the materials, yielding, temperatures above 30% of the melting temperature; contact between the roller and the strip involving tremendous friction; the stress is no longer proportional to the strain, heat transfer non linearities such as radiation from the workpiece, etc.

Material non-linearities

A solution requiring a nonlinear material model is probably the most difficult type of nonlinear problem. The degree of difficulty is proportional to the degree of nonlinearity. A nonlinear elastic problem is easier to solve than a moderately plastic problem. Even the latter is easier to complete than a model with significant plasticity and relaxation. This is the reason why the cold rolling problem is easier from the material modeling point of view, than the hot rolling problem.

The success and efficiency of a nonlinear material solution are dependent on the choice of material model. Even the most complex material models are still significant idealizations of the real situation. The material non-linearities in the cold and hot rolling problem are due to the high degree of plasticity of the rolling stock. In order to properly define the plastic behavior of the rolling stock we have to define the following:

a) Yield Criteria: when plastic behavior is expected, we must tell the solver which criteria to seek to initiate yielding. Yield criteria are a function of the stresses in the model. Both the hot and cold rolling models in this thesis use the von Mises yield criterion which is considered the best criterion for ductile metals

b) Hardening Rule: determines how the material model responds to repeated stress reversals, or switching between tension and compression. In ductile material that has never experienced plasticity, the yield point in tension can be expected to be equal to the opposite of the yield stress in compression. However, once the yielding has occurred, some materials experience a phenomenon known as the Bauschinger Effect, which causes the yield point in compression to be somewhat less than the compressive equivalent of the initial yield stress. Consequently, nonlinear solutions have implemented hardening rules to allow for adjustment of the yield point in stress reversals.
    - An Isotropic hardening model does not take the Bauschinger Effect into account and the compressive yield always equals the tensile yield; the absolute value of both equals the initially defined yield stress.
    - A kinematic hardening model will take into account the reduction in the compressive yield point after a stress reversal. A kinematic model is more computationally intensive and should not be used unless a portion of the model is expected to yield in tension and then in compression. Most materials do experience strain hardening and will see an improvement in accuracy if the kinematic hardening model is used when needed. It is the case of the cold rolling problem which we modeled using the Ramberg-Osgood hardening material model. It is due to the hardening that the cold rolled material undergoes, that the kinematic hardening rule is needed in

order to obtain accurate results. This was the rule used in the FEM models that will be described in the following chapters.

c) Flow rule: establishes the incremental stress-strain relations for plastic material. The flow rule describes differential changes in the plastic strain components $d\varepsilon^p$ as a function of the current stress state. The Prandtl-Reuss representation of the flow rule in conjunction with the von Mises yield function is the flow rule used for the cold rolling model. The Levy-Mises was used for the hot rolling case.

Another important decision that had to be made for the nonlinear material analysis of the hot and cold rolling problems was which material model to use. In our case, the elasto-plastic material model was the model of choice for the cold rolling problem for obvious reasons. As we saw in Section 3.7, the elasto-plastic material model takes into account the path dependent behavior that the material follows as it is cold rolled, with an elastic deformation as the workpiece enters and exits the roll gap, and a plastic deformation as the workpiece undergoes the bulk of the deformation process. In the elastic plastic material model the strain is divided into an elastic part and a plastic part. This type of model also accurately simulates the irreversible deformation that occurs during the cold rolling problem upon reaching a certain stress state.

Many materials experience noticeable hardening after the onset of plasticity. In these materials, the response of the system to large strains will diverge in a bilinear model. Therefore a trilinear model contains a third, hardening modulus to account for this.

For our cold rolling problem a multilinear material model was used. This multilinear model was input using pairs of stress strain values extracted from a standard tensile test of the rolling stock at ambient temperature. This multilinear material model is independent of the strain rate and the temperature unlike the material model used for the hot rolling case. As we saw in Section 2.9, the constitutive equation for the hot rolling problem is a function of the strain rate and the temperature generating a much more complicated material model. Shida's model for high temperature steel was selected for this thesis due to its

Therefore we have that:

$$\text{Cold Rolling} \Rightarrow \sigma = f(\varepsilon) \tag{3.58}$$

$$\text{Hot Rolling} \Rightarrow \sigma = f(\varepsilon, \dot{\varepsilon}, T) \tag{3.59}$$

In the case of the hot rolling problem, the formulation used is the rigid-plastic one. As we saw in Section 3.4, in hot metal forming operations, the non-linear plastic strains are much larger than the elastic ones; these last ones can be neglected allowing the use of a simpler rigid-plastic model in the analysis.

Geometric Non-Linearities

Geometric non-linearities in the cold and hot rolling problems are due to the existence of large strains and deformations.

There are two natural classes of large deformation problems:

- Large displacement – small strain problems: changes in the stress-strain law can be neglected, but the contributions from the nonlinear terms in the strain displacement relations cannot be neglected.
- Large displacement – large strain problems: the constitutive relation must be defined in the correct frame of reference and is transformed from this frame of reference to the one in which the equilibrium equations are written.

Geometric nonlinearity leads to two types of phenomena: change in structural behavior and loss of structural stability. The first one being the case we are concerned with for our rolling problem, as the second one has to do with the collapse load of a structure and is the subject of a nonlinear buckling analysis, which is not the object of this study.

The kinematics of deformation can be described by the following approaches [2,6,18,19]:

- *Lagrangian Formulation*: the finite element mesh is attached to the material and moves through space along with the material. In this case, there is no difficulty in establishing stress or strain histories at a particular material point and this approach also naturally describes the deformation of structural elements and transient problems such as the indentation problem. This method can also analyze steady-state processes such as extrusion and rolling. Shortcomings of the Lagrangian method are that flow problems are difficult to model and that the mesh distortion is as severe as the deformation of the object.

  The Lagrangian approach can be classified in two categories: the total Lagrangian method and the updated Lagrangian method. In the total Lagrangian approach everything is referred to the original undeformed geometry, which is used as a reference. This approach is therefore applicable to problems exhibiting large deflections and large rotations (but with small strains), such as thermal stress, creep, and rubber analysis where large elastic strains are also possible. In the updated Lagrangian method, the current configuration acts as the reference state and the mesh coordinates are updated after each increment. This method is good for problems featuring large inelastic strains such as metal forming and other problems where inelastic behavior such as plasticity causes the large deformations. Thus, this is the approach used for our rolling model.

- *Eulerian Formulation*: where the mesh is fixed in space and the material flows through the mesh. This method is suitable for steady state processes such as extrusion or steady state rolling, and also fluid mechanics problems.
- *Arbitrary Eulerian-Lagrangian (AEL) Formulation*: where the mesh moves independently of the material, yet in a way that it spans the material at any time. Due to its strong resemblance to the pure Eulerian formulation, it is also referred to as the quasi-Eulerian formulation.

Boundary Non Linearities

There are three types of problems associated with nonlinear boundary conditions: contact, non-linear support, and nonlinear loading. In the rolling problem, contact plays a major role as it creates one of the most severe nonlinearities in mechanics. It is therefore very important to have a good understanding of its underlying principles.

Contact by nature, is a nonlinear boundary value problem. During contact, mechanical loads and sometimes heat are transmitted across the area of contact. If friction is present, shear forces are also transmitted. Contact problems are commonly encountered in physical and manufacturing systems. In the rolling problem the contact problem occurs at the interface between the metal workpiece and the rolls [6,19].

Contact problems are characterized by two important phenomena: gap opening/closing, and friction. As shown in Figure 3.5, the gap describes the contact (gap closed) and separation (gap open) conditions of two objects (structures). Friction influences the interface relations of the objects after they are in contact. The gap condition is dependent on the movement (displacement) of the objects, and friction is dependent on the contact force as well as the coefficient of Coulomb friction at contact surfaces. The analysis involving gap and friction must be carried out incrementally. Iterations can also be required in each (load/time) increment to stabilize the gap-friction behavior.

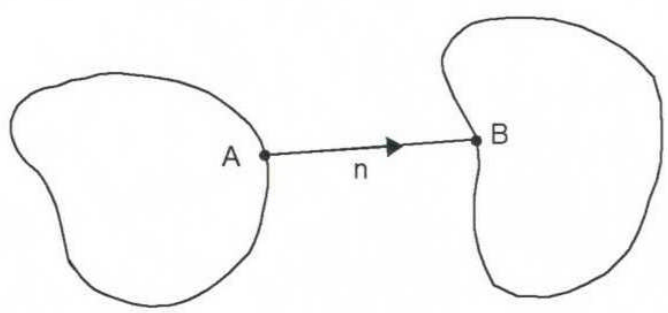

Figure 3.6: Normal gap between potentially contacting bodies [54] © MSC Software Corporation

There are two types of contact situations used in our study of the rolling problem:

a) deformable to rigid body contact
b) deformable to deformable Contact

The first one is used in the case where the workpiece is modeled as a deformable element but the rolls are modeled as a rigid body. This method is computationally inexpensive and it is the one used in most cases in this thesis.
The deformable-deformable case is used when both the rolls and the workpiece are modeled as deformable elements. Since the rolls are rather large, this case generates a

huge amount of elements that cause the model to converge after a very long period of time.

The basics of these two models can be found in Chapter 2, Section 2.7 of this thesis that deals with the mathematical aspects of the rolling problem

Heat Transfer non-linearities

Heat transfer nonlinearities are present in the hot rolling model. For the case of cold rolling since it is conducted at ambient temperature linear heat transfer suffices.

Heat transfer nonlinearities in the hot rolling problem are caused by:

a) temperature dependent conductivity: $K = K(T)$
b) temperature dependent specific heat: $C_p = C_p(T)$
c) temperature dependent film coefficient: $h = h(T)$
d) temperature dependent heat flux
e) radiation boundary condition: $-K\dfrac{\partial T}{\partial n} = \sigma\varepsilon\left(T^4_{workpice} - T^4_{\infty}\right)$

Consequently, heat capacity matrix, conductivity matrix, film matrix and equivalent nodal flux vector are also temperature dependent.

Due to the severe nonlinearities present in this problem transient analysis is required.

The accuracy of the simulation of temperature fields, which develop during plastic deformation processes, depends, in a very significant manger, on the mathematical description of the thermal properties of the deformed material and the boundary conditions. The conductivity, specific heat, and density of the metal have to be introduced into the finite-element model as functions of the current local temperatures if we want to obtain realistic results.
The following sets of formulas describe the conductivity, density and specific heat for the tree main types of steel used in rolling processes [49,56].

1. <u>Low carbon manganese steel</u>

$$k = Conductivity = 23.16 + 51.96 \cdot e^{-2.03\hat{T}} \quad \left(\frac{W}{m}\right) \tag{3.60}$$

$$\rho = Density = \frac{7850}{\left(1 + 0.004\hat{T}^2\right)^3} \quad \left(\frac{kg}{m^3}\right) \tag{3.61}$$

$$C_p = 689.2 + 46.2 \cdot e^{3.78\hat{T}} \text{ for T< 700 ºC} \quad \left(\frac{J}{KgK}\right) \tag{3.62}$$

$$207.9 + 294.4 \cdot e^{1.41\hat{T}} \text{ for T>700 ºC}$$

2. <u>High Carbon Steel</u>

$$k = Conductivity = 23.16 + 51.96 \cdot e^{-2.025\hat{T}} \quad \left(\frac{W}{m}\right) \tag{3.63}$$

$$\rho = Density = \frac{7850}{\left(1 + 0.004\hat{T}^2\right)^3} \quad \left(\frac{kg}{m^3}\right) \tag{3.64}$$

$$C_p = 391 + 0.202T_K \text{ for T< 700 ºC} \quad \left(\frac{J}{KgK}\right) \tag{3.65}$$

$$586 - 0.46T_K + 0.00076T_K^2 \text{ for T>700 ºC}$$

3. <u>Austenitic Steel</u>

$$k = Conductivity = 21.9 + 14.3\hat{T}^{1.82} \quad \left(\frac{W}{m}\right) \tag{3.66}$$

$$\rho = Density = \frac{7850}{\left(1 + \gamma_1\right)^3} \quad \left(\frac{kg}{m^3}\right) \tag{3.67}$$

$$C_p = 474 + 197\hat{T} + 3.79\hat{T}^2 - 59.6\hat{T}^3 \quad \left(\frac{J}{KgK}\right) \tag{3.68}$$

where in all of the above,

$$\hat{T} = \frac{T}{1000} \tag{3.69}$$

$$T_K = T + 273 \tag{3.70}$$

$$\gamma_1 = 0.334 + 0.836\hat{T} + 1.169\hat{T}^2 - 0.4586\hat{T}^3 \tag{3.71}$$

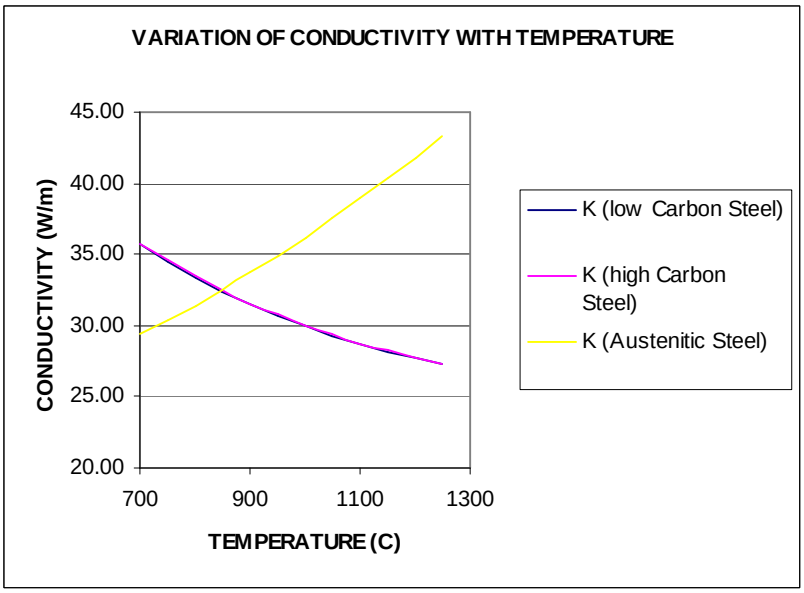

Figure 3.7: Non-linear conductivity in hot rolling

In Figure 3.7 it can be seen how the conductivity decreases as the temperature increases for low carbon steel. This is an important fact especially for the hot rolling process. In hot rolling the roll temperature increases rapidly, and that increase has a significant influence on the heat transfer between the strip and the roll that decreases according to the equation for the conduction coefficient. Thus the effect of the heat transfer coefficient in hot rolling is of great importance.

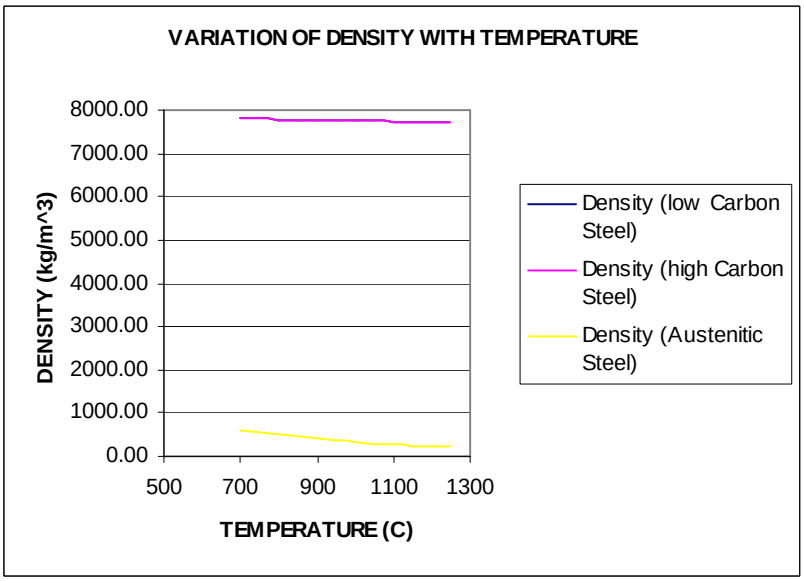

Figure 3.8: Non-linear density in hot rolling

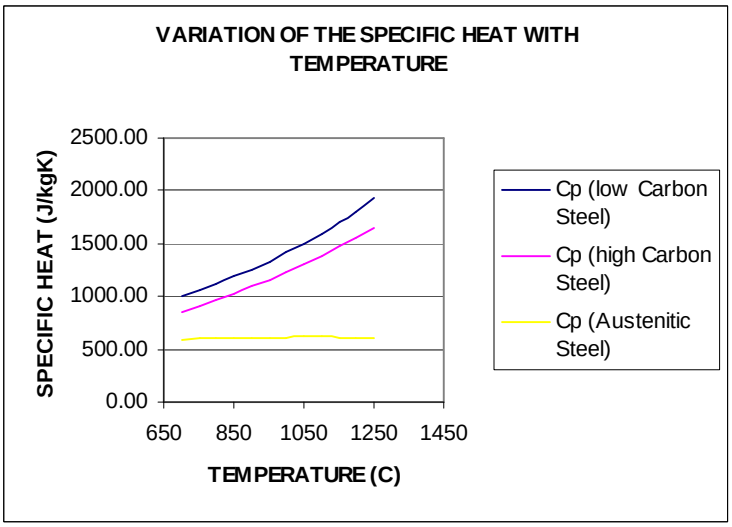

Figure 3.9: Non-linear Specific Heat in Hot Rolling

On the other hand, in cold rolling, due to a smaller temperature difference between the strip and the roll, the effect of the heat transfer coefficient is of less importance than in hot rolling. Nevertheless, as the temperature of the workpiece increases, cooling by the roll becomes more intense and that makes the choice of the heat transfer coefficient for use in modeling of some importance. The temperature rise of the strip, measured in cold rolling, usually will vary between a few degrees and about 50˚C.

3.10 Summary and Concluding Remarks

In this chapter we have taken an exhaustive look to the cold and hot rolling problems from the finite element formulation point of view. The Finite Element Method is our tool of choice for the solution of the complex Initial Boundary Value Problems (IBVP) corresponding to the rolling problem, that were described in detail in Chapter 2, and where the formation of element equations is accomplished by using a variational approach.

The basis of finite element metal flow modeling, using the variational approach, is to formulate proper functionals, depending upon specific constitutive equations. The solution of the initial boundary value problem (IBVP) is obtained by the solution of the dual variational problem in which the first order variation of the functional vanishes.

For our mechanical initial boundary value problem (M-IBVP), the *variational approach* requires that among admissible velocities v_i that satisfy the conditions of compatibility and incompressibility, as well as the velocity boundary conditions, the actual solution give the functional described by Equation (3.5) a stationary value. Using this variational approach, the basic equation for the finite element discretization was developed, Equation (3.8).

Likewise, the Thermal Initial Boundary Value Problem (T-IBVP) was solved using a variational approach that led to the FE discretization Equation, (3.42), that was implemented into the finite element formulation according to Equations (3.48) & (3.49).

We then took a look at the main formulations used in the application of FEM to metal forming, namely, the flow formulation and the solid formulation. Flow formulation assumes that the deforming material has negligible elastic response, while solid formulation includes elasticity. The flow formulation uses the *rigid-plastic* or *rigid-viscoplastic* material models. Since in metal forming operations, the non-linear plastic strains are much larger than the elastic strains, these last ones are usually neglected allowing the use of a simpler rigid-plastic model in the analysis. The resulting constitutive equations in this approach are identical to those of a non-Newtonian fluid
Solid formulation, also known as solid-state incremental approach, employs elastic-plastic or elastic-viscoplastic material models. This approach uses a Lagrangian description of motion

We then developed the finite element equations for each of these two formulations, solid and flow, starting from Equation (3.8), which as we have just seen is the basic equation for finite element formulation.

A complete analysis of the rolling process also requires the simulation of heat transfer in the roll gap, making it necessary to couple the solution for the flow formulation with the thermal model. In order to handle a coupled thermo-viscoplastic deformation problem, it is necessary to solve simultaneously the material-flow problem for a given temperature distribution and the heat transfer equations. The finite element model for the heat transfer and coupled thermal-mechanical problem was based on formulations developed by Kobayashi & Zienkiewicz. These formulations can be used to calculate the temperature distribution as well as the velocity, strain rate, strain and stress fields in the deformation zone during hot and cold rolling.

Finally we took a look at the main sources of non-linearities present in the rolling problems (material, geometric and boundary) and saw how the hot and cold rolling problem we have to deal with these three sources of nonlinearities with permanent deformations and gross changes in geometry that the workpiece acquires as it is rolled; stress values which exceed the elastic limits of the materials, yielding, temperatures above 30% of the melting temperature; contact between the roller and the strip involving tremendous friction; stresses no longer proportional to the strains, and heat transfer non linearities such as radiation from the workpiece, etc.

In the next chapter we will take a look at the 2-D plane-strain non-linear FEM models of the hot and cold rolling processes, which were created in order to verify and demonstrate the goals of this thesis. As we will see, the conditions of perfect symmetry that occur only in the flat rolling process allows us to use the plane strain condition which “occurs whenever the thickness becomes very large compared with its in-plane dimensions, so that the strains in the out-of-plane direction can be ignored” [43]. This approach is very efficient and computationally inexpensive, compared to the 3-D solid modeling approach.

Chapter 4
Results for 2-D Plane Strain Finite Element Models for the Flat Rolling Problem

4.1 Introduction

Thus far in this thesis, we have studied the main mathematical aspects of the rolling problem, such as its mathematical model, equations of motion and equilibrium, friction modeling, material modeling and heat and mass transfer. We have modeled the physics of the problem into a pair of coupled Initial Boundary Value Problems, and we have established the foundation of the finite element model within the context of our problem, explaining how the mathematical model described in Chapter 2 fits within the finite element formulation. We are now ready to start creating and analyzing the 2-D plane strain models developed for this thesis that will in turn allow us to explore and achieve the main goals of this thesis that as stated in Chapter 1 were:

To demonstrate that:

a) the steel in cold rolling can be accurately modeled using the elastic-plastic material model;
b) the steel in hot rolling (at temperatures between 800 and 1200 C) can be modeled using the rigid-plastic material model with the flow stress as a function of the strain, strain rate, and the temperature;
c) in cold rolling, plane sections do not remain plane (as the classic theory assumes in the derivations of formulas for stress) and due to this, all the empirical formulas used in the classical theory of rolling can only be used as an estimate;
d) the degree of deformation, stresses and strains, strain rates, as well as other parameters of interest, on the workpiece and in the rolls can be predicted;
e) the heat transfer from the workpiece to the rolls can be accurately modeled;
f) the stresses developed in the rolls are very similar to the stresses developed in the Hertzian contact problem;
g) the complicated and not well understood friction process between the roll and the workpiece can be accounted for in the FE models
h) the Finite Element Method can be used to predict material flow;
i) the mechanism of bite in rolling

The cold rolling models done for this simulation, utilize the elastic-plastic (solid) formulation. As we saw in Chapter 3, the elastoplastic formulation is more realistic than the rigid-plastic approximation, as it takes into account the elastic contribution to the total strain rate This approach is necessary when we analyze processes in which the elastic effects play a significant role. Such is the case of the cold rolling process. As we have already seen, in cold rolling, as the strip enters the roll gap it is first deformed elastically. As the strip proceeds through the roll gap plastic flow occurs until finally at the exit the roll pressure is removed. The strip is, at that time, unloaded and it returns through an elastic state to the original load free condition.

The solid formulations of the finite element method for metal forming problems are based on the use of the *Prandtl-Reuss* equations for elastic-plastic materials. The formulation is given in the rate form and assumes the infinitesimal theory of deformation

$$\dot{\varepsilon}_{ij}^{p} = \dot{\lambda} s_{ij} \tag{4.1}$$

$$\dot{\lambda} = \frac{1}{\tau_Y}\sqrt{\frac{1}{2}\dot{\varepsilon}_{ij}\dot{\varepsilon}_{ij}}$$

On the other hand, the hot rolling models utilize the rigid-viscoplastic (flow) formulation, which assumes that the deforming material has a negligible elastic response. The flow formulation of the finite element method for metal forming processes is based on the *Levy-Misses* plasticity model for rigid plastic materials, which assumes that work hardening is negligible, and is given by the flow rule (constitutive equations):

$$\dot{\varepsilon}_{ij} = \dot{\lambda}\frac{\partial f(\sigma_{ij})}{\partial \sigma_{ij}} = \frac{3}{2}\frac{\dot{\bar{\varepsilon}}}{\bar{\sigma}}s_{ij} \tag{4.2a}$$

$$\dot{\lambda} = \frac{3}{2}\frac{\dot{\bar{\varepsilon}}}{\bar{\sigma}} \tag{4.2b}$$

$$\dot{\bar{\varepsilon}} = \sqrt{\frac{2}{3}\dot{\varepsilon}_{ij}\dot{\varepsilon}_{ij}} \tag{4.2c}$$

$$\bar{\sigma} = \sqrt{\frac{3}{2}s_{ij}s_{ij}} \tag{4.2d}$$

As to the yield surface, for both the hot and cold rolling it will be the von Misses yield that we will use for all the models. Finally about hardening rule is Isotropic for the cold rolling case. The hot rolling case uses rigid-viscoplastic flow formulation so no hardening is necessary.

4.2 2-D Plane Strain Model for Flat Cold Rolling

The purpose of the 2-D plane strain flat cold rolling models is to help the roll designer predict the main flat rolling parameters, namely, the rolling loads, temperature & velocity fields, the overall geometric changes of deformed pieces, and the metal flow under different temperatures, as well as the optimum conditions for the flat rolling process. The process can be modeled as a two-dimensional or a three-dimensional problem. Both have their advantages and trade-offs. The 3-D model is more accurate in its description of the process because it takes into account the spread (deformation in the direction of the thickness) that the workpiece undergoes. This important factor is ignored by the 2-D plane strain models where $\varepsilon_z=0$. The 3-D method is however more computationally expensive as the number of elements is increased. One of the most efficient approaches to the simulation of the flat rolling process is the plane-strain method. Since in flat rolling we have perfect symmetry with respect to a plane that cuts the workpiece in two through its midplane, and since the rolls are prefect cylinders, we will assume that the plane strain conditions apply, even though in reality this ignores the spread effect.

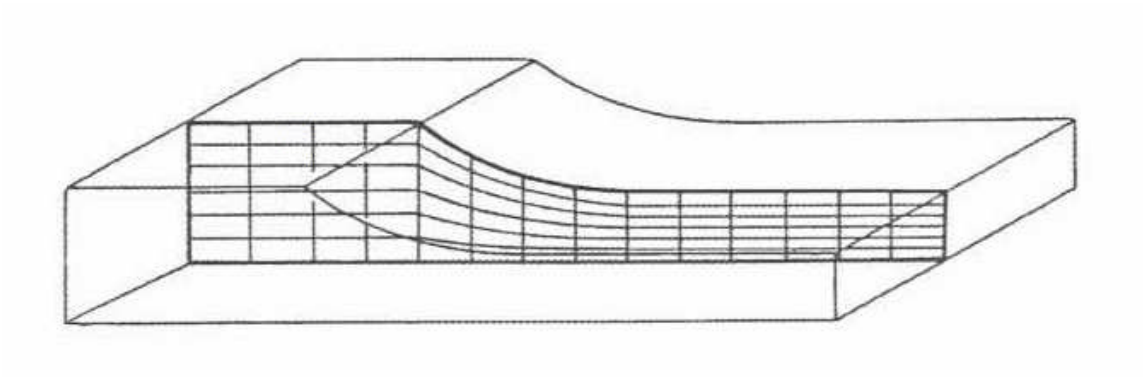

Figure 4.1: Plane strain model of the flat rolling process [49] © Elsevier Science

Due to the thermo-mechanical interactions that this manufacturing process has, the process is modeled as a coupled thermo-mechanical transient dynamic problem (transient heat transfer & dynamic mechanical).
There are three types of analyses we can do for the plane-strain flat-rolling problem:

1. Deformable-Rigid coupled analysis: where the slab is modeled as a deformable body and the rolls as rigid.
2. Deformable-Rigid with heat transfer coupled analysis: where the slab is again modeled as a deformable body, but the rolls are modeled as a rigid body with heat transfer (this approach utilizes a special kind of element)
3. Deformable-Deformable Coupled analysis: where both the steel strip and the rolls are modeled as deformable bodies.

The cold rolling model will use the work hardening material model that is implemented using the elastic-plastic material formulation that we discussed in Chapter 2, section 2.9. The cold rolling process is the right starting point, as it is much simpler than the hot rolling one, and from it we can learn invaluable lessons.
The non-linear FEM software used in this project was MSC MARC, one of the leading FE software developers with over twenty years of experience in the field.

<u>2-D Plane-Strain Model Description</u>

Cold rolling of a 0.5 m thick 0.1% Carbon steel slab, reduced by 20 % in one pass is presented below.

<u>Geometry</u>

Roll Diameter = 3.1 m	Slab Length = 2 m	% Reduction= 20 %
Slab Thickness = 0.5 m	Slab Width = 1 m	$\varpi = 1.5 rad/s$

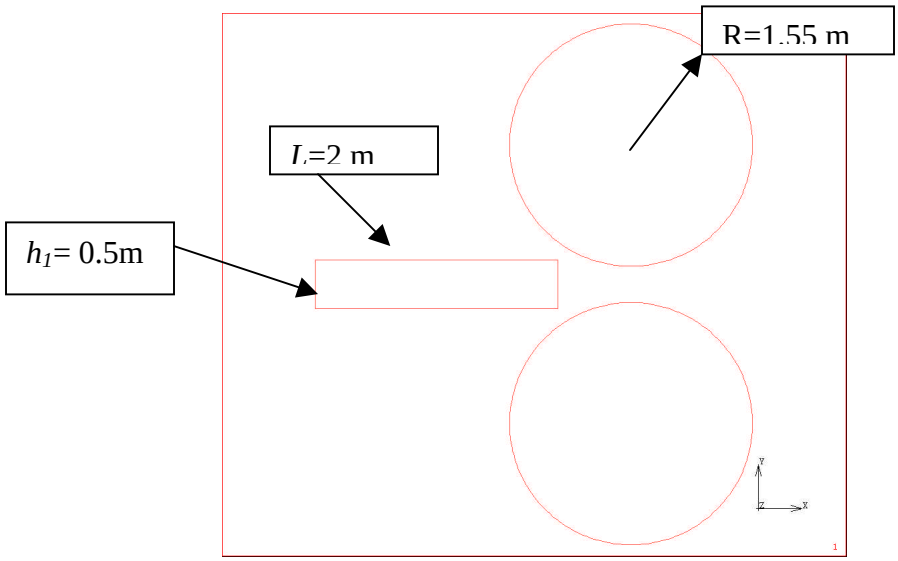

Figure 4.2: 2-D model geometry

Initial Conditions

Initial Temperature of the slab = 298.15 K

Boundary Conditions

1. Plastic Heat Generation with $\eta = 0.9$, i.e. 90% of the mechanical energy of deformation is converted into heat. The remaining 10% mechanical energy is used on dislocations, etc
2. Conduction across the edges of the slab with $k = 8000 \frac{W}{m^2 K}$
3. Film convection to the environment with $h = 50 \frac{W}{m^2 K}$ with an environment temperature of $T_\infty = 298.15K = 25°C$

Slab Properties

Plasticity : Elastic-Plastic (Solid) Formulation

Yield Surface: von Mises

Hardening: Isotropic

Friction coefficient μ= 0.5 [56]

According to Krupkowski, the strain-hardening curve for 0.1% carbon steel has the following constitutive equation:

$$\sigma = 66 \times 10^{7} \varepsilon^{0.248} \quad \left(\frac{N}{m^2} \right) \tag{4.3}$$

Young's Modulus: $E = 210x10^{9} \frac{N}{m^2}$

Poisson's Ratio: $\mu = 0.3$

Coefficient of Thermal Expansion = $1.17x10^{-5} / K$

Mass density: $\rho = 7860 \frac{kg}{m^3}$

Conductivity: $K = 8000 \frac{W}{m^2 K}$

Specific Heat: $C_p = 500 \frac{J}{kgK}$

Emissivity: $\varepsilon = 0.8$

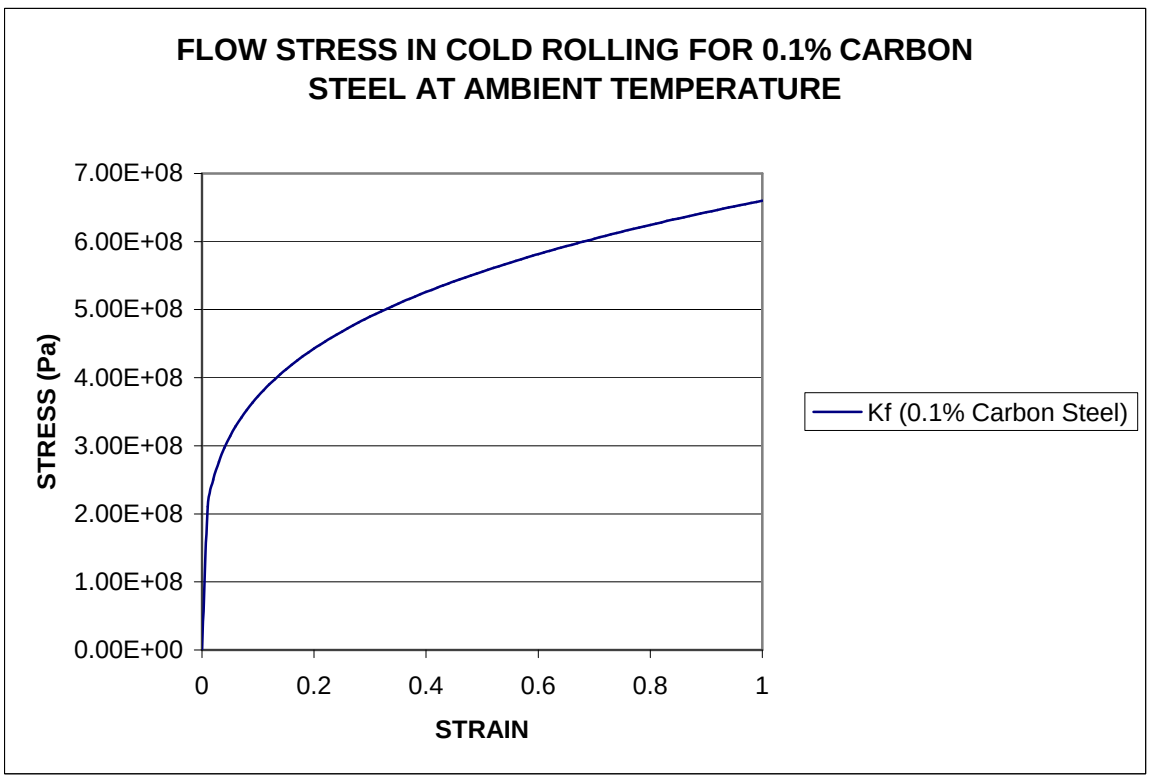

Figure 4.3: Strain Hardening curve for 0.1 % Carbon Steel where K_f is the yield stress

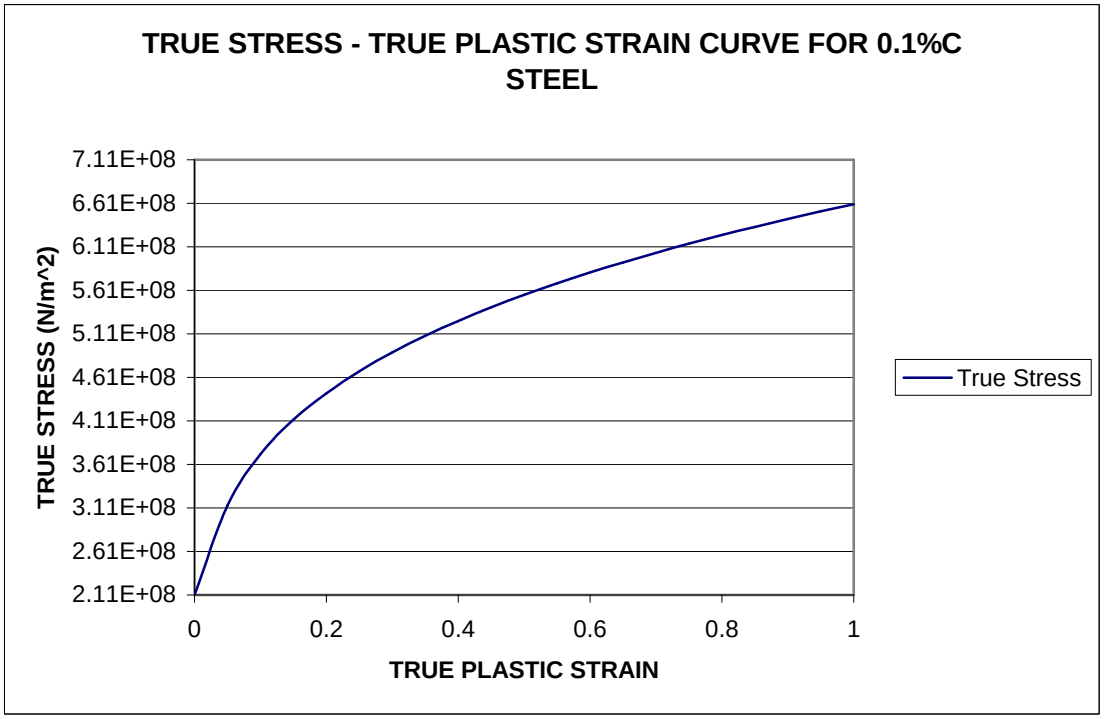

Figure 4.4: True stress – true plastic strain curve for 0.1% Carbon Steel

Where the true plastic strain is $\varepsilon^p = \varepsilon - \varepsilon^e = \varepsilon - \dfrac{\sigma}{E}$

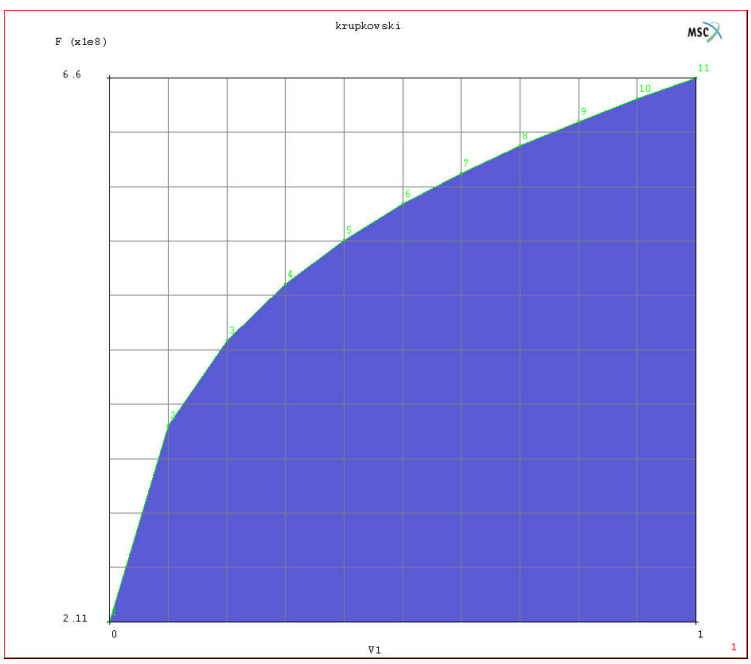

Figure 4.5: Krupkowski's True stress – true plastic strain curve for 0.1% Carbon Steel input in MARC

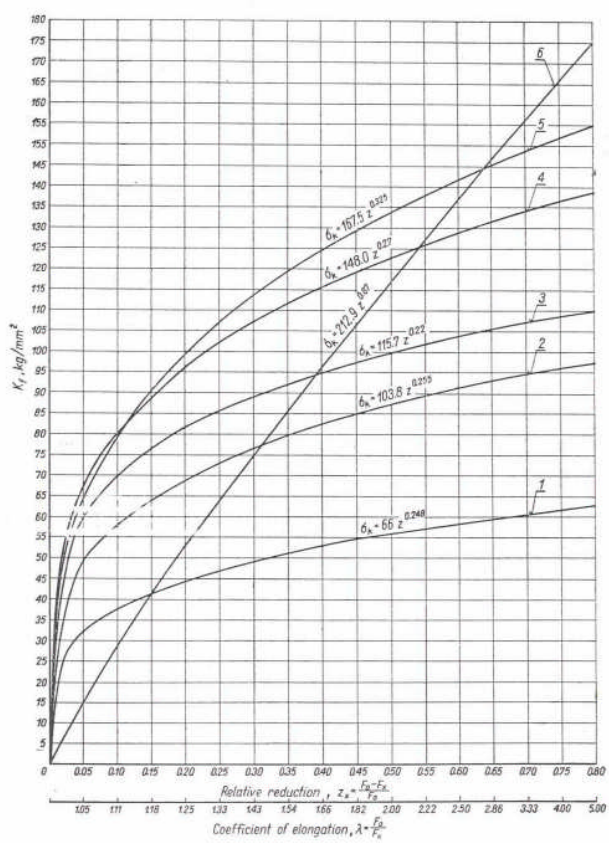

Figure 4.6: Strain hardening curves for steel according to Krupkowski: 1- 0.1% Carbon steel; 2- 0.33% Carbon Steel; 3- 0.42% Carbon Steel; 4- N Steel 0.9%C; 5 – T55 Steel 0.55%C; 6 – 18-8 Steel [72] © Pergamon Press / Elsevier Science

For a uniaxial test, the true strain is equal to the equivalent strain because in a uniaxial test, the other two strains are zero. The true strain rate is also equal to the equivalent strain rate. In a uniaxial tensile test, the usual material data is given in the form of true stress vs. true strain. However when we introduce this data in MARC, it has to be in the form of true stress vs. true plastic strain, and the first point for the true stress must be the yield stress.

4.2.1 Deformable-Rigid with Heat Transfer Case

The first case analyzed corresponds to the cold rolling of a deformable workpiece with the properties and the boundary conditions previously described. The rolls are rigid with infinite stiffness but take into account the heat transfer by conduction from the workpiece to the rolls. This heat transfer to the rolls however cannot be recovered.

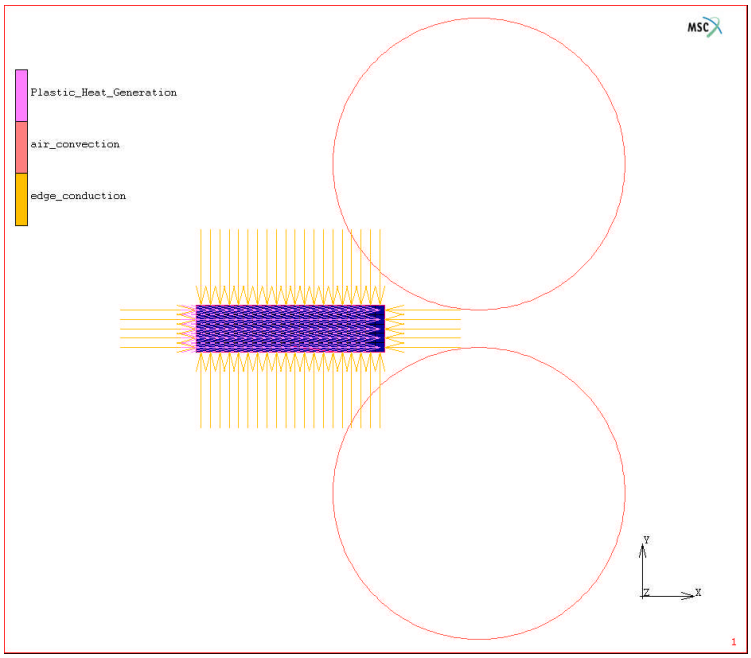

Figure 4.7: Boundary Conditions on the deformable – rigid case

The workpiece is subject to a 20% reduction and the rolls are spinning with an angular velocity of w =1.5 rad/s

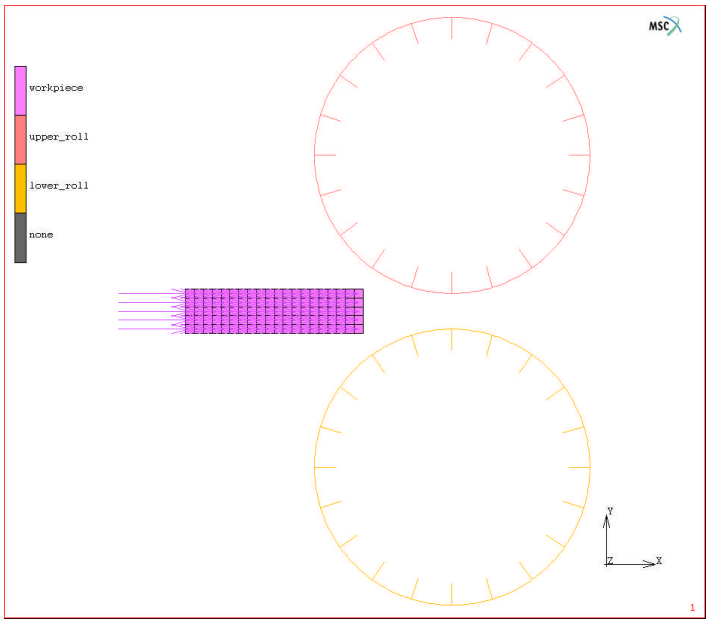

Figure 4.8: Contact definition

The contact problem is defined as follows: workpiece is a deformable body as previously mentioned, and the rolls are rigid bodies and have rigid-deformable body contact with the workpiece. The contact distance tolerance is set at 0.0005, with a bias *B*=0.99 and a separation force F_s= 1 x 10^{-9}. Double sided contact is enforced. The values for the contact distance tolerance, bias, and separation force, were the ones needed to assure convergence of our model. The bias factor B is the delta tolerance that the program uses to know whether the node is in contact with the roll or radius *R*. MARC then uses concentric circles or radii *R+Bias* and *R-Bias* respectively, to determine the node contact zone and find the node forces during contact. The program then evaluates the corresponding equations to find the contact force at the nodes to then perform a check:

- if Contact Force *F* > Separacion force *Fs* => no contact. The node is released and a new set of equations is made followed by a new iteration until convergence is found
- if Contact Force *F* < Separation force *Fs* => stay in contact

The distance tolerance is 5% of the smallest element length. The distance tolerance bias is a very important parameter. A bias B=0.9 means that 90% of the 2*Delta Tolerance zone will be inside the body and 10% will be outside the body. This is very helpful because it will not pull nodes in contact with the rolls. This is consistent with the contact study performed in Chapter 2, Section 2.7.

The workpiece was meshed using plane-strain 4-node quadrilateral quad (4) linear function elements with full integration (Marc element #11)

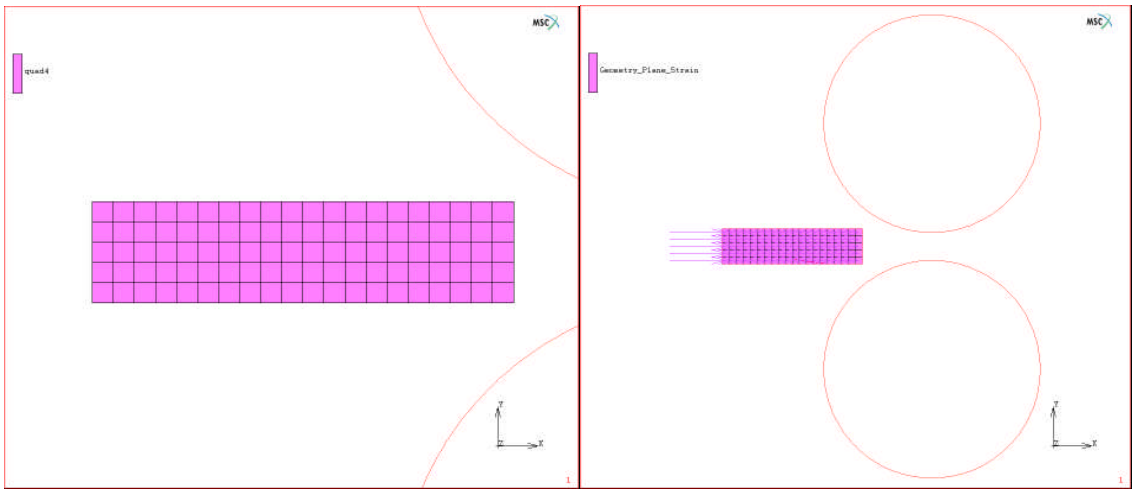

Figure 4.9: mesh detail and plane strain geometry

The simulation was run as a coupled thermo-mechanical transient dynamic problem. The convergence testing was set to auto switch (uses both relative and residuals). The total loadcase time was 3 seconds and the number of steps was 200. For the solution control, the maximum number of recycles was set to 20. The iterative procedure selected was the full Newton-Raphson method with a convergence of 10^{-5}.

The results corresponding to the simulation are shown in the following figures 4.10 thru 4.20.

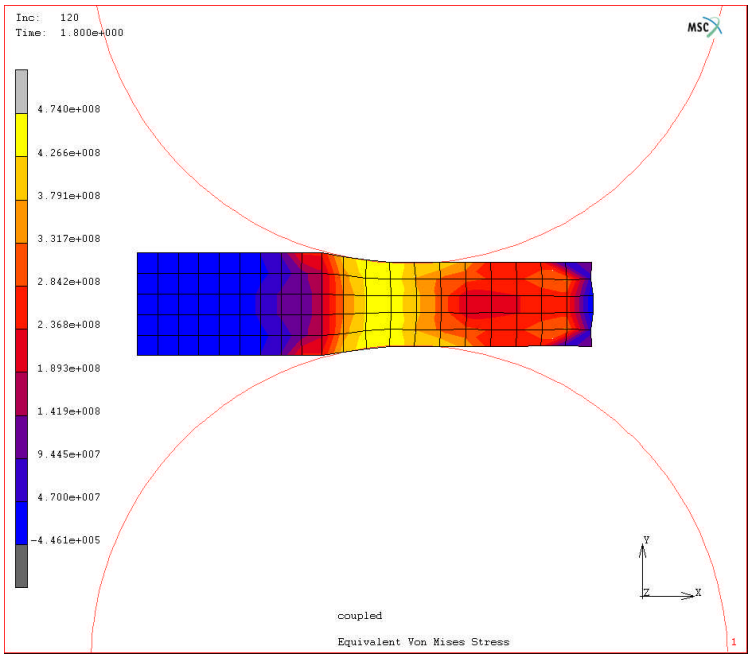

Figure 4.10: Equivalent Von Mises Stress

The maximum von Mises stress is 4.74×10^8 Pa, which is in agreement with the constitutive equation used for the 0.1% Carbon steel.

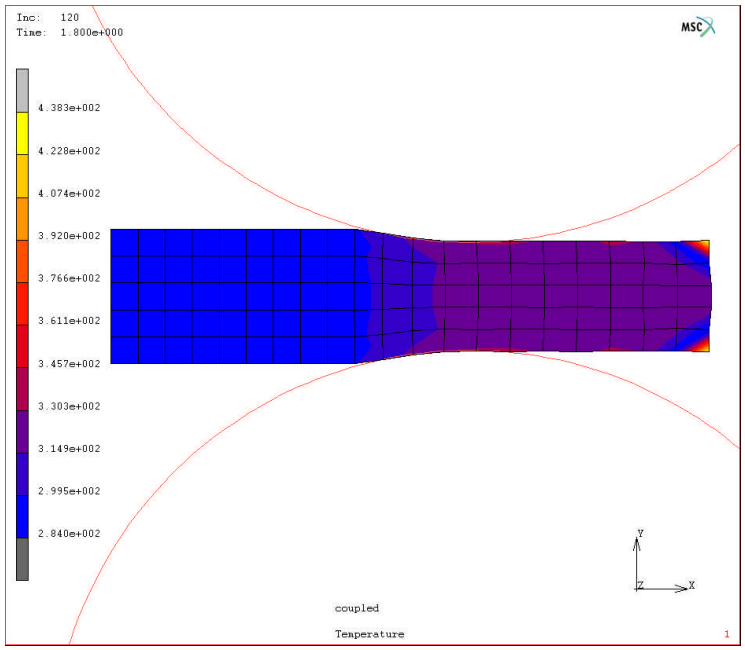

Figure 4.11: Temperature distribution

The temperature of the workpiece increases from 298K to an average of 330 K. Notice how there are local areas that see higher temperature increases such as the corners where the rolls first contact the slab, and the arc of contact where all the high friction forces take place.

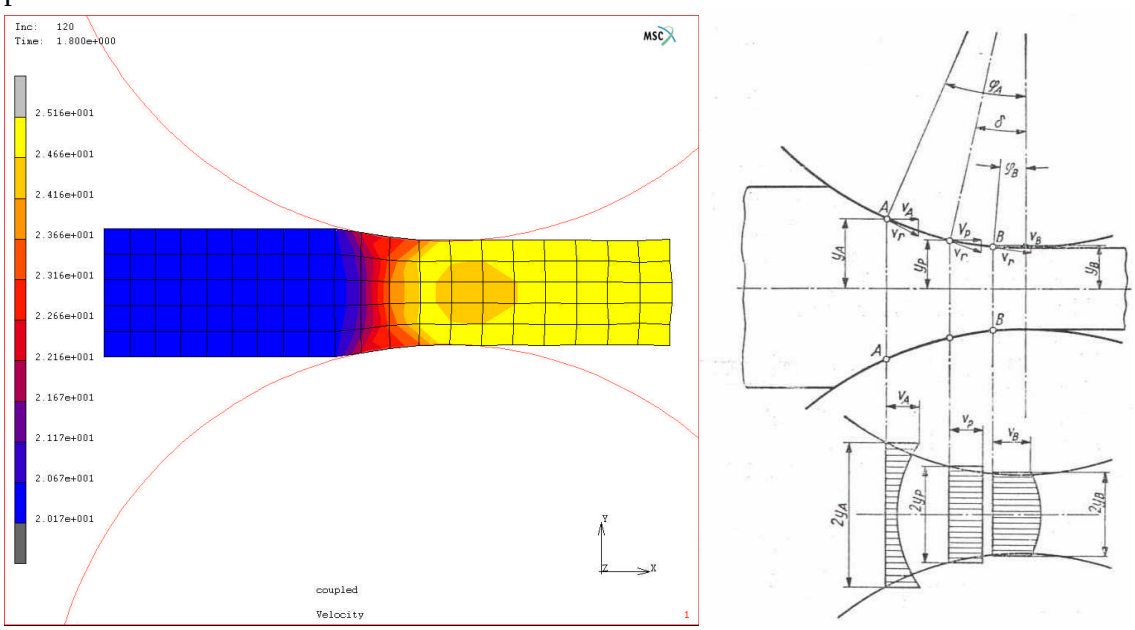

Figure 4.12: Velocity distribution according to FEM and to the classical theory of rolling [72] © Pergamon Press / Elsevier Science

As it can be seen in Figure 5.12, the assumptions made in the classical theory of rolling that were used to derive the formulas for the resistance to deformation, torque, roll load, etc, are not accurate. Here we can clearly see that plane sections do not remain plane and that at the neutral plane the velocity distribution is not uniform but parabolic.

In classical theory according to Tselikov, the speed conditions in rolling along the arc of contact are directly connected with the build up of a sticking zone. He bases his assumption on the definition of the neutral plane, that in that plane all particles of the rolled stock of a cross-sectional height of $2y_p$ and width of b=1 have the same horizontal speed

$$V_p = V_r \cos\delta \tag{4.4}$$

where

V_r = peripheral speed of rolls
δ = neutral angle

Subsequently, Tselikov considers the speed distribution over the cross-sectional height of the rolled stock for two other arbitrary chosen planes A-A and B-B positioned in the sticking zone, one on each side of the neutral plane. The heights of the rolled stock in the considered planes are denoted $2y_A$ and $2y_B$. Owing to the disappearance of slip between rolls and the stock within the sticking zone all particles in contact with the rolls along the whole zone will have the same speed as the peripheral speed of the rolls. Therefore it follows that the horizontal speed component of the rolled stock at points A and B is

$$\begin{aligned} V_A &= V_r \cos\varphi_A \\ V_B &= V_r \cos\varphi_B \end{aligned} \tag{4.5}$$

where φ_A and φ_B indicate rolling angles at points A and B. The volume per second of the rolled stock passing through any cross section should be constant

$$Volume = 2y_p V_r \cos\delta \tag{4.6}$$

in the previous figure we can also notice the non-uniform speed distribution in cross sections A-A and B-B.

It is true that the speed distributions in sections A-A and B-B are non-uniform, but they actually have the opposite shape, i.e. speed distribution in section A-A is concave and the one corresponding to section B-B is convex. His error was due to the fact that he did not fully understood the mechanics of the problem and due to the very general assumptions he made for his model, mainly the assumption that plane sections remain plane throughout the deformation process.

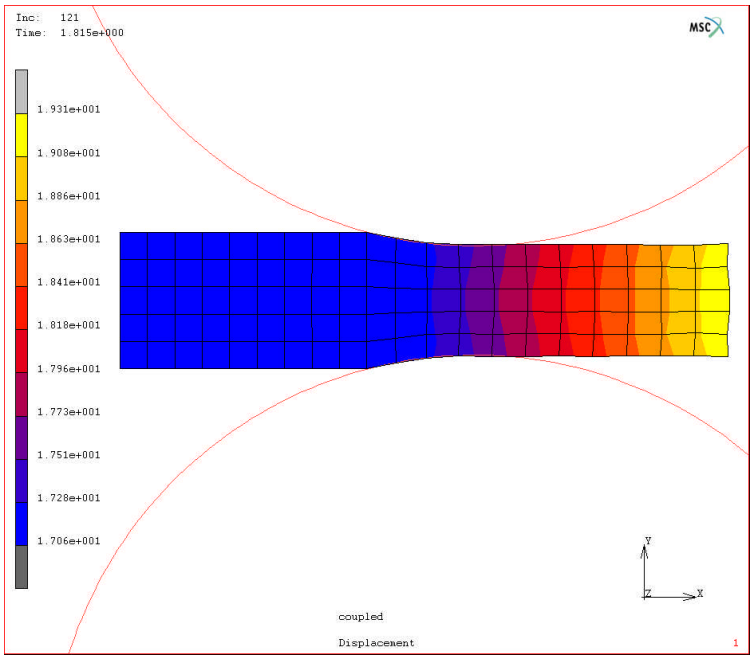

Figure 4.13: Displacement distribution

Figure 4.13 also demonstrates results, which support that plane sections do not remain plane. This figure agrees with the results obtained in practice done with soft materials such as plasticine and putty. Figure 4.14 shows how the plasticine takes the same shape only that the shape is even more pronounced because it is a lot softer and malleable than the steel. Also, the greater the influence of friction on metal surface, the more pronounced are the distortions it causes, and the metal is forced to move together with the roll surface. Thus, in cold rolling, vertical plane sections become curved in the direction of rolling under the action of frictional forces.

If we compare this with the case of the compression of a block of steel we can see that a similar displacement field occurs. Thus we have proved objective c) of the list of goals we set for this thesis.

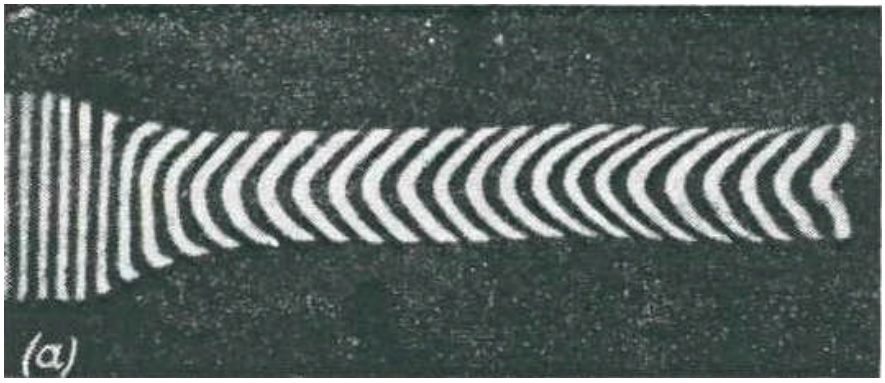

Figure 4.14: Plasticine bar rolled between wooden rolls [72] © Pergamon Press / Elsevier Science

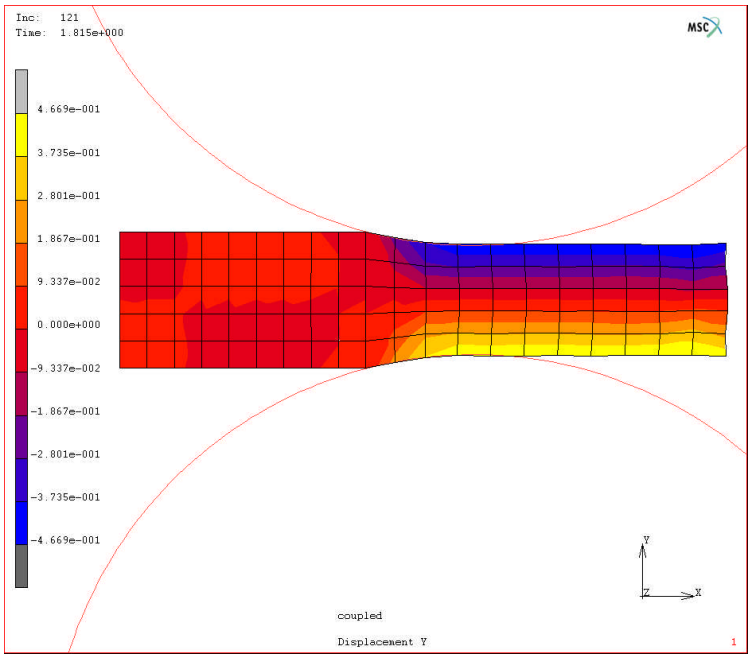

Figure 4.15: Displacement in y direction

In this previous figure we can see how the material flows in the vertical direction as it is compressed

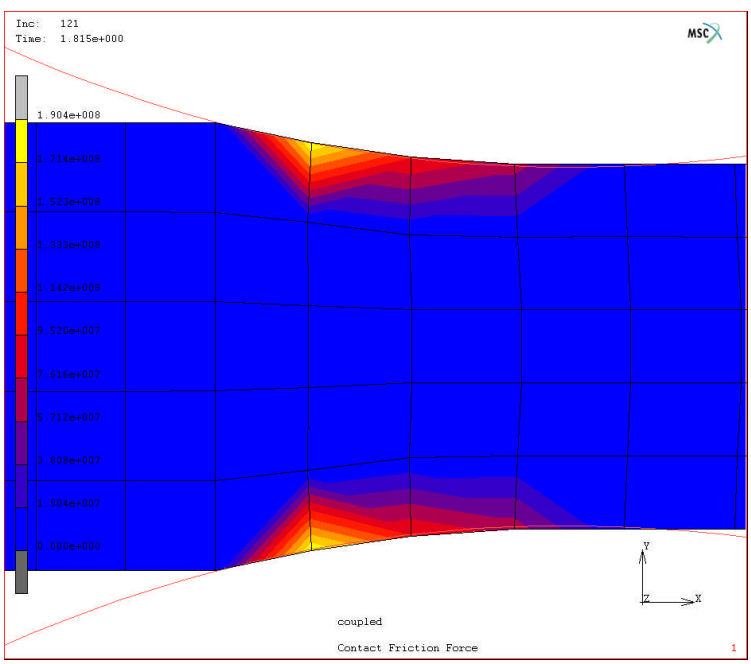

Figure 4.16: Detail of the contact Friction force

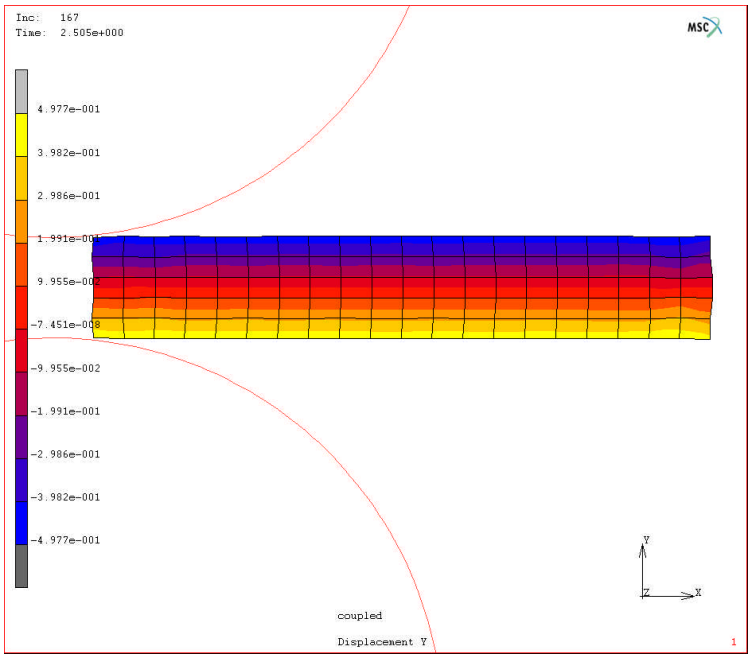

Figure 4.17: The rolled strip comes out perfectly flat

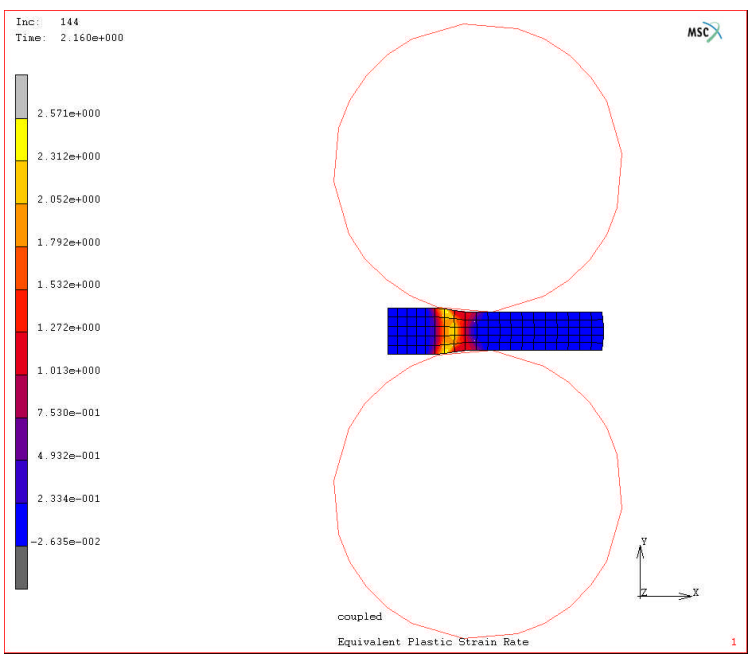

Figure 4.18: Equivalent Plastic Strain Rate $\dot{\bar{\varepsilon}}^{p}$

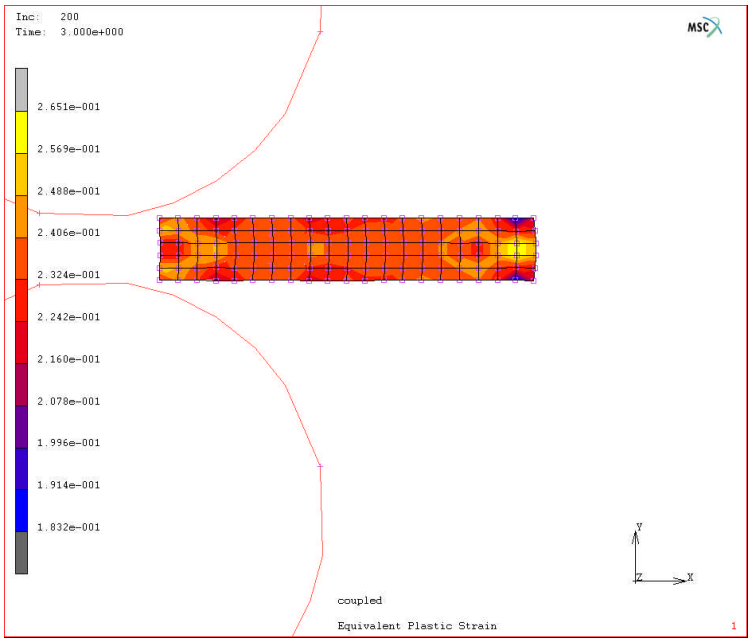

Figure 4.19: Equivalent Plastic Strain $\bar{\varepsilon}^{p}$

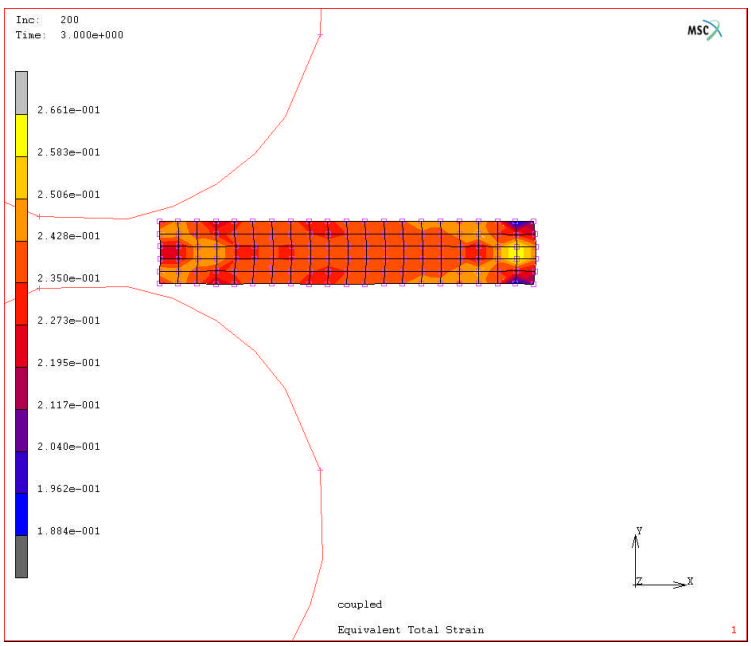

Figure 4.20: Equivalent Total Strain $\bar{\varepsilon}$

The results agree with published results by Lenard & Pietrzyk [56], and Kobayashi [44]

4.2.2 Deformable-Rigid with Heat Transfer Case

In this model, the rolls are modeled as “rigid with heat transfer”, taking advantage of a special type of element (#39) that is available in MSC MARC. This element #39 employs a heat conduction planar 4 node quadrilateral linear function. The purpose of using this element in the rolls is that this time we will be able to recover heat flux from the cold worked slab to the rolls, something that we were not able to do previously. The following figures illustrate the results. The rolls still have infinite stiffness and so no stresses will appear in the rolls (they are rigid for all purposes) and the results for the von Mises stress in the workpiece will be exactly the same as in the previous case. Thus we will only focus on the heat flux from the workpiece as it heats up due to friction and plastic deformation.

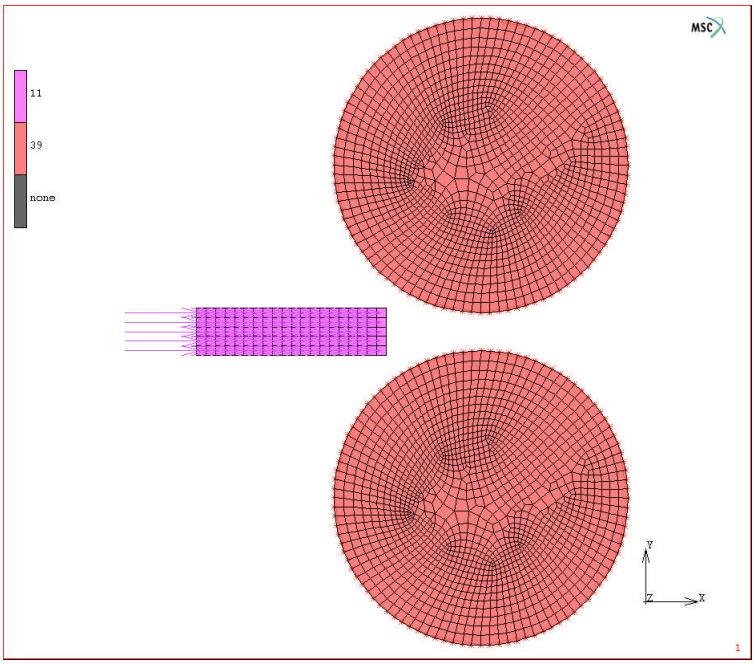

Figure 4.21: Detail of the model with the two types of elements

Figure 4.22 shows how the heat generated during the plastic deformation is transferred to both the rolls and the workpiece whose temperature also increases slightly.

The heat generated during the friction process heats up the outer edge of the rolls and also the outer surface of the workpiece. The maximum temperature occurs at the corners of the workpiece due to the “roll bite phenomenon” during which the rolls grab the workpiece if and only if the tangent of the angle of contact is less than the friction coefficient. The increase in the temperature in the inside of the workpiece is due to the plastic heat generation.

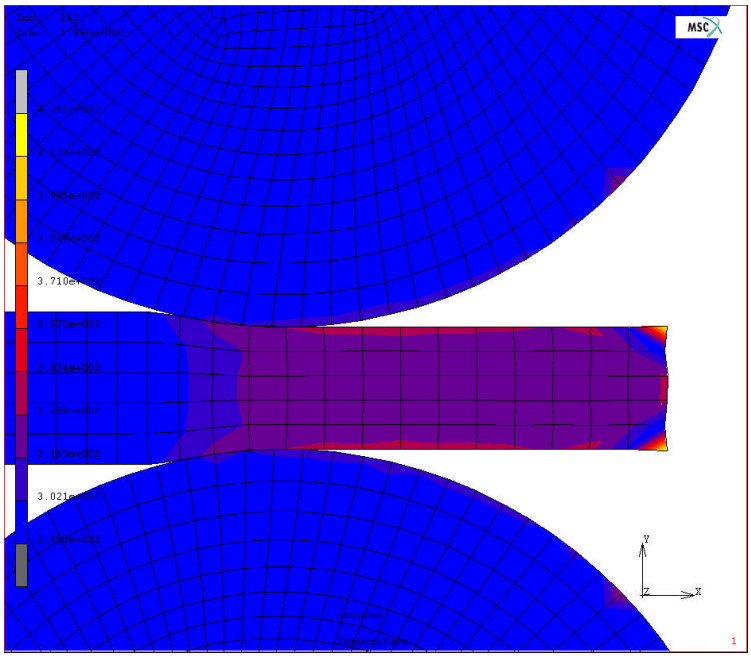

Figure 4.22: Detail of the slight increase in temperature on the outer edge of the rolls

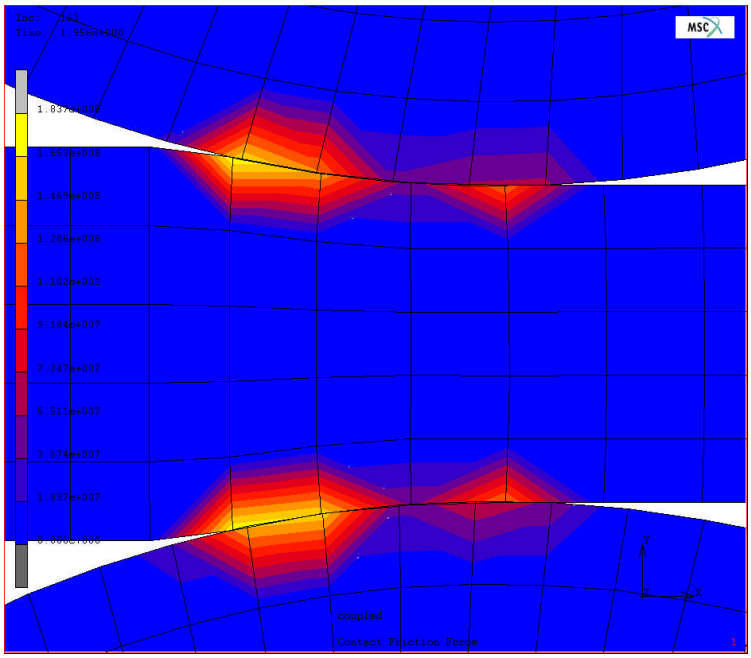

Figure 4.23: contact friction force

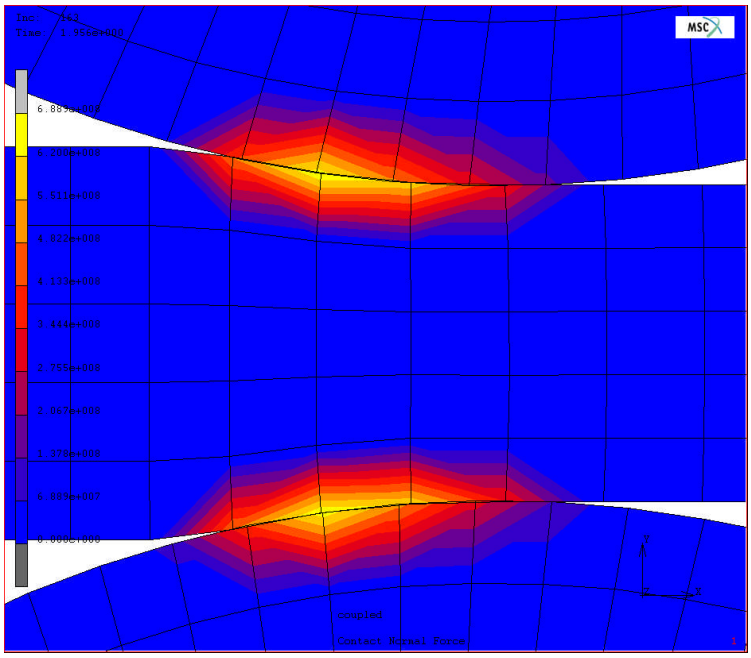

Fig 4.24: contact normal force

4.2.3 Deformable-Deformable Case

In this case, the rolls will be modeled as deformable, so now we will be dealing with a deformable-deformable contact problem. The coupled thermal mechanical analysis with both rolls and workpiece modeled as deformable should yield the most accurate and realistic results in terms of the stresses on both the workpiece and the rolls.

This case presents the challenge that since the rolls, now modeled as deformable bodies rotate, the rotation of the rolls generates rigid body motions, which have smaller deformations on them. The solution used to work around this problem was to create a small rigid disc within the roll representing a rigid body. Then a ring of deformable elements was attached to the outside of the rigid disc. The rigid body control and angular velocity are defined as part of the disc properties. Figure 4.25a shows the stress distribution in the rolls which is quite different from what it was thought to be according to the classical theory (Figure 4.25 b)

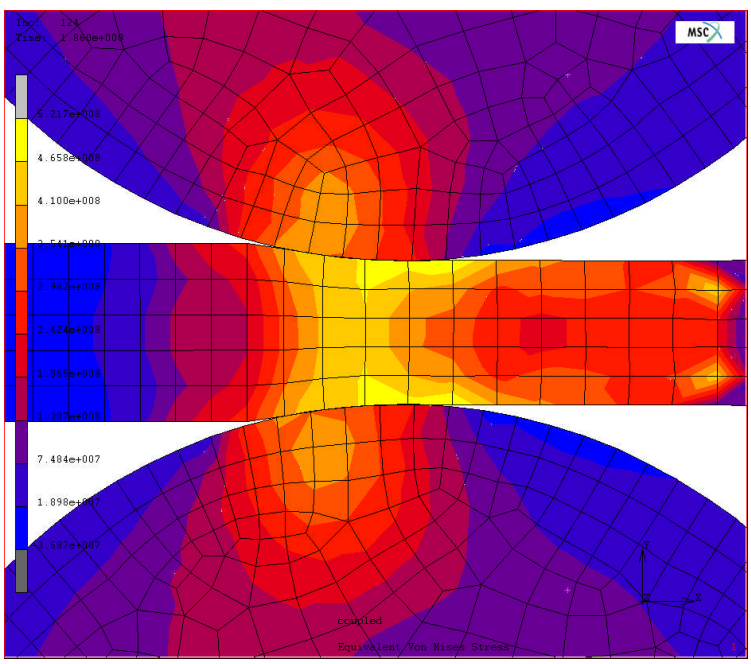

Figure 4.25 a: Stress distribution in rolls and slab

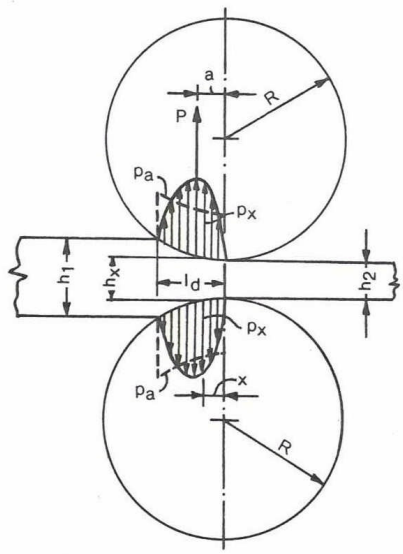

Figure 4.25 b: Distribution of normal pressure and roll separating force in rolling [32] © Marcel Dekker / Taylor & Francis Group

$$P = \int_0^{ld} p_x dx = \int_0^{\alpha} R p_\theta d\theta \tag{4.7}$$

where

p_x = normal pressure at distance x from the exit plane

p_θ = normal pressure at the roll angle θ

l_d = projected arc of contact between the rolls and the workpiece

α = roll bite angle

As it can be seen, the classical theory determines that the stress distribution in the rolls has a parabolic shape with a maximum at the neutral angle. The model shows how in reality, the stress distribution is much larger in magnitude, and has a much different shape where instead of a parabolic stress distribution, we have a series of concentric "balloons". This distribution seems correct because it resembles very much the stress distribution for the Hertzian stress contact problem that we will look at in the next Section 4.2.4. Both distributions look exactly the same with the difference that the rolls' stress distribution is not symmetric with respect to the y-axis. This is expected because the FE model for the Hertz contact stresses is between a disc and a flat surface, whereas, in our rolling problem, instead of a flat surface we have a curved surface. In the limiting case, we could say that the flat surface is a curved surface of infinite radius. We then feel confident that our result is correct even though no literature on this subject has been found.

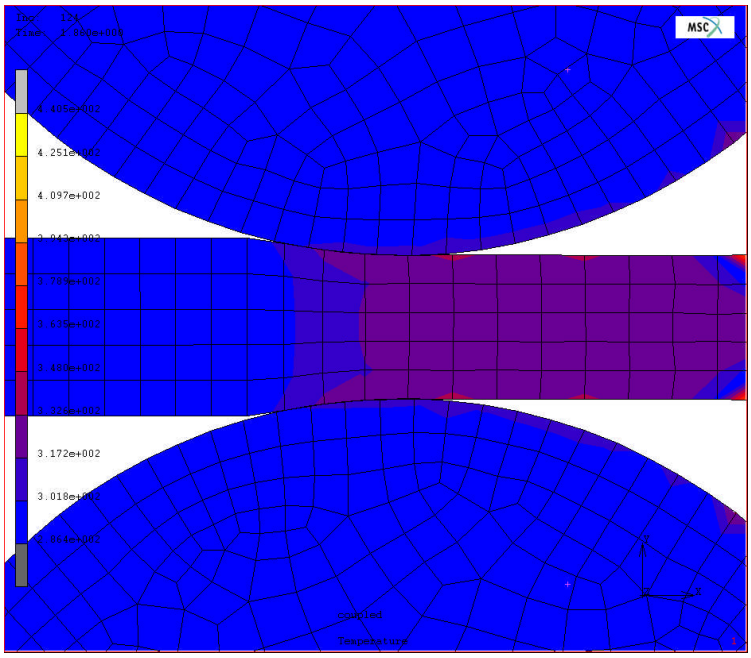

Fig 4.26: Temperature distribution

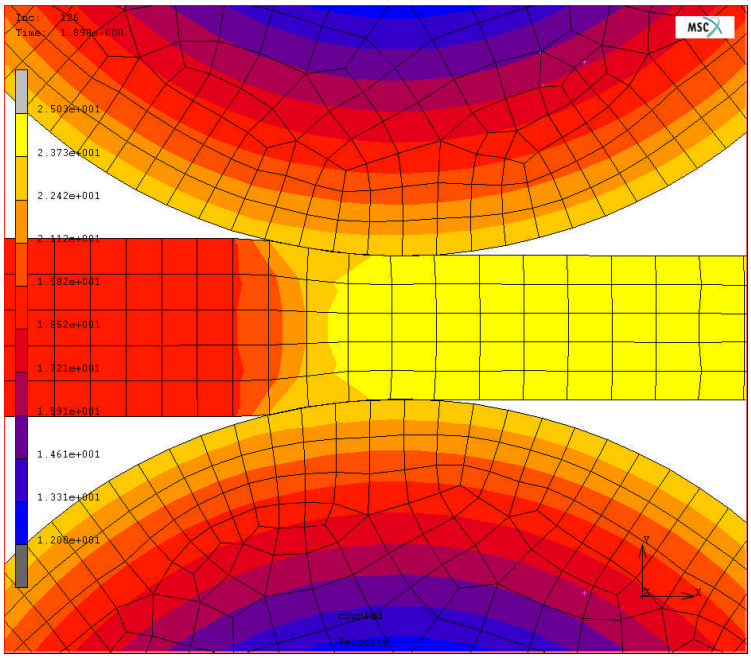

Figure 4.27: Velocity Distribution and the Neutral plane

Figure 4.26 shows how the outer part of the rolls heats up due to friction and the temperature of the workpiece increases due to plastic work heat generation. Temperature in the rolls goes from 25 ºC to 56ºC. The temperature in the workpiece goes from 25 ºC

to an average of 60ºC although at the edges of the workpiece it increases up to 90ºC in the points of maximum friction.

Figure 4.27 clearly shows how the plane in which the velocity of the rolls equals the velocity of the workpiece (definition of neutral plane) actually has a C shape against the belief in the classical rolling theory that plane sections remained plane. Also, the slab increases its velocity. This is due to the fact that the volume stays constant and because of conservation of mass in order to be able to "process" all the material the workpiece has to pick up speed the same way a fluid such as air or water increases its speed when flowing through a constricted or narrow passage.

The numerical results for the main parameters of interest, namely, equivalent Mises stress, maximum strain rate, temperature increase, strip length increase, strip width increase (spread), % reduction achieved after rolling, and strip velocity increase, and the main conclusions obtained from the above figures corresponding to the 2-D cold rolling case are summarized in section 4.2.6.

4.2.4 Analysis of the Hertzian stresses in the rolls due to contact

The most interesting result in the previous section is without a doubt the combined look at the stress distribution in the rolls and the workpiece. The result is very similar to the problem of Hertzian contact stresses between a disc and a flat surface. The rolling problem is somewhat similar except that the disc is "rolling" at the same time that is pressing down on the flat surface.

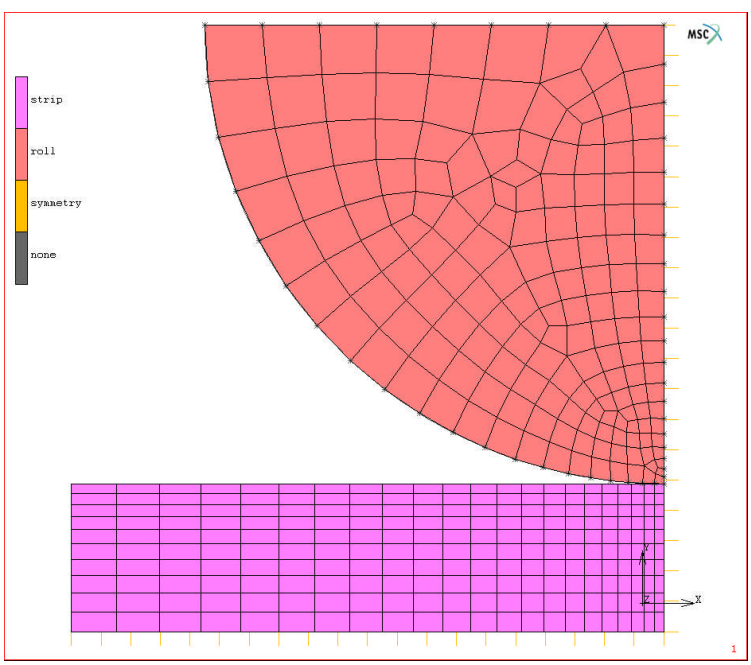

Figure 4.28: FE model for hertz contact stress between a disc and a flat surface

In order to obtain a better understanding of the stresses in the rolls we modeled the classic Hertz contact problem. In the following figures we can see the model and stress analysis corresponding to this well-known case whose result has been published. As we will see, the stress distribution is similar to the one we just saw in the deformable-deformable rolling problem as we can see in Figure 4.28:

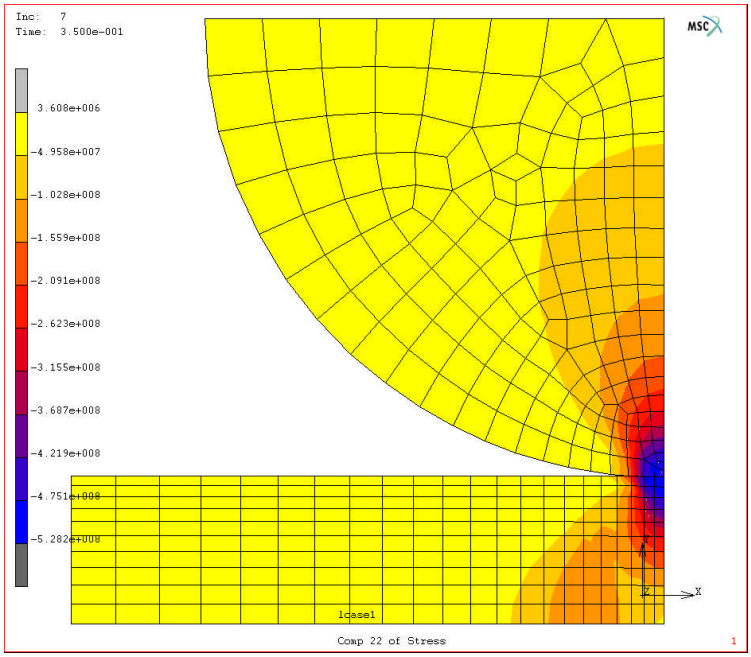

Figure 4.29: Hertzian Stresses in a symmetric model

In this case, a load somewhat equivalent to the one applied by the rolls is applied for one second. A maximum compressive stress of -5.28×10^8 is obtained. The most interesting result is the shape of the stress distribution in the disc that simulates the upper roll. The distribution is somewhat similar to the one we saw on the deformable-deformable case. In this case there is perfect symmetry in the loading and consequently in the stress distribution. In our rolling problem we do not have such perfect symmetry, as the rolls do not apply the load perpendicularly, but at an angle. Therefore the stress distribution in the rolling problem becomes asymmetric. Also, the part of the model representing the workpiece is perfectly flat, whereas in the rolling problem, it is curved.

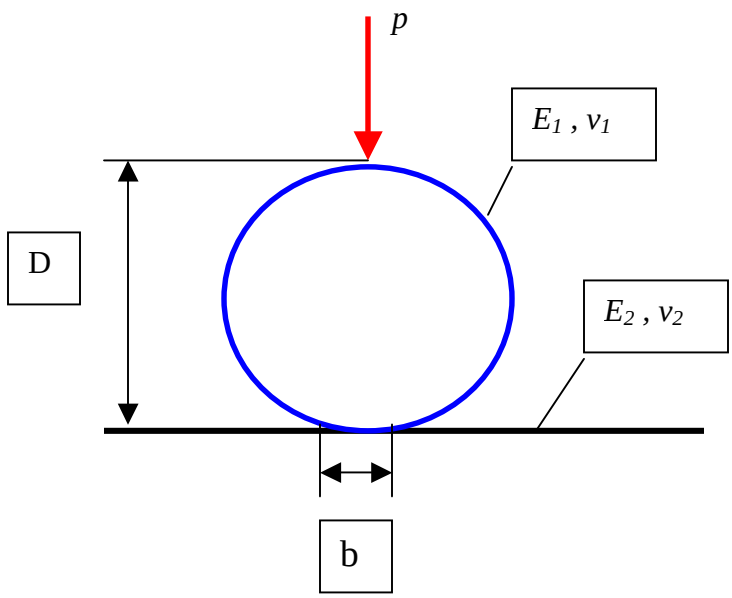

Figure 4.30: The Hertz Contact Problem

The solution agrees with the theoretical solution as given by Roark & Young, pg 651 Given a cylinder of length L, large as compared to its diameter D, subject to a load per unit length *p*, the contact patch is found through the formula

$$b = 1.60\sqrt{pK_D C_E} \tag{4.8}$$

where, K_D= D

$$C_E = \frac{1-v_1^2}{E_1} + \frac{1-v_2^2}{E_2}$$

The maximum compressive stress in the y direction is then given by

$$\sigma_{\max} = 0.798\sqrt{\frac{p}{K_D C_E}} \tag{4.9}$$

Substituting values for our model, we get a result, which is just 0.76% off the FEM solution.

4.2.5 Upsetting of a Square Block between flat dies

Another part of our stepping-stone approach was to first analyze the upsetting of a square block between flat dies. This process is similar in nature to the rolling process. The difference here is that the dies are not rolling over the surface of the workpiece, but stationary.

For this purpose, a non-linear finite element model of this problem was created. The problem is again modeled as a coupled thermo-mechanical dynamic transient problem. The material is also 0.1%C steel, is modeled following the elasto-plastic material formulation, with a von Mises yield surface, and it follows the same constitutive equation (Krupkowski's) used in the flat cold rolling problem. The dies, shown in the model as horizontal red lines, are modeled as rigid bodies.

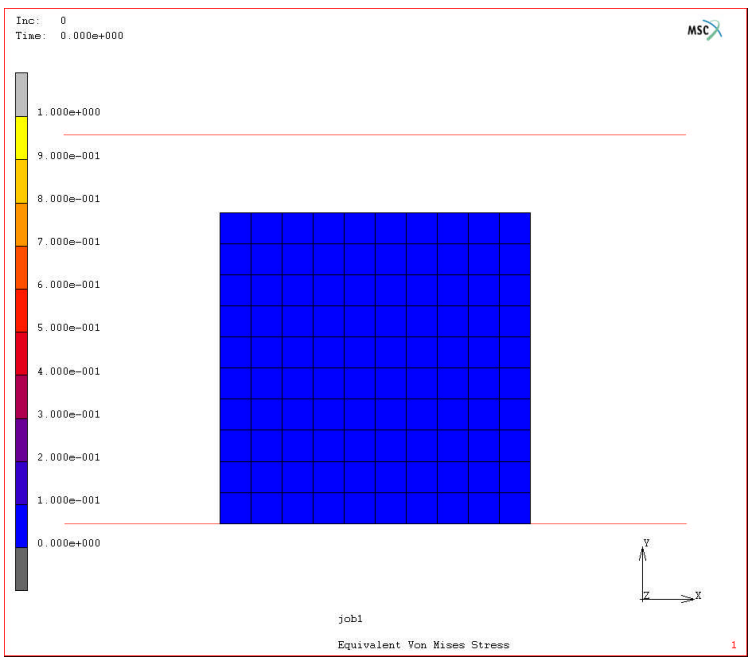

Figure 4.31: Initial shape and mesh of square block model

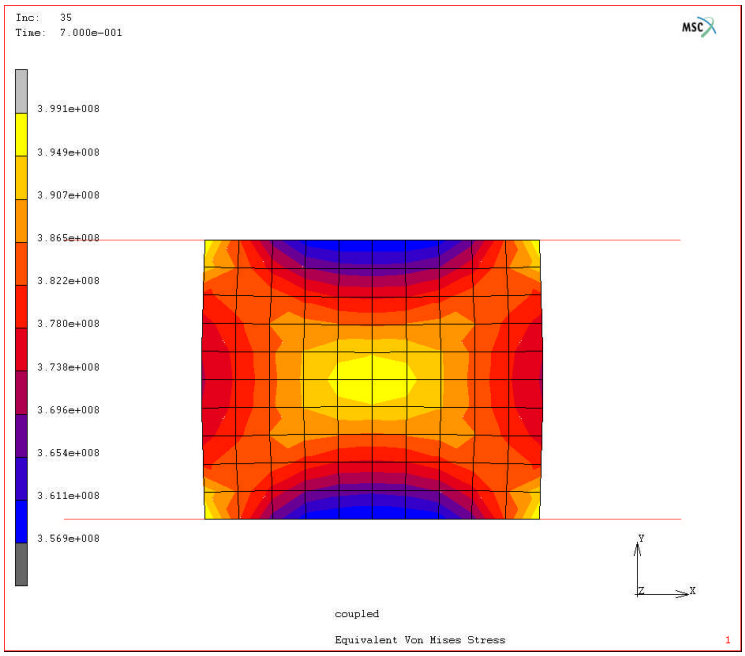

Figure 4.32: Plane Strain Upsetting of a Square Block: Equivalent von Mises stress after a 10% reduction

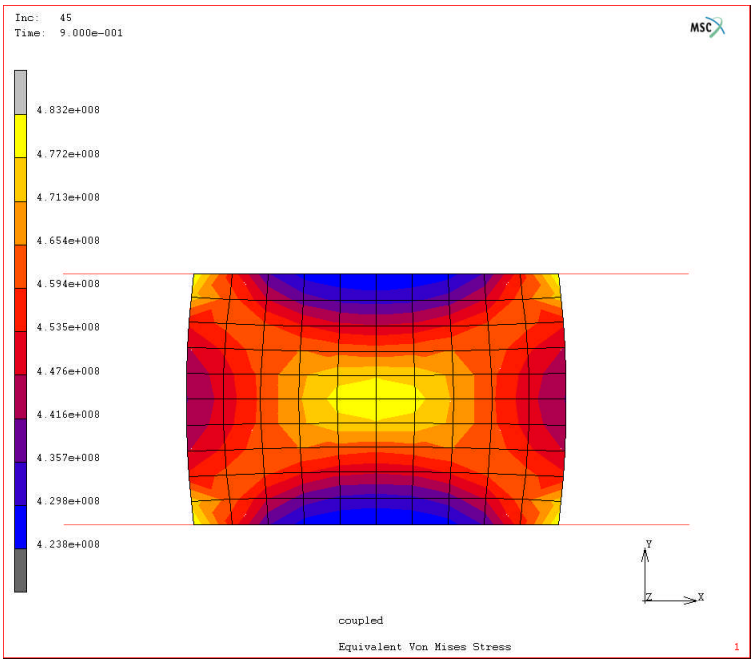

Figure 4.33: Plane Strain Upsetting of a Square Block: Equivalent von Mises stress after a 20% reduction

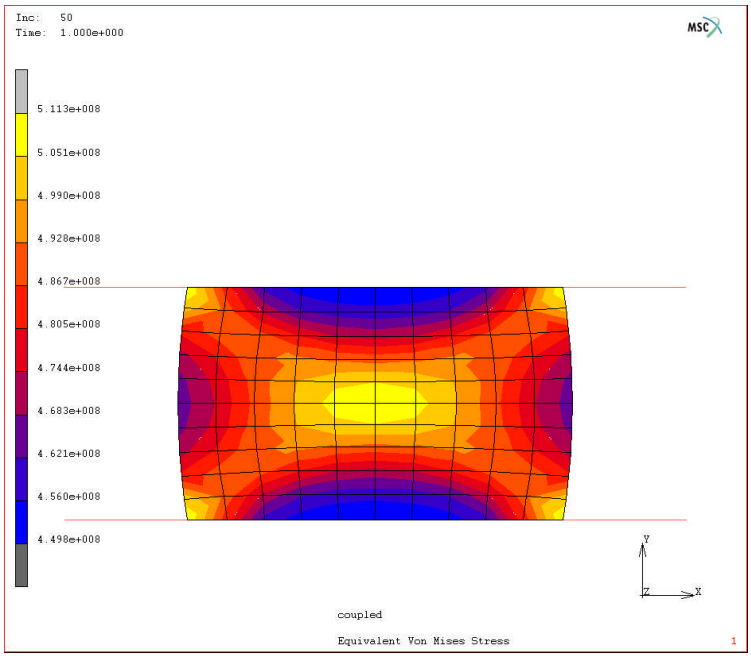

Figure 4.34: Plane Strain Upsetting of a Square Block: Equivalent von Mises stress after a 25% reduction

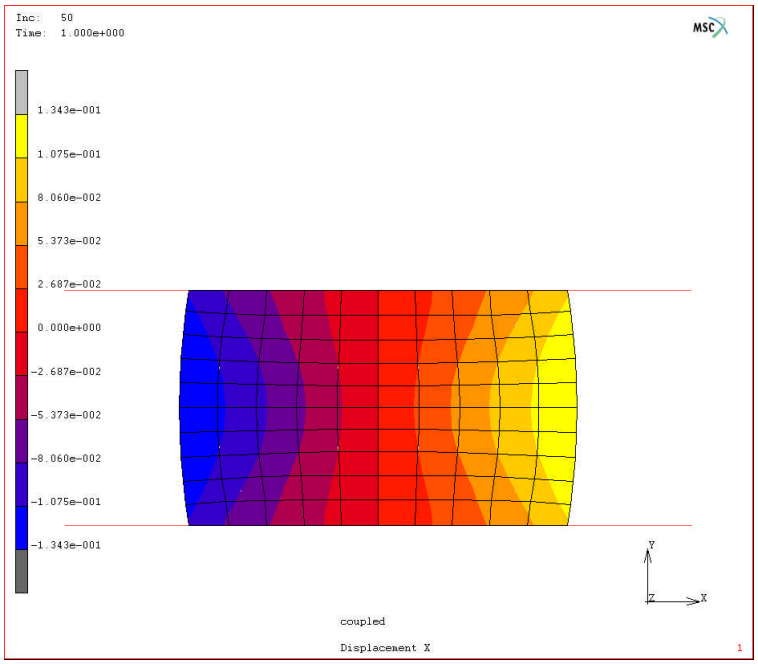

Figure 4.35: Displacement in the x direction

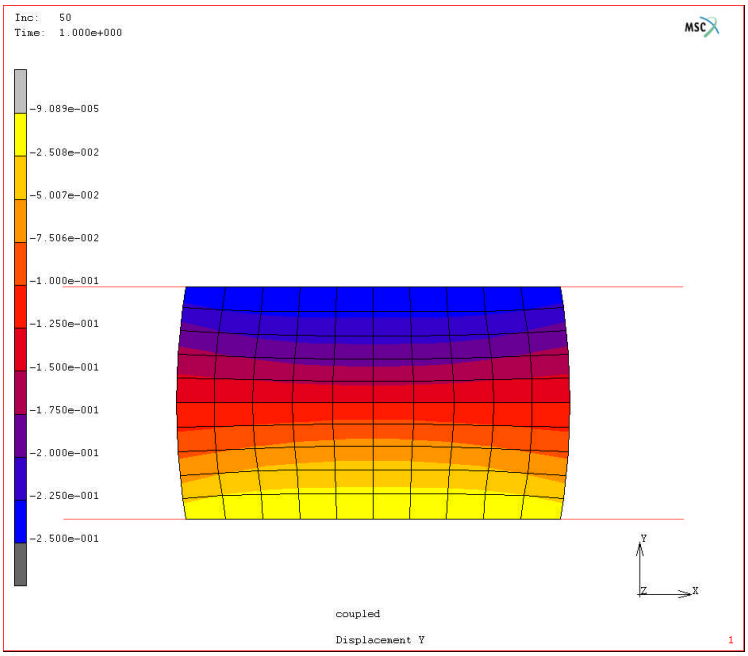

Figure 4.36: Displacement y-direction

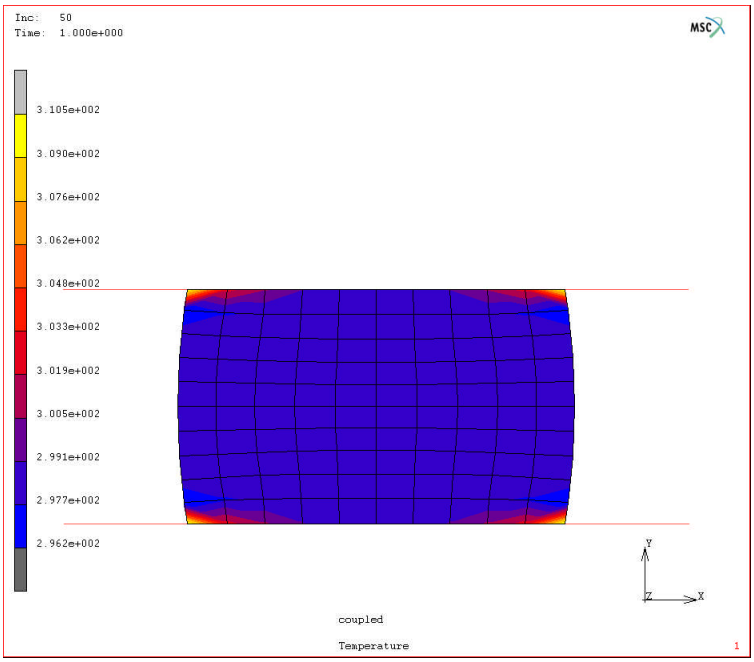

Figure 4.37: Temperature increase

Note that the external friction results not only in non-uniform stress distribution, but also in formation of regions with varying capability of deformation. Consequently, the metal undergoes non-uniform deformation, resulting in barreling of the square specimen (Figure 4.37).

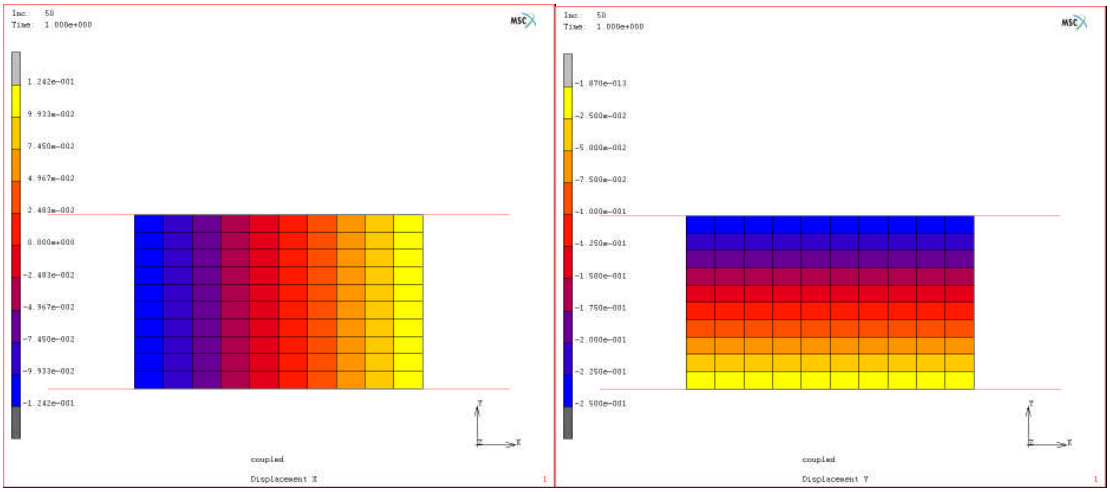

Figure 4.38: Deformation of square block with no friction

As it can be seen in Figure 4.38, if no friction is present, the deformation is homogeneous in both the x and y directions and plane sections remain plane. This simple simulation shows the critical role that friction plays in the deformation process.

The temperature increase is higher towards the corner nodes because those go through a higher displacement and thus also have a larger contact friction force.
Figures, 4.31 thru 4.37, show that the x-displacement distribution in our simulation of the upsetting of a square block with Coulomb friction, looks very similar to the one in a cross section of a workpiece in flat rolling. The von Mises stress is almost exactly the same (4.8×10^8 vs 4.74×10^8) and the actual stress distribution looks the same. For a comparison with the flat rolling process refer to Chapter 4, Section 4.2.1. The differences are due to the different nature of these two processes. The upsetting of a square block between two flat dies is a forging process and in it the material flows and deforms in a different way than in the rolling process. The temperature increase after a 20% deformation is 12˚C. The temperature increase is less than in the cold rolling process because the friction forces in the cold rolling problem are much larger due to the shearing action between the rolls, and thus a lot more friction heat is generated.

So as we can see the results between the upsetting of the square block between flat dies and the cold rolling process correlate fairly well. Again, the same temperature, friction coefficient, friction model (Coulomb), % reduction, etc. were used in both models in order to make a fair comparison. Between the results from the Hertzian stress and the results from this forging simulation of a square block we can conclude that the results obtained for the cold rolling process simulation are acceptable and reasonable.

The results for the upsetting of this square block, agree 100% with published results by Rowe et al.[64], and Kobayashi et al [44].

4.2.6 Results & Analysis

The results we obtained for the 2-D Plane Strain cold rolling problem can be summarized in the following table:

Table 4.1: Results for 2-D Plane Strain Cold Rolling FE models

Roll designer Parameters	COLD ROLLING	
	Classic Theory	**2-D plane strain FEM**
Equivalent Stress (Pa)	3.42×10^{8}	4.74×10^{8}
Equivalent Plastic Strain	NA	2.65×10^{-1}
Total Equivalent Strain	NA	2.66×10^{-1}
Maximum Strain Rate (s^{-1})	2.59	2.57
Temperature Increase (˚C)	21.1	32
Strip Length Increase (%)	12.50	12.45
Strip Width Increase / Spread (%)	35	NA
% Reduction Achieved after Rolling	20	19.91
Strip Velocity Increase (%)	25	24.74

The 2-D results can be considered as good and in agreement. . The slight differences between them can be attributed to the fact that the 2-D model ignores the strain in the z direction (depth), which in reality is not the case.

Resistance To Deformation/Equivalent von Mises Stress:. There is a significant difference between the FE results and the results obtained through the "classical rolling theory". As we saw, in order to simplify the problem, the classical theory makes many assumptions that are not entirely accurate. Among the main inaccurate assumptions we must point out the following:

a) The frictional forces do not produce the internal distortion of the metal and do not change the orientation of the principal directions,
c) Plane vertical sections remain plane and therefore, the deformation is homogeneous in regard to determination of induced strain,
d) Elastic deformation of the workpiece is negligible in comparison with the plastic deformation,
e) There is no elastic deformation of the tool in the contact zone,
f) The compressive strength is constant throughout the contact length,
g) The workpiece does not spread laterally as we assume a state of plane strain,
h) There is no roll flattening in the arc of contact,
i) Material does not undergo work hardening during its passage between the rolls.

All of the formulas used in the classical theory are empirical and differ significantly among rolling researchers. Each researcher tailored his set of formulas in order to match the results he obtained in the rolling mill. There are many sources of uncertainty when taking these measurements, which are particularly difficult given the nature of the rolling process with very high temperatures and a quite rudimentary instrumentation available at the time. It is quite possible therefore that some of the readings of the researchers were inaccurate. Each of the researchers likely had a different setup and a different set of conditions in terms of the radii of the rolls, thickness of the workpiece, rolling speed, temperature of the stock, etc. In a non linear process with so many variables and parameters the differences in the set up of each of the researchers' experiments, plus the assumptions that each of them made, led to the differences that can be observed on the formulas that each of them arrived to when trying to empirically predict the values of stress, torque, roll pressure, etc. The FE stress results obtained in this thesis are within the same order of magnitude but are 38% higher in the cold rolling case. Such differences can be attributed to the previously mentioned reasons. The FEM results are more accurate and are in agreement with comparable results published by other researches such as Lenard & Pietrzyk [56,49], Kobayashi et al. [44], Rowe et al. [64].

Maximum Strain Rate: the results for this important parameter of the cold rolling process are all basically in agreement. The FE results are 1% smaller than the cold rolling theory.

Temperature Increase: the FE results for the cold rolling case are 50% higher than the ones predicted by the classic rolling theory that predicts a temperature increase of 21.1˚C.

Strip Length Increase: the FE results are in perfect agreement with the classical theory ones. This parameter is one of the easiest to measure and as expected, the differences are extremely small and in the neighborhood of 0%.

% Reduction achieved after rolling: the FE results make more sense than the theoretical ones. When planning for a 20% reduction in the thickness of the workpiece it is impossible to obtain such reduction because as we saw in previous Chapters, the material deforms elastically recuperating some of its thickness. The FE results agree perfectly with this phenomenon. The reduction in cold rolling comes in 3.1% lower than expected by the classical theory.

Strip Velocity Increase: the results are very close for the cold rolling case.

4.3 2-D Plane Strain Model for Flat Hot Rolling

In this section we will look at the results obtained through the simulation of the flat hot rolling process using MSC MARC. The model geometry stays the same. In this case, the material model is changed in order to properly model the behavior of steel at high temperatures. For this purpose, Shida's equation [56], which models the flow stress as a function of strain, strain rate, and temperature, will be implemented. The most interesting part of this simulation is to see and understand the interaction between the stress, strain rate, strain and temperature, and the added difficulty of the radiation boundary condition, as well as the material non-linearities due to the density, specific heat, and conductivity changing as a function of the temperature.

2-D Plane Strain Model Description

Hot rolling of a 0.5 m thick 0.1% Carbon steel slab, reduced by 20 % in one pass is presented below.

Geometry

Roll Diameter = 3.1 m	Slab Length = 2 m	% Reduction= 20 %
Slab Thickness = 0.5 m	Slab Width = 1 m	$\varpi = 1.5 rad/s$

Initial Conditions

Initial Temperature of the slab = 1473.15 K = 1200 ˚C

Boundary Conditions

1. Plastic Heat Generation with $\eta = 0.9$, i.e. 90% of the mechanical energy of deformation is converted into heat. The remaining 10% mechanical energy is used on dislocations, etc
2. Conduction across the edges of the slab with $k = 8000 \frac{W}{m^2 K}$
3. Film convection to the environment with $h = 50 \frac{W}{m^2 K}$ with an environment temperature of $T_\infty = 298.15K = 25°C$
4. Radiation to the environment with an emissivity of $\varepsilon = 0.8$

Slab Properties

Plasticity: Rigid-Plastic (flow) Formulation (Levy-Mises flow rule)
Yield Surface: von Mises

Friction coefficient = 0.5

Young's Modulus: $E = 210x10^{9}\,\dfrac{N}{m^{2}}$

Poisson's Ratio: $\mu = 0.3$

Coefficient of Thermal Expansion = $1.17x10^{-5}\,/\,K$

Mass density: $\rho = Density = \dfrac{7850}{\left(1+0.004\hat{T}^{2}\right)^{3}}\quad\left(\dfrac{kg}{m^{3}}\right)$

Conductivity: $k = Conductivity = 23.16 + 51.96\cdot e^{-2.03\hat{T}}\quad\left(\dfrac{W}{m}\right)$

Specific Heat: $C_p = 207.9 + 294.4\cdot e^{1.41\hat{T}}$ for T>700 ºC $\left(\dfrac{J}{KgK}\right)$

Emissivity: $\varepsilon = 0.8$

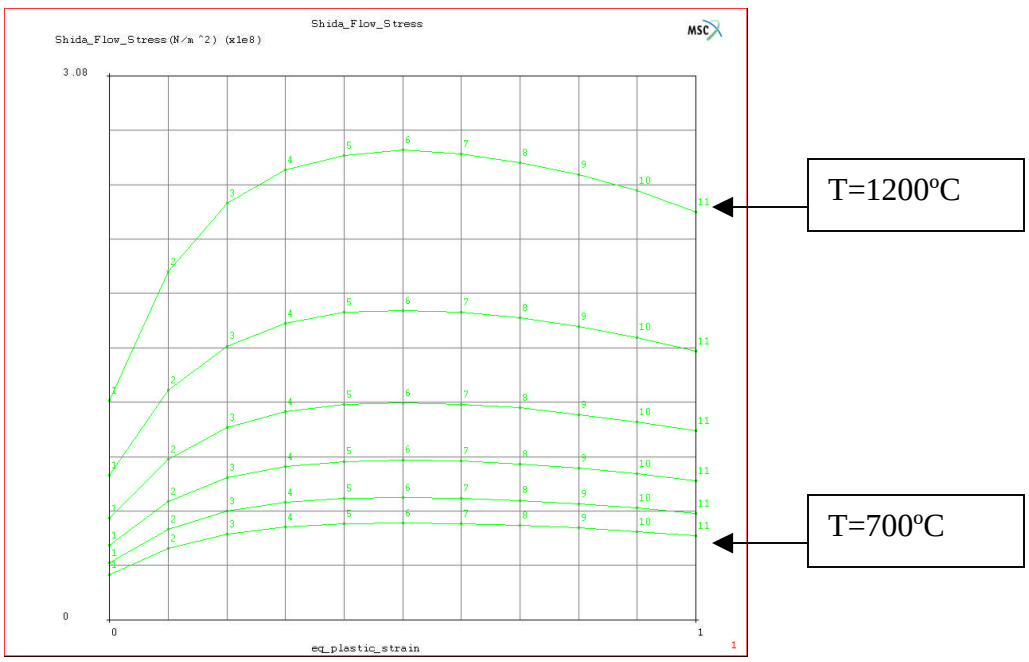

Figure 4.39: Shida flow curves (front view). Temperature axis is perpendicular to the plane of the paper

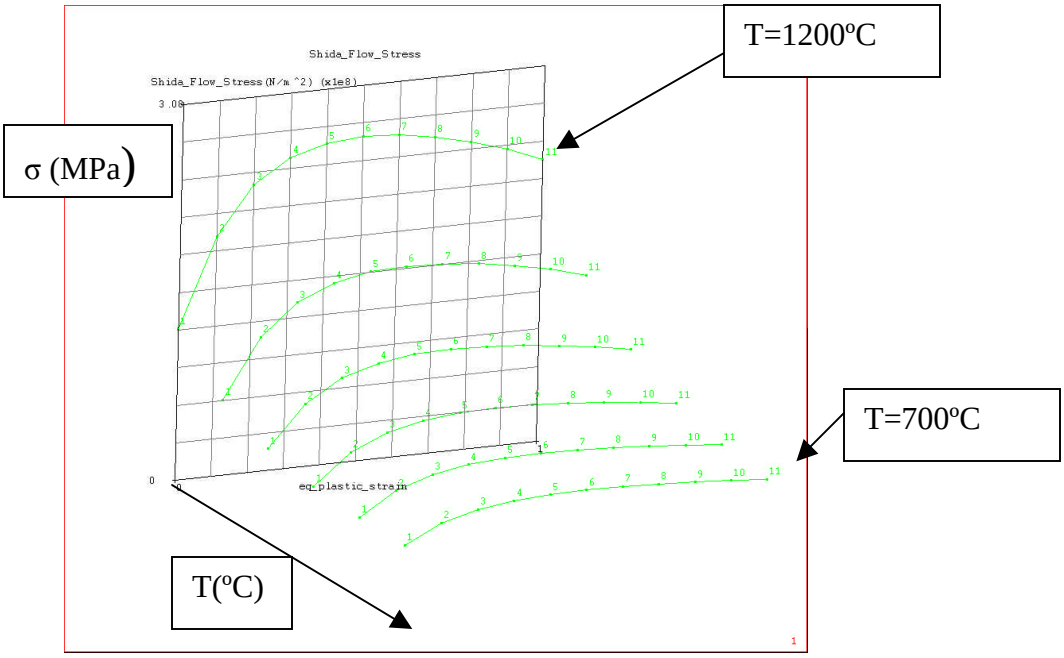

Figure 4.40: perspective view of the Shida flow curves for a strain rate = 2 s^{-1}

Each of the curves corresponds to a temperature. First one is 700ºC and last one 1200ºC. Notice the "relaxation" in the curves as the temperature increases.

The Shida equation is implemented using the rigid-plastic material formulation, as explained in Chapter 2, Section 2.9 of this thesis.

4.3.1 Deformable-Rigid Case

The first case analyzed corresponds to the hot rolling of a strip at 1200 ºC. The workpiece is subject to a 20% reduction and the rolls are spinning with an angular velocity of ω=1.5 radians per second.

The FE model has the following boundary conditions:

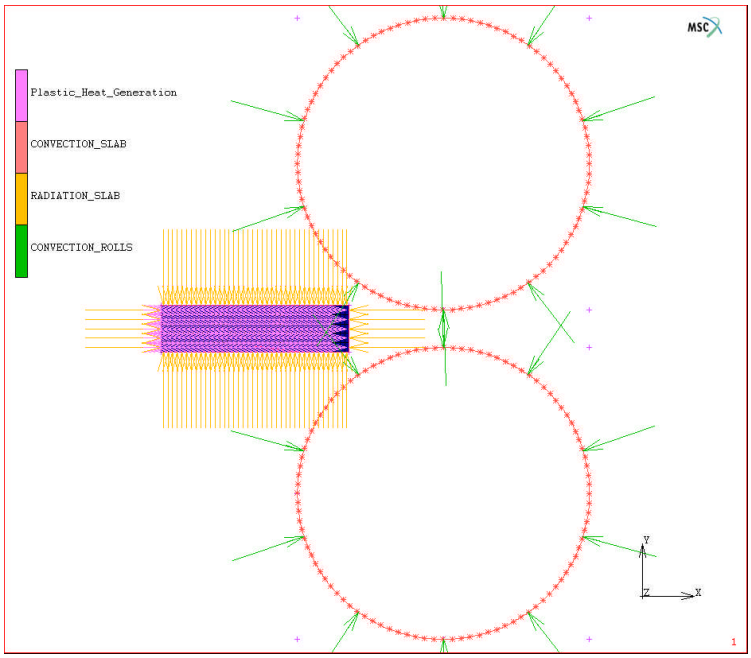

Figure 4.41: Boundary conditions

The contact boundary condition is specified as part of the contact part of the problem. In the contact table the conductivity of the rolls and workpiece is specified. Thus, when the workpiece and the rolls come in contact, the conduction part of the problem is "activated" and heat can be conducted from the "yellow-hot" steel bar to the rolls at ambient temperature. The main difference with respect to cold rolling is the introduction of the radiation boundary condition that will allow the slab to dissipate some heat to the environment through radiation. The environment is modeled as being at 25 ºC. The workpiece can also cool through convection (non-forced) to the environment. The rolls can also cool down through convection.

The workpiece is meshed using plane strain 4 node quadrilateral quad (4) linear function elements with full integration (Marc element #11). The simulation is run as a coupled thermo-mechanical transient dynamic problem. The results corresponding to the simulation are shown in the following figures:

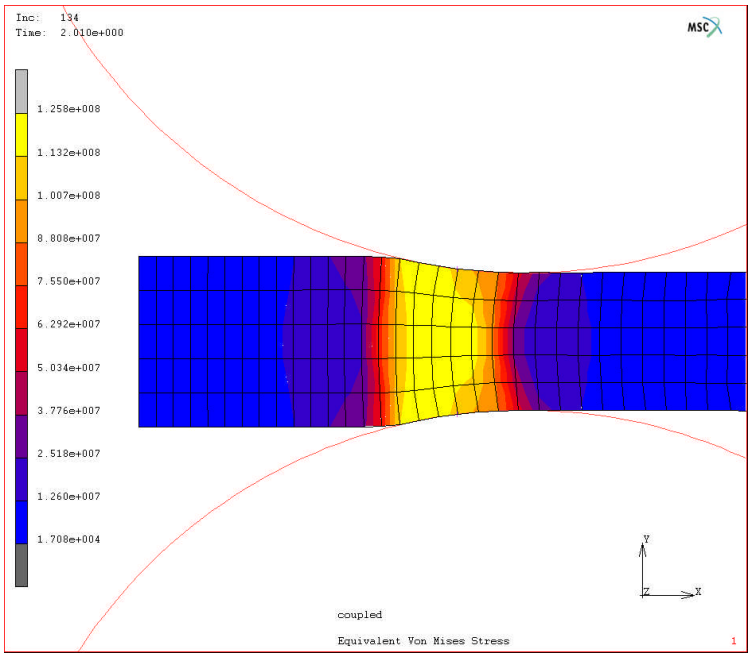

Figure 4.42: Equivalent von Mises Stress

The particular conditions at each point of strain, strain rate, and temperature, unequivocally determine a state of stress according to Shida's equation. Compressive stresses appear in the whole deformation zone.

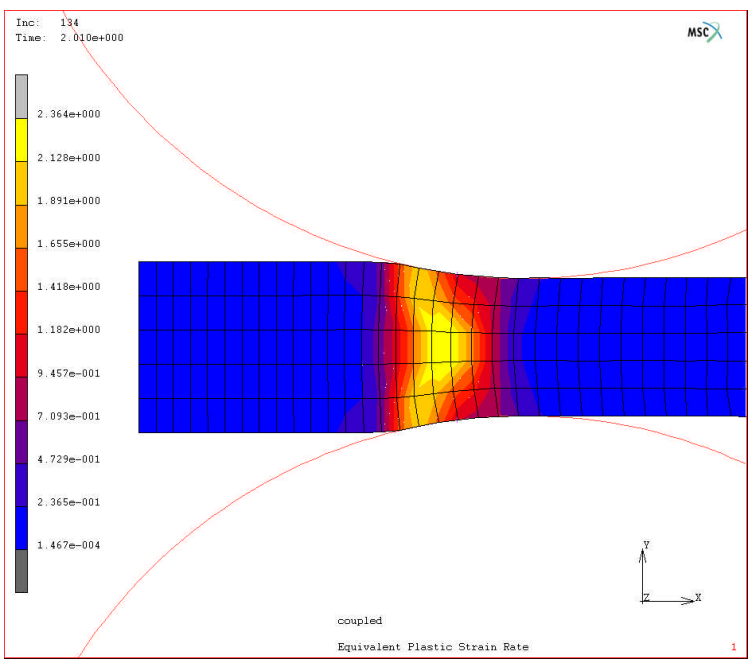

Figure 4.43: Equivalent plastic strain rate distribution

The strain rate is obviously not constant. In the deformation zone it has a maximum value of 2.36 s^{-1}. The strain rate concentrations in the contact zone cause a non-uniform strain distribution.

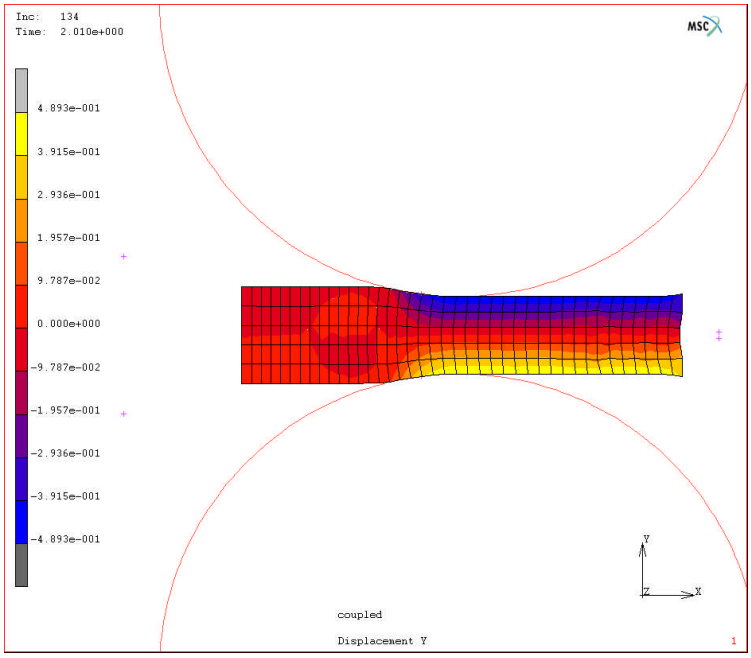

Figure 4.44: Detail of how the material flows in the y direction

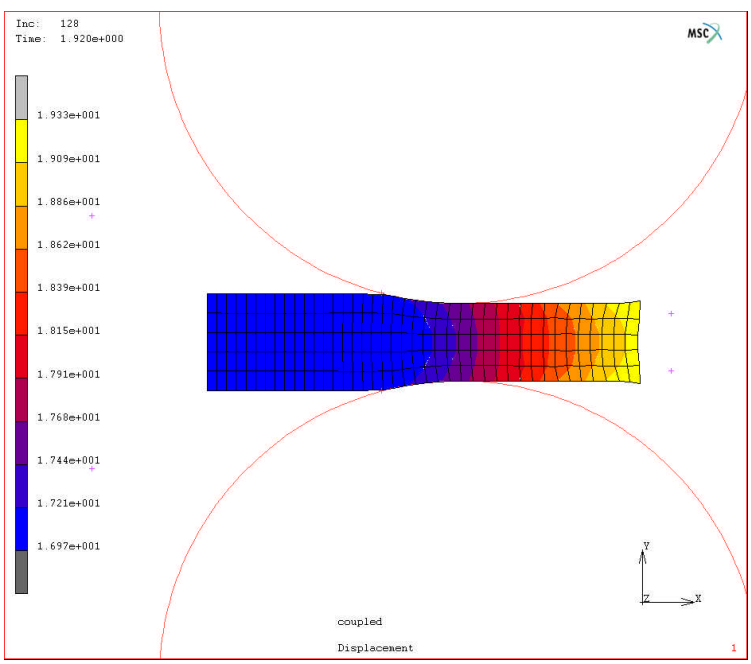

Figure 4.45: Displacement distribution

The hot rolled material displaces in a direction opposite to the rolling direction looking like an inverted C, the opposite as in cold rolling. This is due to conditions existing in hot rolling when considerable friction and sticking of metal to the rolls occur. In cold rolling, when smooth, well-lubricated rolls are used, the phenomenon of sticking seems to be eliminated or at least reduced, and thus plane sections are curved on the same direction as the rolling direction.

In general it can be said that if there were no influence of friction on the metal surface, the deformation would be closer to parallelepipedal with all the edges remaining straight, parallel and vertical. The greater the influence of friction, the greater is the deformation of the bar.

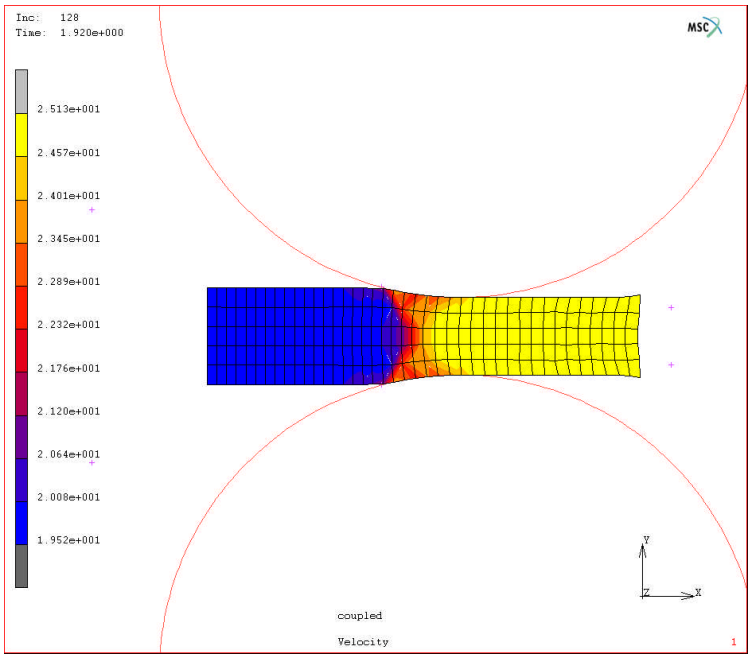

Figure 4.46: Velocity distribution. Notice the neutral plane

The velocity distribution in hot rolling is similar though not exact as the one in cold rolling.

Figure 4.47 shows how the temperature goes up but only by 5 ˚C. The temperature field agrees with the numerous experimental data presented by Pietrzyk and Lenard [49,56]. As expected, the coolest part of the plate is the one near the contact zone and on the outer edge of the workpiece, and a sharp temperature gradient towards the strip center is observed. Low rate of heat loss of the central portion, before entering the roll gap, is also noticed. The strip also experiences some heating (5˚C) in the roll gap, the result of work done on the plastically deforming metal.

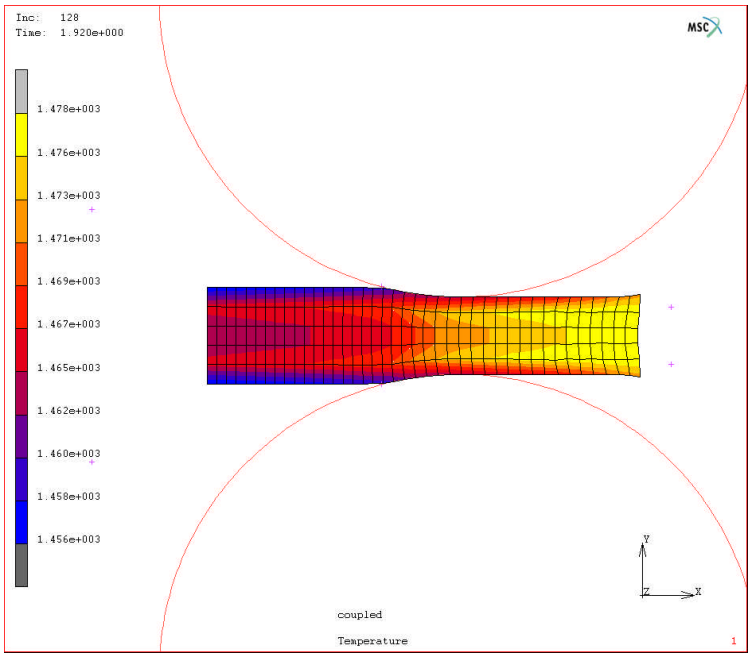

Figure 4.47: Temperature distribution

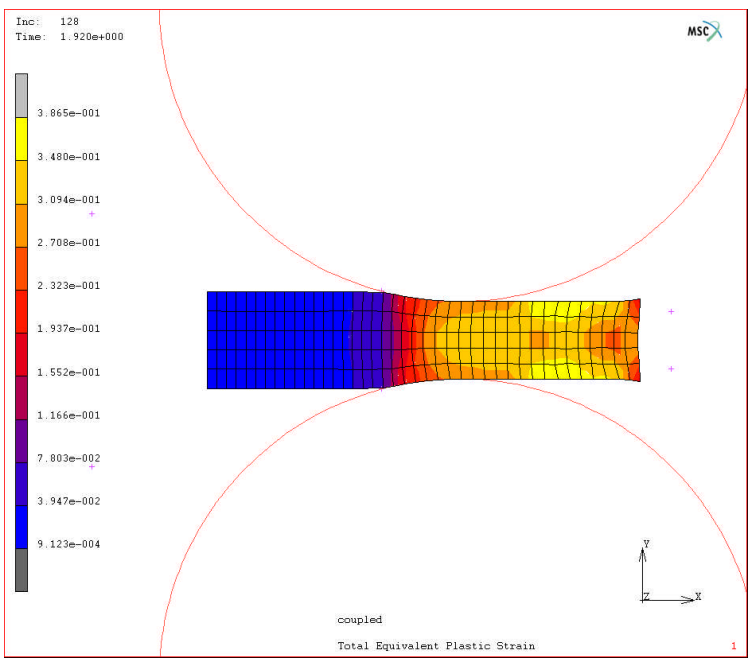

Figure 4.48: Total equivalent plastic strain. The largest strains appear near the surface

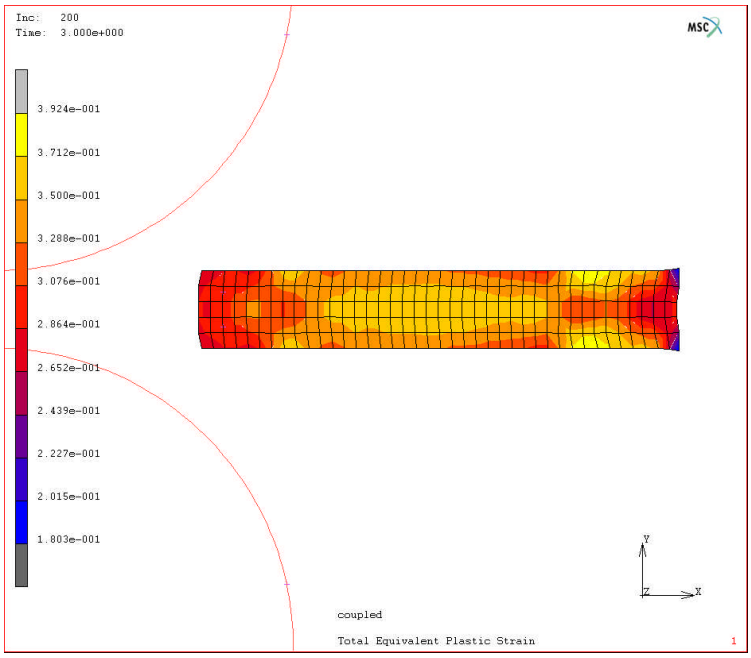

Figure 4.49: workpiece comes out perfectly flat

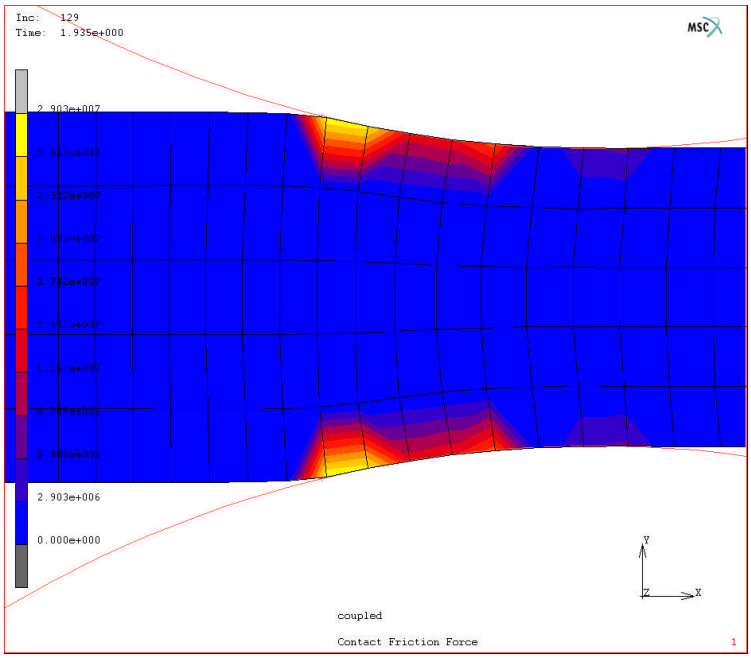

Figure 4.50: Detail of the contact friction

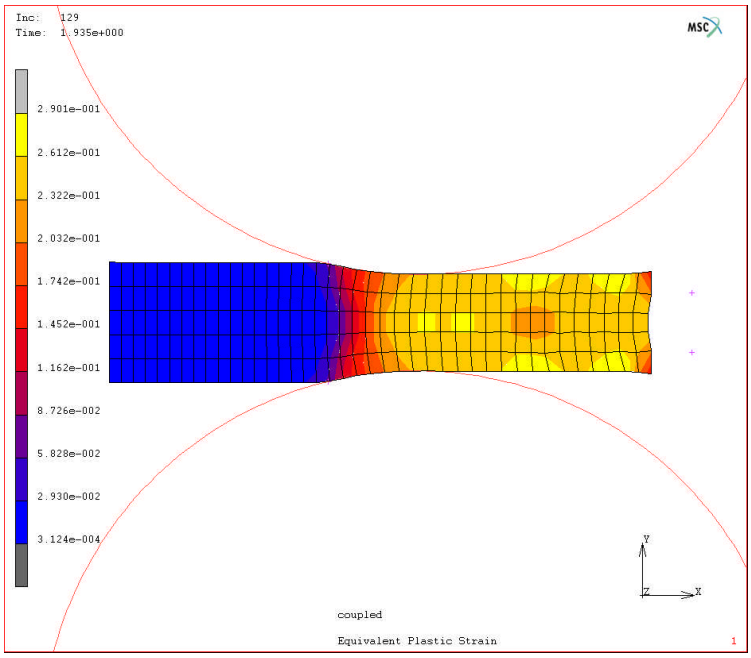

Figure 4.51: Equivalent Plastic Strain $\bar{\varepsilon}^{p}$

The numerical results for the main parameters of interest, namely, equivalent Mises stress, maximum strain rate, temperature increase, strip length increase, % reduction achieved after rolling, and strip velocity increase, and the main conclusions obtained from the above figures corresponding to the 2-D hot rolling case are summarized in Section 4.3.3

4.3.2 The Mechanism of Bite in Hot Rolling

There are many situations when while during cold or hot rolling, the slabs or strips will not be able to enter through the roll gap and they are literally spit out of the mill, or they keep bouncing against the rolls while unsuccessfully trying to enter the roll gap.

Depending on the conditions under which the slab is introduced into the roll gap two situations can occur:

1. The metal is gripped by the rolls and pulled along the roll gap
2. The metal slips over the roll surface and the slab does not enter in the roll gap

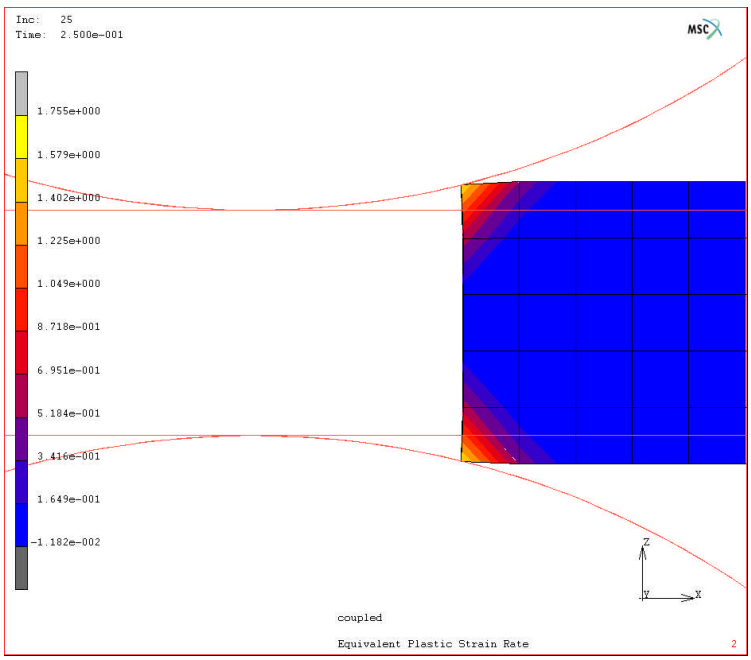

Figure 4.52: The mechanism of bite in rolling: workpiece as it enters the roll gap

Roll bite happens when the horizontal component of the friction force vector is larger than the horizontal component of the normal N, i.e.

$$F_{R_x} > N_x \tag{4.10}$$

but

$$F = \mu N \tag{4.11}$$

$$N_x = N \sin\alpha \tag{4.12}$$

$$F_x = F \cos\alpha \tag{4.13}$$

where $\alpha =$ roll bite angle

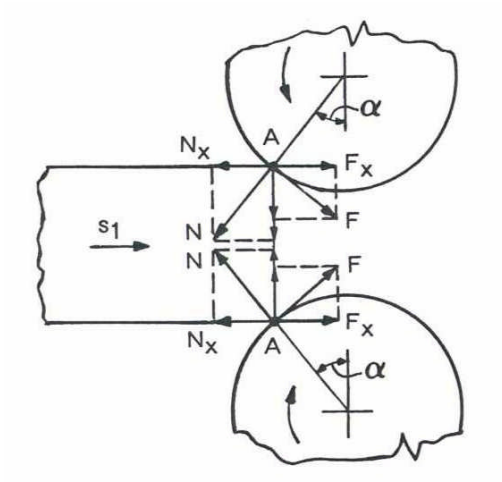

Figure 4.53: Forces acting in the roll bite during initial entry of the workpiece [32] © Marcel Dekker / Taylor & Francis Group

Therefore substituting in inequality (4.10) we have that

$$F\cos\alpha > N\sin\alpha \tag{4.14}$$

$$\mu N\cos\alpha > N\sin\alpha \tag{4.15}$$

$$\mu > \frac{\sin\alpha}{\cos\alpha} = \tan\alpha \tag{4.16}$$

Thus, the roll bite takes place if the entry coefficient of friction μ is larger than the tangent of the roll bite angle α

Also since

$$\tan\alpha = \frac{\sqrt{R\Delta h}}{R - \frac{\Delta h}{2}} \tag{4.17}$$

where $\Delta h = draught$, then the condition for roll bite becomes

$$\mu > \frac{\sqrt{R\Delta h}}{R - \frac{\Delta h}{2}} \tag{4.18}$$

From this relation we have an important practical application. In the industry it is hard sometimes to determine the coefficient of friction. Based on the previous equation, if we find out the draught for the very first slab that is bitten by the rolls, which we can denote as $\Delta h_{\min}$, then the coefficient of friction will be exactly equal to

$$\mu = \frac{\sqrt{R\Delta h_{\min}}}{R - \frac{\Delta h_{\min}}{2}} = \tan\alpha_{\max} \tag{4.19}$$

that is, the coefficient of friction is equal to the tangent of the maximum roll bite angle $\alpha_{\max}$

Therefore:

1. The rolls bite the metal when the coefficient of friction is larger than the tangent of the roll bite angle α
2. Free rolling takes place within the limits $\mu > \tan\alpha > 0$
3. Using the maximum angle of bite α (or the minimum draught for which the roll bite occurs) the coefficient of friction μ can be found.
4. During rolling, the coefficient of friction decreases. Therefore the friction force also decreases and so the angle of contact becomes $\frac{\alpha}{2}$. Thus,

$$\mu \geq \tan\frac{\alpha}{2} \tag{4.20}$$

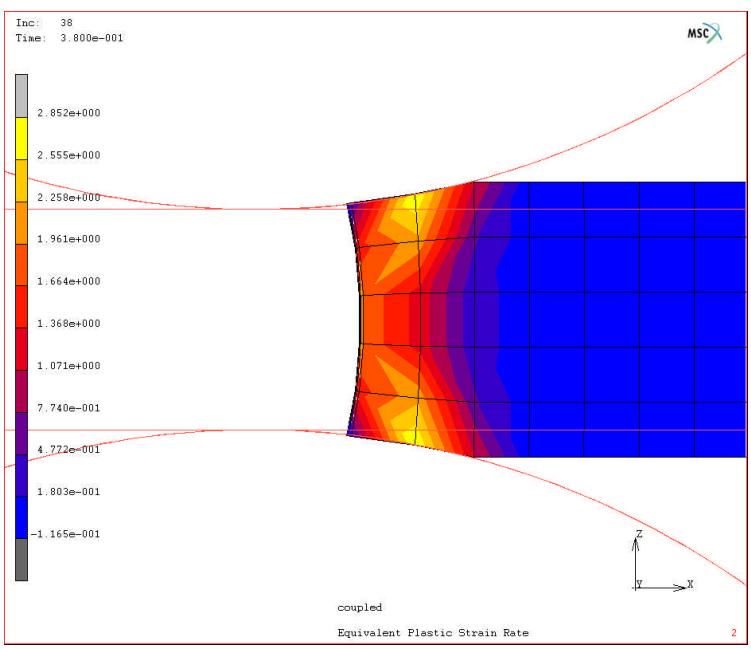

Figure 4.54: The entry coefficient of friction μ is larger than the tangent of the roll bite angle α and the rolls bite the workpiece.

4.3.3 Results & Analysis

The results for the 2-D plane-strain hot rolling FE models are summarized in the following table

Table 4.2: Results for 2-D Plane Strain Hot Rolling FE models

	HOT ROLLING	
	Classical Theory	2-D Plane Strain FEM
Equivalent Stress (Pa)	1.17×10^{8}	1.26×10^{8}
Equivalent Plastic Strain	NA	2.9×10^{-1}
Total Equivalent Strain	NA	2.90×10^{-1}
Maximum Strain Rate (s^{-1})	2.59	2.36
Temperature Increase (˚C)	5.1	5
Strip Length Increase (%)	12.50	12.50
Strip Width Increase / Spread (%)	50	NA
% Reduction Achieved after Rolling	20	19.57
Strip Velocity Increase (%)	25	28.74

The 2-D FEM results can be considered as good and in agreement with the classical hot rolling theory.

Resistance To Deformation/Equivalent von Mises Stress:. There is a significant difference between the FE results and the results obtained through the "classical rolling theory". As we saw, for the cold rolling 2-D case, in order to simplify the problem, the classical theory makes many assumptions that oversimplify the problem. The most inaccurate assumptions are the ones regarding the friction forces, the plane vertical sections, the neglection of the elastic deformation in the workpiece and in the contact zone, the lack of lateral spread since this is a plane strain model, and the lack of work hardening and roll flattening.
As it was in the case of cold rolling, the classical formulas used in hot rolling are all empirical and vary enormously among the researchers due to differences in setup, tooling, instrumentation, mill size, etc.
The FE stress results obtained in this thesis are within the same order of magnitude but are 7% higher in the hot rolling case. Such differences can be attributed to the previously mentioned reasons. The FEM results are more accurate and are in agreement with comparable results published by other researches.

Maximum Strain Rate: the results for this important parameter of the cold rolling process are all basically in agreement. The FE results are 7% smaller than the hot rolling classical theory.

Temperature Increase: the FE results for the hot rolling case are extremely close however, the difference being just 2%.

Strip Length Increase: the FE results are in perfect agreement with the classical theory ones. This parameter is one of the easiest to measure and as expected, the differences are extremely small and in the neighborhood of 0%.

% Reduction achieved after rolling: the FE results make more sense than the theoretical ones. When planning for a 20% reduction in the thickness of the workpiece it is impossible to obtain such reduction because as we saw in previous chapters, the material deforms elastically recuperating some of its thickness. The FE results agree perfectly with this phenomenon. The reduction in cold rolling comes in 4% lower than expected by the classical theory.

Strip Velocity Increase: The FE hot rolling result comes in 4% lower than the classical rolling theory result.

4.4 Summary and Concluding Remarks

In this chapter we created and analyzed the 2-D plane strain developed for this thesis, which in turn allowed us to explore and achieve the main goals of this thesis.
The purpose of the 2-D plane strain flat cold rolling models is to help the roll designer predict the main flat rolling parameters, namely, the rolling loads, temperature & velocity

fields, the overall geometric changes of deformed pieces, and the metal flow under different temperatures, as well as the optimum conditions for the flat rolling process

The 2-D plane strain cold rolling models done for this simulation, utilized the elastic-plastic (solid) formulation, which uses the Prandtl-Reuss flow rule. The elastoplastic formulation is more realistic than the rigid-plastic approximation, as it takes into account the elastic contribution to the total strain rate and it accurately describes the cold rolling process where the workpiece undergoes a elastic-plastic-elastic deformation.

The 2-D plane strain hot rolling models utilize the rigid-viscoplastic (flow) formulation, which assumes that the deforming material has a negligible elastic response. The flow formulation of the finite element method for metal forming processes is based on the *Levy-Misses* plasticity model for rigid plastic materials, which assumes that work hardening is negligible

Both the cold and hot rolling processes were modeled using the von Mises yield surface, and the hardening rule for the cold rolling case was the kinematic one.

For the 2-D plane strain cold rolling models, 3 different scenarios were analyzed:

- Deformable-Rigid coupled analysis: where the slab is modeled as a deformable body and the rolls as rigid.
- Deformable-Rigid with heat transfer coupled analysis: where the slab is again modeled as a deformable body, but the rolls are modeled as a rigid body with heat transfer (this approach utilizes a special kind of element)
- Deformable-Deformable Coupled analysis: where both the steel strip and the rolls are modeled as deformable bodies.

The results we obtained for the cold rolling problem were in good agreement with the classical theory except for the equivalent Mises stress and the temperature. The FE stress results obtained in this thesis are within the same order of magnitude but are 38% higher in the cold rolling case. The temperature was 50% higher for the FE results. Such differences can be attributed to the over-simplifying assumptions that were done when developing the classical theory of cold rolling. The numerical results for the rest of the main parameters of interest: maximum strain rate, strip length increase, strip width increase (spread), % reduction achieved after rolling, and strip velocity increase were closer to the ones predicted by the classical theory.

Also, two baseline models were created in order to compare the stresses we obtained with well known published results. Specifically, the problem of Hertz contact stress was analyzed, where a cylinder was pressed against a flat surface representing the workpiece. Also, the upsetting of a square block was simulated. From this simulation we were able to draw conclusions regarding the influence of friction on the stresses and the temperature.

Based on the excellent results we have obtained, from this set of 2-D plane-strain cold rolling models we are able to conclude and verify that:

a) the steel in cold rolling can be accurately modeled using the elastic-plastic material model;
b) in cold rolling, plane sections do not remain plane (as the classic theory assumes in the derivations of formulas for stress) and due to this, all the empirical formulas used in the classical theory of rolling can only be used as an estimate;
c) the degree of deformation, stresses and strains, strain rates, as well as other parameters of interest, on the workpiece and in the rolls can be predicted;
d) the heat transfer from the workpiece to the rolls can be accurately modeled and consequently, the increase in temperature in the rolls due to friction heating, and in the workpiece due to plastic deformation heat inside, and friction heating on the surface of the workpiece can also be predicted.
e) the stresses developed in the rolls are very similar to the stresses developed in the Hertzian contact problem;
f) the complicated and not well understood friction process between the roll and the workpiece can be accounted for in the FE models
g) the Finite Element Method can be used to predict material flow in cold rolling

For the 2-D plane strain hot rolling models the rigid-deformable case was analyzed. The model included conduction, convection, and radiation heat transfer as required.
The 2-D FEM results can be considered as good and in agreement with the classical hot rolling theory. The largest difference between the FEM results and the published results was 7%. FEM results were comparable with published results by Lenard et. al, Kobayashi et al, and Rowe et al, Wagoner & Chenot.

For the 2-D plane strain hot rolling models we were able to demonstrate that

a) the steel in hot rolling (at temperatures between 800 and 1200 C) can be modeled using the rigid-plastic material model with the flow stress as a function of the strain, strain rate, and the temperature;
b) the degree of deformation, stresses and strains, strain rates, as well as other parameters of interest, on the workpiece and in the rolls can be predicted for hot rolling
c) the heat transfer from the workpiece to the rolls can be accurately modeled and therefore the increase in temperatures of both the rolls and the workpiece can be simulated
d) that the FEM can be used to predict material flow in hot rolling
e) the mechanism of bite in hot rolling can be modeled using FEM.

Chapter 5
Summary & Concluding Remarks

5.1 Summary

Although the cold rolling of non-ferrous materials has been practiced since the fourteenth century, the hot rolling of steel was begun in the latter half of the seventeenth century, just over 300 years ago. Since that time, the rolling industry has been constantly evolving and taking advantage of the latest technological developments.
More and more sectors of the metalforming industry are beginning to recognize the benefits that finite-element analysis of metal-deformation processes can bring in reducing the lead-time and development costs associated with the manufacture of new components. The rolling industry, which processes more tonnages of metal than any other, has been no stranger to the FEM revolution. Finite element analyses of non-linear problems, such as the ones found in the cold and hot rolling processes, require powerful computing facilities, and large amounts of computer running time but advances in computer technology in the latter part of the twentieth century and the beginning of this century, and the falling price of computing hardware are bringing these techniques within the reach of even the most modest company [14].

Virtual manufacturing involves the simulation of a product and the processes involved in its fabrication. Simulation technology has the potential to enable rolling companies to optimize key factors directly affecting the profitability of their manufactured products such as the reduction of the number of trials needed to correctly design the rolls, the generation of less material waste, the reduced cost of tooling, the increase in confidence in the manufacturing process, the improved quality, the reduced time to market, and the lower manufacturing cost. Virtual manufacturing utilizes nonlinear finite element technologies to provide detailed analysis information about a product, which is then used for optimization of factors such as manufacturability, final shape, residual stress, and life-cycle estimations.

Nonlinear finite element analysis facilitates the simulation of the fabrication in a more realistic manner than ever before, especially in the hot rolling industry where only a few people have a clear understanding of the behavior of steel at high temperatures, and where most companies need to use a trial and error approach before they obtain the desired results.

The goal of this work was to develop a fully nonlinear finite element analysis model that can be used as a tool in order to analyze the rolling of cold and hot steel strips under a series of different parameters and scenarios. The purpose is to provide the roll designer with a tool that he can use in order to understand the behavior of the steel as it flows through the different kinds of passes in the rolls, by computing the main process parameters, given the desired mechanical and metallurgical properties and the final dimensions of the product along with its initial metallurgical make-up. Currently, this is a very difficult industry problem that requires skilled engineers with many years of experience.

In order to achieve this, the author took a look at the flat and cold and hot rolling problem from the following aspects: materials science, mathematical models of rolling, theory of plasticity, machine and mechanical design aspects, heat transfer issues, etc, then focusing on the Finite Element Analysis issues concerning this problem, such as coupled thermo-mechanical analysis, thermo-mechanical finite element modeling, and all the non-linear aspects of the rolling problem. Flat products are a good starting point since they all have a simple rectangular geometry, and there is symmetry with respect to the neutral plane of the section, which facilitates the analysis. Hence, they are used as a stepping-stone to the more challenging and interesting problem of non-symmetrical products such as structural shapes, etc.

We began by setting up the theoretical mathematical and engineering mechanics foundations upon which we can build on. By having a great understanding of the physics of the problem we can then model these physics into our finite element model. After all, the results the model will produce are only as good as the mechanics of the model created. The mathematical physics of this problem lead to a second order homogeneous partial differential equation (PDE), for the thermal portion of the problem, that together with the boundary and initial conditions constitutes a thermal Initial Boundary Value Problem (T-IBVP). The mechanical portion of the problem lead to another set of PDEs given by the equilibrium conditions, the compatibility conditions, the constitutive equations, and the yield criterion, which together with the boundary conditions lead to another Initial Boundary Value Problem (M-IBVP)

The final solution to our problem will be determined by the simultaneous solutions of these two IBVPs due to the strong coupling between the mechanical and the thermal problems. There are two primary causes of coupling. First, coupling occurs when deformations result in a change in the associated heat transfer problem. Such a change can be due to either large deformation or contact. The second cause of coupling is heat generated due to inelastic deformation. The irreversibility of plastic flow causes an increase in the amount of entropy in the body, which in turns results in changes to the associated mechanical problem.

We then went ahead and took an exhaustive look to the cold and hot rolling problems from the finite element formulation point of view. The Finite Element Method is our tool of choice for the solution of the complex Initial Boundary Value Problems (IBVP) corresponding to the rolling problem, that were described in detail in chapter 2, and where the formation of element equations is accomplished by using a variational approach.

The basis of finite element metal flow modeling, using the variational approach, is to formulate proper functionals, depending upon specific constitutive equations. The solution of the initial boundary value problem (IBVP) is obtained by the solution of the dual variational problem in which the first order variation of the functional vanishes.

For our mechanical initial boundary value problem (M-IBVP), the *variational approach* requires that among admissible velocities v_i that satisfy the conditions of compatibility and incompressibility, as well as the velocity boundary conditions, the actual solution give the functional described by equation (3.2.5) a stationary value. Using this

variational approach, the basic equation for the finite element discretization was developed, Equation (3.2.8).
Likewise, the Thermal Initial Boundary Value Problem (T-IBVP) was solved using a variational approach that led to the FE discretization equation, (3.6.3), that was implemented into the finite element formulation according to Equations (3.6.10) & (3.6.11).

We then took a look at the main formulations used in the application of FEM to metal forming, namely, the flow formulation and the solid formulation. Flow formulation assumes that the deforming material has negligible elastic response, while solid formulation includes elasticity. The flow formulation uses the *rigid-plastic* or *rigid-viscoplastic* material models. Since in metal forming operations, the non-linear plastic strains are much larger than the elastic strains, these last ones are usually neglected allowing the use of a simpler rigid-plastic model in the analysis. The resulting constitutive equations in this approach are identical to those of a non-Newtonian fluid
Solid formulation, also known as solid-state incremental approach, employs elastic-plastic or elastic-viscoplastic material models. This approach uses a Lagrangian description of motion

We then developed the finite element equations for each of these two formulations, solid and flow, starting from Equation (3.2.8), which as we have just seen is the basic equation for finite element formulation.
A complete analysis of the rolling process also requires the simulation of heat transfer in the roll gap, making it necessary to couple the solution for the flow or solid formulation with the thermal model. In order to handle a coupled thermo-viscoplastic deformation problem, it is necessary to solve simultaneously the material-flow problem for a given temperature distribution and the heat transfer equations. The finite element model for the heat transfer and coupled thermal-mechanical problem was based on formulations by Kobayashi & Zienkiewicz. As we saw, these formulations can be used to calculate the temperature distribution as well as the velocity, strain rate, strain and stress fields in the deformation zone during hot and cold rolling.

Later on the thesis, we took a look at the main sources of non-linearities present in the rolling problems (material, geometric and boundary) and saw how the hot and cold rolling problem we have to deal with these three sources of nonlinearities with permanent deformations and gross changes in geometry that the workpiece acquires as it is rolled; stress values which exceed the elastic limits of the materials, yielding, temperatures above 30% of the melting temperature; contact between the roller and the strip involving tremendous friction; stresses no longer proportional to the strains, and heat transfer non linearities such as radiation from the workpiece, etc.

At that point we started to create and analyze the 2-D plane strain cold and hot rolling models developed for this thesis that in turn allowed us to explore and achieve the main goals of this thesis.

The models were validated using a stepping-stone approach by which simplified versions of the problem will be first analyzed to demonstrate the results obtained. New parameters and physical phenomena were progressively added to the initial basic models. In each case the updated models will be analyzed and verified until arriving at the full model of flat rolling for both hot and cold rolling. The validation of the models uses classical stress analysis techniques and methodology, or proofs in the existing literature via the classical theory of rolling or published data and/or photos of actual rolling tests. From the models we obtained results for the main parameters of interest to the roll designer, and we also obtained proof of the hypothesis and goals we had set for this thesis.

The following table summarizes the main results obtained from the 2-D FE models shown in Chapter 4.

Table 5.1: Summary of Results for 2-D Plane Strain Cold and Hot Rolling

	Classical Theory		**2-D Plane Strain**	
	Cold	Hot	**Cold**	Hot
Equivalent Stress (Pa)	3.42×10^{8}	1.17×10^{8}	4.74×10^{8}	1.26×10^{8}
Equivalent Plastic Strain	NA	NA	2.65×10^{-1}	2.9×10^{-1}
Total Equivalent Strain	NA	NA	2.66×10^{-1}	2.90×10^{-1}
Maximum Strain Rate (s^{-1})	2.59	2.59	2.57	2.36
Temperature Increase (˚C)	21.1	5.1	32	5
Strip Length Increase (%)	12.50	12.50	12.45	12.50
Strip Width Increase / Spread (%)	35	50	NA	NA
% Reduction Achieved after Rolling	20	20	19.91	19.57
Strip Velocity Increase (%)	25	25	24.74	28.74

The results can be considered as good and in agreement. The slight differences between them can be attributed to the fact that the 2-D model ignores the strain in the z direction (depth), which in reality is not the case. The results for a 3-D model however, would have been more accurate since this modeling approach takes into account the deformation in the z direction, also known as spread that as we know has a very important role in the flat rolling process.

Resistance To Deformation/Equivalent von Mises Stress: the 2-D FE results are very close to each other for both the hot and cold rolling cases. There is a significant difference between the FE results and the results obtained through the "classical rolling theory". As we saw in chapters 10 and 11, in order to simplify the problem, the classical theory makes many assumptions that are not entirely accurate. All the formulas used in the classical theory are empirical and differ significantly among rolling researchers. Each researcher tailored his set of formulas in order to match the results he obtained in the rolling mill. There are many sources of uncertainty when taking these measurements, which are particularly difficult given the nature of the rolling process with very high temperatures and a quite rudimentary instrumentation available at the time. It is quite possible therefore that some of the readings of the researchers were inaccurate. Each of the researchers likely had a different setup and a different set of conditions in terms of the radii of the rolls, thickness of the workpiece, rolling speed, temperature of the stock, etc. In a non linear process with so many variables and parameters the differences in the set up of each of the researchers' experiments, plus the assumptions that each of them made, led to the differences that can be observed on the formulas that each of them arrived to when trying to empirically predict the values of stress, torque, roll pressure, etc. The FE stress results obtained in this thesis are within the same order of magnitude but are 38% higher in the cold rolling case and 7.7% in the hot rolling case. Such differences can be attributed to the previously mentioned reasons.

Maximum Strain Rate: the results for this important parameter of the rolling process are all basically in agreement. The FE results are 1% smaller for the cold rolling case, and 7% smaller for the hot rolling case.

Temperature Increase: the FE results for the cold rolling case are 50% higher than the ones predicted by the classic rolling theory that predicts a temperature increase of 21.1˚C. FE results for the hot rolling case are extremely close however, the difference being just 2%.

Strip Length Increase: the FE results are in perfect agreement with the classical theory ones. This parameter is one of the easiest to measure and as expected, the differences are extremely small, between 0% and 0.4%.

Strip Width Increase (Spread): the FE results are in very good agreement with the theory. The FE hot rolling result comes in only 4% lower than the classical rolling theory result.

% Reduction achieved after rolling: the FE results make more sense than the theoretical ones. When planning for a 20% reduction in the thickness of the workpiece it is impossible to obtain such reduction because as we saw in previous chapters, the material deforms elastically recuperating some of its thickness. The FE results agree perfectly with this phenomenon. The reduction in cold rolling comes in 3.1% lower than expected by the classical theory, and the reduction in hot rolling comes in 0.5% lower. The reason why the hot rolling reduction comes in closer to the theoretical and ideal result is that the rigid-plastic formulation used in order to model the material behavior of the steel at high temperature, ignores the elastic deformation of the material because it is so small that it can be neglected. Therefore, in the hot rolling case, the deformation will always be closer to the ideal one since there is very little or no elastic recovery of the workpiece.

Strip Velocity Increase: the results are very close for the cold rolling case but slightly higher for the hot rolling one. The FE models have a 2% and 15% difference for the cold and hot rolling processes respectively.

5.2 Conclusions

The goal of this work was to develop an advanced non-linear finite element model of the cold and hot flat rolling processes that can subsequently be used to analyze the rolling process under a series of changing parameters. Many of the mechanisms that govern the hot rolling process are still not fully understood, and there exists a need to provide engineers with comprehensive tools that allow them to design the rolls right the first time, thus reducing the number of trials in the design of the rolls, the amount of material waste, the cost of tooling, and therefore increasing the time that roll designers can spend on engineering as well as the confidence in the manufacturing process and the quality of the final product. All of the above also lead to a reduced time to market, and a lower overall manufacturing cost.

The models developed here, take into account all of the non-linearities present in the rolling problem: material, geometric, boundary, and heat transfer, and used a coupled thermal-mechanical analysis method to take into account the coupling between the mechanical and thermal phenomena resulting from the pressure-dependent thermal contact resistance between the steel slab and the steel rolls.

Through our analysis, we were able to demonstrate the goals of this thesis:

a) that the steel in cold rolling can be accurately modeled using the elastic-plastic (solid Prandtl & Reuss) formulation, using also the von Mises yield surface, and the kinematic hardening rule.
b) that the steel in hot rolling (at temperatures between 800 and 1200 C) can be modeled using the rigid-plastic (flow Levy-Mises) material model with the flow stress as a function of the strain, strain rate, and the temperature, using also the von Mises yield surface.
c) that in cold rolling, plane sections do not remain plane (as the classic theory assumes in the derivations of formulas for stress). We saw this through the displacement distributions obtained through our simulations, and also through photos of actual tests performed on plastic material, and explained its physics by arguing, that the frictional work is consumed at the interface between the deforming metal and tool faces that constrain the metal. The redundant work is due to internal distortion in excess of that needed to produce the desired shape. It is affected by such factors as the tool and workpiece geometry and lubrication at the tool-workpiece interface. Figure 5.1 illustrates an ideal deformation process in which the plane sections remain plane. In reality, internal shearing causes distortion of plane sections. As a consequence, the metal experiences a strain that is greater than in the case of its ideal deformation.

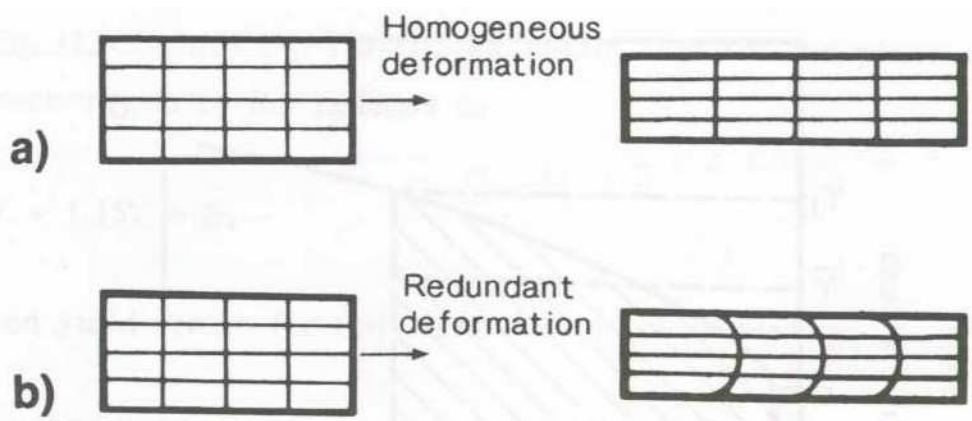

Figure 5.1: Homogeneous vs. Redundant Deformation [63] © Marcel Dekker / Taylor & Francis Group

From this, we concluded that all the empirical formulas used in the classical theory of rolling can only be used as a good estimate or reference, and that the results will not necessarily need to match the ones we obtain from the FEM but they should be in the neighborhood.

d) the degree of deformation, stresses and strains, strain rates, as well as other parameters of interest, on the workpiece and in the rolls can be predicted, as we measured them through our simulations and were proven to be even more accurate than the results from the classical theory of rolling.

e) the heat transfer from the workpiece to the rolls can be accurately modeled, as we did using by incorporating all the thermal properties of the rolls and the slabs into our finite element model to take into account conduction, convection, radiation, friction heating, and plastic work heat generation,
f) the stresses developed in the rolls are very similar to the stresses developed in the Hertzian contact problem. This was done to check that the stress distribution we obtained on the rolls resembled the one form the Hertz contact problem from which the solution is well known
g) the complicated and not well understood friction process between the roll and the workpiece can be accounted for in the FE models, as we did by modeling the friction according to the Coulomb friction also used by other researchers like Kobayashi, Lenard, Pietrzyk, etc.
h) the Finite Element Method can be used to predict material flow, as we did by using Shida's viscoplastic material model to simulate the flow stress of steel at high temperatures.

And we also examined successfully:

e) The mechanism of bite in rolling and saw that the roll is “bitten” by the roll gap when the entry coefficient of friction μ is larger than the tangent of the roll bite angle α
f) the influence of friction in the rolling process, which we did by trying all of the different friction models one by one and realizing that the only one that provided good results was the Coulomb model.
g) the role that plastic heat generation and friction generated heat plays in the rolling process, which we modeled in all of our FE models and allowed us to see how the temperature of the rolls increased, and also the temperature on the slabs,
h) the main heat transfer aspects present in the rolling problem, which we did by looking and deriving the heat thermal balance equation
i) the non-linear finite element approach to solving the problem, which was done by translating the engineering science and mechanics issues of the problem into two Initial Boundary Value Problems (mechanical and thermal) which were solved using a variational approach that led to the FE discretization equations that were implemented into the finite element formulation. The final solution to our problem will be determined by the simultaneous solutions of these two IBVPs due to the strong coupling between the mechanical and the thermal problems. In order to do this, we took advantage of the solid & flow formulations for the mechanical problem, and also from the FEM formulations for the heat transfer and the coupling. These formulations were used to calculate the temperature distribution as well as the velocity, strain rate, strain and stress fields in the deformation zone during hot and cold rolling.

j) the main issues from the theory of plasticity point of view, analyzing and finding the adequate yield surface and work hardening rule for both the cold and hot rolling problem, as well as studying the main constitutive equations that have been proposed for low carbon steel at low (power/hardening law) and high temperatures (Shida), and selecting the appropriate ones for the FEM models used in this thesis.

The ability of our models have therefore been demonstrated by showing the computed distributions of the equivalent stress, strain, strain rate, temperature, etc, are accurate and valid. Consequently, the FEM models developed have allowed us to obtain a greater understanding all the issues involved with non linear FEM modeling applied to flat rolling, namely, the modeling of the material, the types of plastic models used, hardening rules, yield surfaces, the types of FEM elements needed to model the problem in 2-D plane strain, the setup of the contact parameters within the software in order to achieve convergence (the contact problem is extremely complicated), etc, etc, etc.

We are now in a good situation to try to move into the more complicated problem, which is the one that the industry is really interested in regarding the design of rolls for roll pass design of non-symmetric structural shapes, i.e. shape rolling.

5.3 Recommendations and Future Work

The application of finite element techniques to metalforming is still the subject of much research. Researchers are constantly trying to improve their constitutive models of material behavior as well as the FEM portion of their models. The following are areas in which the author would like to study in depth:

a) Automatic Adaptive meshing: the effects of mesh size are obvious. It is desirable to have a fine enough mesh to reveal all of the necessary detail of information or other features, but this must be balanced against CPU time and costs. The aspect ratio and type of element can influence the result (e.g. simple triangular elements tend to be overstiff in large plastic deformation). Intelligent routines for re-meshing of continuum elements are needed. One that is currently available and that I would like to explore further is the Automatic/Adaptive meshing. If the error estimate, based on residuals, or strain energy, or geometrical considerations, or on invariants of stress and strain tensors, is not fulfilled, the FE mesh can be adapted according to:
    a. r-method: change the location of nodal points
    b. p-method: change the order of the element shape functions
    c. h-method: change the element size (global remeshing or local mesh refinement)
b) Non Linear Adaptive analyses: if the solution does converge, this routine checks if the mesh is sufficiently fine. If it is not the mesh is modified and a new iteration is started until there is convergence and also the mesh is sufficiently fine. We must keep in mind that the error criteria for non-linear analyses are the same as for linear plus nodes in contact, and equivalent plastic strain. Now modifying an FE mesh involves local rezoning, since nodal and integration point values must be transferred to the newly created nodes and elements.
c) 3-D FEM modeling also produces particular difficulties, which are enhanced by the need to reduce the total number of elements involved. Boundary contact conditions also cause difficulties. It is necessary to match the initial geometric shape as well as possible, but also to introduce test to determine when a node comes into contact with a rigid or elastic tool. This can be done geometrically, and the node then restored to the surface if it has apparently crossed the boundary. It is then necessary to determine whether the normal force has become tensile, before re-sitting the node. I used this approach in my models but I would like to look into it even further.
d) Boundary friction: The friction problem needs to be addressed further. An even better and more realistic modeling friction method is desirable. It is usual to assume a coefficient of friction relating the normal and tangential forces or stresses. For most metal forming operations this is not valid, since the tangential stress is limited to the shear yield stress, which is independent of the stress acting normal to the surface. There is already a composite model with shear limitation in some zones and Coulomb friction in others that could work very well in our rolling problem.

e) Expert systems: computer programs that emulate the cognitive, reasoning and explanatory processes of a human expert within a specialized field of interest, using theoretical or empirical rules and knowledge of the problem domain. The complementary natures of expert systems and FE analysis make them eminently suitable for integration with a roll design package. In such a package, the expert system would design the rolls for each stage of the rolling process (roll pass), and specify the initial billet size and the rolling conditions. An FE analysis would only be needed if it were uncertain whether the rules built in to the expert system could be applied satisfactorily to an unfamiliar component. The results of the FE analysis would help in the design of the rolls in this instance, and they would also provide information about the general applicability of the expert-system rule base. The FE results might even suggest how the rules could be modified in order to deal with future components of similar type. This way, the rage of application of the expert-system die-design procedure increases with time, while the need for expensive FE analysis becomes less and less. The integration of the roll design and FE programs requires the use of an Intelligent Knowledge Based System (IKBS) to compare the components that are to be manufactured with previous examples and to decide whether FE analysis is required. A start has already been made in achieving this kind of integrated facility, through much work still needs to be done in this area (Rowe et al., 174).

f) Plastic work heat generation & friction heat generation: two physical phenomena that are not fully understood and are still the subject of much research today.

g) Viscoplasticity material models: more accurate models need to be developed within the field of viscoplasticity. In this area I would personally like to explore more the Sellars-Tegart Law, the Norton-Hoff Law, and others.

h) Shape Rolling: this is the main problem the industry is interested in regarding the design of rolls for roll pass design of non-symmetric structural shapes. Planning the details of this process, in spite of the large amount of scrutiny and study they received, is still considered an art, not science. The problems and the unknowns are daunting. They involve the ability of the hot metal to fill the grooves of the rolls and attend the effects of the process and material parameters. Finite element analysis can reduce these difficulties. This problem is of enormous difficulty due to the fact that it is yet not understood how the material at 1,200 ºC behaves when there is no symmetry with respect to the neutral axis of rolling. For flat products, both rolls are perfectly cylindrical, and the workpiece goes right through the middle of the roll gap. However, for structural shapes of complex geometry, the top roll is different from the bottom roll, and the roll designer must estimate based on his judgment and experience how much each roll will work the slab, ensuring that the amount of deformation fills the roll gap completely yet trying to minimize the number of passes that are needed in order to achieve the final desired cross section. The main problem seems to be that currently there is no material model that accurately predicts the behavior of the steel at high temperatures. Also, certain mechanisms like friction in the roll gap, and the modeling of the contact problem are not fully understood. The heat generation due to friction and work of plastic deformation are also areas of current research. Thus, the problems that remain are connected with the boundary conditions, that is, the coefficients of

friction and heat transfer at the contact surfaces are still not 100% understood. How exactly are these coefficients affected by the process parameters? The ultimate goal is to be able to model the roll passes using non linear FEM in order to allow the roll designer to do virtual tests on the computer, that will always be a lot cheaper than having to manufacture the rolls, to then test them, which requires a lot of tooling, labor, and associated costs. This is the area to which I now intend to focus my research, now that I have achieved a good comprehension of the cold and hot rolling of flat products.

Alejandro Rivera
January 7th, 2007

Bibliography & References

[1] Asaro, R.J., & Lubarda, V.A., "Mechanics of Solids and Materials", Cambridge University Press, New York, (2006), pp. 461-501

[2] Askenazi, A., & Adams, V., "Building Better Products with Finite Element Analysis", Onword Press, Santa Fe, (1999), pp 425-464

[3] Barrett, C.R., Nix, W.D., & Tetelman, A.S., "The Principles of Engineering Materials", Prentice-Hall, Englewood Cliffs, New Jersey, (1973)

[4] Bathe, K-J., Wilson, E.L., "Numerical Methods in Finite Element Analysis", Prentice Hall, NJ, (1976), pp.82-83, 172-173, 176,184, 208, 246-249

[5] Bathe, K.-J., "Finite Element Procedures in Engineering Analysis", Prentice Hall, Englewood Cliffs, New Jersey, (1982), pp. 301-305, 407-418

[6] Belytschko, T., Liu, W.K., and Moran, B., "Nonlinear Finite Elements for Continua and Structures", John Wiley & Sons, Chichester, (2001), pp. 570-580

[7] Birchenall, C.E., "Physical Metallurgy", McGraw Hill, New York, (1959)

[8] Brick, R.M., Pense, A.W., & Gordon, R.B., "Structure and Properties of Engineering Materials", McGraw Hill, New York, (1977)

[9] Boresi, A.P., & Chong, K.P., "Elasticity in Engineering Mechanics", 2nd edition, John Wiley & Sons, New York, (2000)

[10] Boresi, A.P., & Schmidt, R.J., "Advanced Mechanics of Materials", 6th edition, John Wiley & Sons, New York, (2003)

[11] Burnett, D.S., "Finite Element Analysis: from concepts to applications", Addison-Wesley Publishing, Menlo Park, California, (1987)

[12] Callister, W.D., "Materials Science and Engineering – An Introduction", 3rd edition, John Wiley & Sons, New York, (1994), pp. 149-153, 165-167, 349-350

[13] Chadwick, P., "Continuum Mechanics: concise theory and problems", Dover, New York, (1999)

[14] Champion, E.R., "Finite Element Analysis in Manufacturing Engineering", McGraw Hill, New York, (1992), pp. 1-4

[15] Christensen, R.M. ,"Theory of Viscoelasticity", 2nd edition, Academic Press, New York, (1982), pp. 90-94

[16] Cianci, M., "Leonardo da Vinci's Machines", Becocci Editore, Florence, (1999), p. 89.

[17] Clark, D.S., "Physical Metallurgy for Engineers", 2nd edition, Van Nostrand, Princeton, New Jersey, (1962)

[18] Crisfield, M.A., "Non-linear Finite Element Analysis of Solids and Structures – Volume 1: Essentials", John Wiley & Sons, Chichester, (2001)

[19] Crisfield, M.A., "Non-linear Finite Element Analysis of Solids and Structures – Volume 2: Advanced Topics", John Wiley & Sons, Chichester, (2003), pp. 99-105, 182-184, 411-424

[20] Cook, R.D., et al., "Concepts and Applications of Finite Element Analysis", 4th edition, John Wiley & Sons, New York, (2002)

[21] Cook, R.D., "Finite Element Modeling for Stress Analysis", John Wiley & Sons, New York, (1995)

[22] Cook, R.D., & Young, W.C., "Advanced Mechanics of Materials", 2nd edition, Prentice Hall, Upper Saddle River, New Jersey, (1999)
[23] DeGarmo, E.P., Black, J.T., and Kohser, R.A., "Materials and Processes in Manufacturing", 8th edition, John Wiley & Sons, New York, (1999)
[24] Dhondt, G., "The Finite Element Method for Three-dimensional Thermomechanical Applications", John Wiley & Sons, Chichester, UK, (2004)
[25] Dowling, N.E., "Mechanical Behavior of Materials: engineering methods for deformation, fracture, and fatigue", 2nd edition, Prentice Hall, New Jersey, (1999)
[26] Eriksen, J.L., "Introduction to the Thermodynamics of Solids", Chapman & Hall, London, (1991)
[27] Ewing, G.M., "Calculus of Variations with Applications", Dover, New York, (1985)
[28] Farlow, S.J., "Partial Differential Equations for Scientists and Engineers", Dover, New York, (1993), pp. 3-7, p.27.
[29] Fung, Y.C., "A First Course in Continuum Mechanics", 3rd edition, Prentice Hall, Englewood Cliffs, New Jersey, (1994)
[30] Fung, Y.C., & Tong, P., "Classical and Computational Solid Mechanics", World Scientific, Singapore, (2005)
[31] Gaskell, D.R., "Introduction to Metallurgical Thermodynamics", Scripta Publishing, Washington, D.C., (1973)
[32] Ginzburg, V., "Steel-Rolling Technology", Marcel Decker, New York, (1989)
[33] Ginzburg, V., "High-Quality Steel Rolling", Marcel Decker, New York, (1993)
[34] Ginzburg, V., & Ballas, R., "Flat Rolling Fundamentals", Marcel Decker, New York, (2000)
[35] Haslach, H.W., & Armstrong, R.W., "Deformable Bodies and their Material Behavior", John Wiley & Sons, New York, (2004), pp. 277-278, 316-377, 258-261
[36] Higgins, R.A., "Engineering Metallurgy: applied physical metallurgy", Krieger, Malabar, Florida, (1983)
[37] Hill, R., "Mathematical Theory of Plasticity", Oxford University Press, London, (1950), pp. 15-17, 188-206.
[38] Hughes, T.J.R., "The Finite Element Method: linear static and dynamic finite element analysis", Dover Publications, New York, (2000)
[39] Incropera, F.P., & DeWitt, D.P., "Fundamentals of Heat and Mass Transfer", 4th edition, John Wiley & Sons, New York, (1996), pp. 4,8,10
[40] Kachanov, L.M., "Fundamentals of the Theory of Plasticity", Dover Publications, New York, (2004), pp. 22-23, 38-41, 240-241.
[41] Kalpakjian, S., "Manufacturing Engineering and Technology", 3rd edition, Addison-Wesley Publishing Company, New York, (1995), pp. 357-359.
[42] Khan, A., & Huang, S., "Continuum Theory of Plasticity", John Wiley & Sons, New York, (1995)
[43] Knight, C.E., "The Finite Element Method in Mechanical Design", PWS-KENT Publishing, Boston, (1993)
[44] Kobayashi, Oh, and Altan, "Metal Forming and the Finite Element Method", Oxford University Press, New York, (1989), pp. 41-44, 70-71, 83-86, 131-133, 291-292, 305-308, 321-322.

[45] Kythe, P.K., and Wei, D., "An Introduction to Linear and Nonlinear Finite Element Analysis – A Computational Approach", Birkhäuser, Boston, (2004)
[46] Lanczos, C., "The Variational Principles of Mechanics", 4th edition, Dover, New York, (1986)
[47] Langhaar, H.L., "Energy Methods in Applied Mechanics", Krieger Publishing, Malabar, Florida, (1962), p.78.
[48] Lemaitre, J. & Chaboche, J.L., "Mechanics of Solid Materials", Cambridge University Press, Cambridge, (2000), pp. 195-215, 253-256.
[49] Lenard, J., Pietrzyk, M., and Cser, L., "Mathematical and Physical Simulation of the Properties of Hot Rolled Products", Elsevier, Amsterdam, (1999), pp. 59, 66, 71, 85-95, 110-11, 131-134.
[50] Logan, D.L., "A First Course in the Finite Element Method", 2nd edition, PWS Publishing, Boston, (1993)
[51] Malvern, L.E., "Introduction to the Mechanics of a Continuous Medium", Prentice Hall, Englewood Cliffs, New Jersey, (1969)
[52] Meyers, M.A. Chawla, K.K., "Mechanical Metallurgy: principles and applications", Prentice-Hall, Englewood Cliffs, New Jersey, (1984)
[53] MSC, "MSC MARC 2003: Volume A: Theory & User Information Guide", Analysis Research Corporation, Palo Alto, (2003)
[54] MSC, "MSC Marc 2003 Introductory Course", MSC Software Corporation, Santa Ana, California, (2003)
[55] Modest, M.F., "Radiative Heat Transfer", McGraw Hill, New York, (1993)
[56] Pietrzyk, M. & Lenard, J., "Thermal-Mechanical Modeling of the Flat Rolling Process", Springer-Verlag, Berlin, (1999), pp. 1-14, 98-102,121-125, 135, 142-143.
[57] Roark & Young, "Formulas for Stress and Strain", 6th edition, McGraw Hill, New York, (1989), p.697
[58] Rees, D.W.A., "Basic Engineering Plasticity", Elsevier, Oxford, (2006)
[59] Reddy, J.N., "An Introduction to Nonlinear Finite Element Analysis", Oxford University Press, New York, (2004)
[60] Reddy, J.N., "An Introduction to the Finite Element Method", 2nd edition, McGraw Hill, London, (1993)
[61] Reddy, J.N., "Energy Principles and Variational Methods in Applied Mechanics", 2nd edition, John Wiley & Sons, New York, (2002), pp. 433-434
[62] Roberts, W.L., "Cold Rolling of Steel", Marcel Decker, New York, (1978), pp. 1-19
[63] Roberts, W.L. "Hot Rolling of Steel", Marcel Decker, New York, (1983)
[64] Rowe, G., et al., ""Finite-Element Plasticity and Metalforming Analysis", Cambridge University Press, Cambridge, (1991)
[65] Sagan, H., "Introduction to the Calculus of Variations", Dover, New York, (1992)
[66] Savitsky, E.M., "The Influence of Temperature on the Mechanical Properties of Metals and Alloys", Stanford University Press, Stanford, (1961)
[67] Spencer, A.J.M., "Continuum Mechanics", Dover, New York, (1980)
[68] Temam, R.M., & Miranville, A.M., "Mathematical Modeling in Continuum Mechanics", 2nd edition, Cambridge University Press, Cambridge, (2005)
[69] The United Steel Companies, "Elements of Rolling Practice", Lund &

Humphries, London, (1963)
[70] Timoshenko, S.P., “History of Strength of Materials”, Dover, New York, 1983
[71] Wagoner, R.H., & Chenot, J.L., “Metal Forming Analysis”, Cambridge University Press, Cambridge, UK, (2001), pp. 208-209
[72] Wusatowski, Z., “Fundamentals of Rolling”, Pergamon Press, Oxford, (1969)
[73] Zienkiewicz, O.C., “The Finite Element Method in Engineering Science”, McGraw Hill, London, (1971)
[74] Zienkiewicz, O.C., “The Finite Element Method”, 3rd edition, McGraw Hill, London, (1977), pp. 450-526, 607-644.
[75] Zienkiewicz, O.C., & Taylor, R.L., ”The Finite Element Method – Volume 1: The Basis”, 5th edition, Butterworth-Heineman, Oxford, (2000)
[76] Zienkiewicz, O.C., & Taylor, R.L., ”The Finite Element Method – Volume 2: Solid Mechanics”, 5th edition, Butterworth-Heineman, Oxford, (2000)
[77] Zienkiewicz, O.C., & Taylor, R.L., ”The Finite Element Method – Volume 3: Fluid Dynamics”, 5th edition, Butterworth-Heineman, Oxford, (2000)